Numerical and Experimental Modeling of Atherosclerosis related to MRI

Master's Thesis
by
Stefan Bernsdorf

Declaration

I, Stefan Bernsdorf, hereby declare that the work contained in this thesis is my own original work and has not previously, in its entirety or in part, been submitted at any university for a degree.

Signed by candidate

Abstract

This thesis was motivated by the idea of employing non-invasive investigations of atherosclerosis using Magnetic Resonance Imaging (MRI). MRI has the advantage of being able to detect atheroma in blood vessels with no risk to the patient but is still limited in its application to large blood vessels by the low geometrical resolution obtainable. The capability of MRI to measure velocities as well leads to the idea of correlating atheroma dimensions with measured velocities downstream of the blockage.

This thesis makes a first step towards obtaining results that can be applied in investigations of atherosclerosis employing MRI. The fluid dynamics of arterial blood flow, the medical procedure of diagnosing and treating atherosclerotic diseases, and the physical principle of MRI are investigated to find out "if" and "how" the correlation between a blockage and the resulting downstream velocities can contribute to the diagnosis of atheroma. Parallel to this background research, experimental and numerical modeling of atheroma is carried out. These two approaches use identical geometrical and fluid parameters to enable a direct validation of the results.

An experimental test-rig is designed. Experiments with different types of blockages are performed. The measured flow parameters are pressure and velocity profiles in a cross-section of the modeled artery. A commercial software package is employed for the numerical simulation of blockages with similar geometries to those used in the experiments. The pressure and absolute velocities are again the derived parameters. Both approaches are validated with analytical results obtainable for flow without any blockages. Blockages are then inserted and the results are compared and analyzed for their potential to contribute to the medical application.

The results obtained with the two models give good correspondence. The transitional length of the laminar pipe flow corresponds very well to the expectations. A laminar velocity profile is completely built up before the fluid enters a blockage. Blockages with a small flow area cause a high peak velocity and a large wake. Blockages that slightly reduce the flow area have only a small influence on the flow. The length of a blockage has only a secondary influence on the downstream velocity distribution, while the influence of the surface roughness of the blockage is small. The peak velocities and pressure loss caused by the different blockages give good correlation.

The prediction of the diameter of the blockage from peak velocities measured with MRI is an improvement on that which is possible from the theory only. In particular, the results obtained in this thesis show that the true maximum velocities are significantly lower than those obtained with theoretical predictions. The change in the velocity profiles, due to angioplasty, is shown in a simplified form with the models. Typical values of reduced areas before and after such surgery, where the atheroma is squeezed against the arterial walls, are analysed. The influence of the post-surgery blockage on the flow is very small, while the pre-surgery blockage shows a dominant influence. A prominent wake exists downstream of a highly reduced flow area, and high velocities occur. A wake is a potential risk area for atherosclerosis, as low shear rates and high turbulence intensities are possible. The blockage with the less reduced area has almost no influence on the flow, and a wake is hardly formed. The influence of different shapes of atheroma, while having a similar reduced area, is also demonstrated. The perfectly symmetrical blockage has less negative influence on the flow than one which is highly asymmetrical. The asymmetrical blockage causes a larger wake and higher maximum velocities.

Acknowledgements

It is a pleasure to thank all the people who have contributed to this work, in particular:

Prof. A. Sayers
for his supervision and support, especially for all the answered questions concerning the experimental field.

Dr. H. Pearce
for his support on the numerical field and the inspiring discussions.

Dr. S. Wynchank
for his attention and patient support and especially for his prompt response to all requests.

Kathy Tagg
for always being, and thus enabling the finishing of this thesis.

Julian Meyer
for helping in virtually every aspect.

Horst Emmrich and everybody else in the mechanical workshop
for the wonderful craftsmanship and a lot of cheerful breaks.

Susan Batho, Diann Donald and Dawn Beckett
for being always friendly and helping me to adjust into a new environment.

My friends and my fellow students.

Thanks to all those mentioned above for the excellent personal relationship.

This thesis is dedicated to my parents who made it possible in the first place and always believed in me.

Table of Contents

Nomenclature

Latin Letters

A	m^2	area
B_0	T, Tesla	magnetic field strength
d	m	diameter
$\underline{f}$	N	external volume force
g	m/s^2	gravitational acceleration
G	Hz/T	gyromagnetic ratio
m	kg	mass
p	Pa	pressure
$\underline{q}$	J/s	heat flux
r	m	radius
T	K, °C	temperature
t	s	time
T1, T2	s	time constants
TE	s	echo time
TR	s	repetition time
u, v, w, v_i	m/s	velocity components
V	m^3	volume
$\underline{v}$, $[u\ v\ w]^T$, $[v_1\ v_2\ v_3]^T$	m/s	velocity vector
w_0	Hz	precessional frequency
$\underline{I}$		normal matrix
$\underline{n}$		normal vector
x, y, z		cartesian coordinates
r, θ, z		cylindrical coordinates

Greek letters

ϕ		general flow variable
ρ	kg/m^3	density
μ	$N\cdot s/m^2$	dynamic viscosity
ν	m^2/s	kinematic viscosity
$\underline{\tau}$	N/m^2	stress tensor

Subscripts

a	ambient
rel	relative
max	maximum
mean	average value

1. Introduction

This thesis deals with two different fields of science. The original problem is located in the medical field. The corresponding medical expressions, which might not be familiar to every reader, are explained in the appendix.

1.1. Motivation

The original idea behind this thesis arose from the investigation of atherosclerosis, especially in coronary arteries. A complete blockage of only one of the three main coronary arteries can cause a heart attack, while even a partial blockage of coronary arteries can decrease the performance of the heart and cause serious chest pain.
Up to now, the investigation of atherosclerotic blockages has mostly been done with catheters, which is an invasive procedure. This implies a certain risk for the patient, the mortality rate being estimated at 0.2%. Furthermore, the cost of this procedure is high due to the necessity of single use items like the catheter and large quantities of contrast medium.
The replacement of the catheterisation with a non-invasive procedure would eliminate these problems. Magnetic Resonance Imaging (MRI) is such a procedure, with the potential to replace invasive investigations. The main current disadvantage of MRI, the relatively low resolution, will decrease in the future as the application of MRI to coronary arteries is still a developing technique. Besides the obvious advantage of bearing no risk for the patient, MRI also offers the possibility of measuring velocities in blood vessels.
This leads to the idea of correlating atheroma dimensions with measured velocities downstream of the blockage. Additional information, besides the tissue geometry, would then be available to judge the severity of an arterial blockage.

1.2. Objectives

The aim of this thesis is to make a first step towards obtaining results that can be applied in the investigations of atherosclerosis with MRI.
The fluid dynamics of arterial blood flow, the medical procedure of diagnosing and treating atherosclerotic diseases, and the physical principle of MRI are investigated to find out "if" and "how" the correlation between a blockage and the resulting downstream velocities can contribute to the diagnosis of atheroma.
Parallel to this background research, experimental and numerical modeling of atheroma is carried out. These two approaches use identical geometrical and fluid parameters to enable a direct validation of the results An experimental test-rig is designed and its performance tested. Experiments with different types of blockages are performed. The measured flow parameters are the pressure and the velocity profile in a cross-section of the modeled artery.
The numerical software is installed and learnt. Blockages with similar geometries to those used in the experiments are simulated. Colored contour plots are created with absolute velocity and pressure as parameters.
Both approaches are validated with analytical results ~~obtainable~~ obtained for configurations without blockage. Blockages are then inserted and the results are compared and analyzed for their potential to contribute to the medical application.

2. Medical Aspects

2.1. Diagnosis and Treatment of Atherosclerosis

2.1.1. Disease

The medical problem of interest is called *atherosclerosis*. The origin of this word is in the words *artery* and *skleros*, which means hard. Atherosclerosis is basically a blockage of an artery, caused by a deposit of plaques containing cholesterol, lipoid material, and lipophages, that are formed within the intima and the inner media of arteries. The material is called atheroma. It can cause turbulence and reduce the blood flow rate. The deposit also changes the elastic behaviour of the blood vessel significantly. Atherosclerosis is not uniformly distributed in the body, it only appears at certain sites in the arterial tree. The atheroma can be a symmetrical blockage on the inner wall of an artery, an asymmetrical or a highly irregular shaped deposit (see figures 2-1a to c).

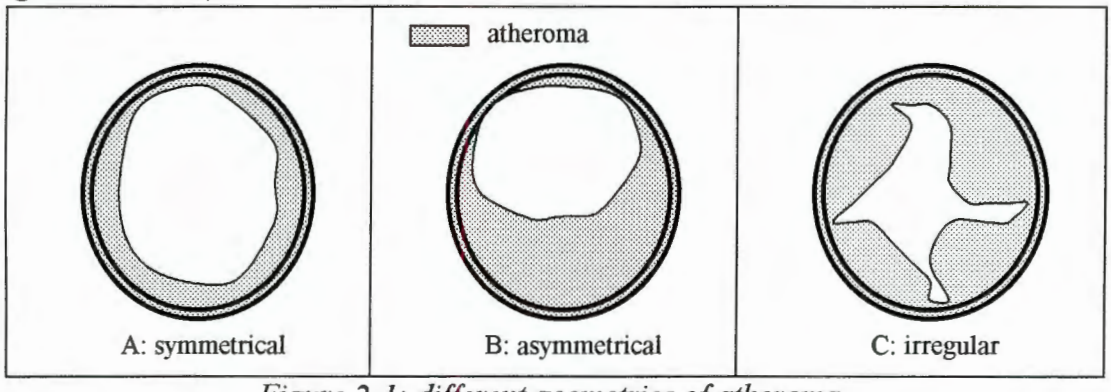

Figure 2-1: different geometries of atheroma

This human disease is the reason for a high number of deaths in the developed countries, as it is the cause for heart attacks. Increased incidence in the developing countries has also been reported.

2.1.2. Diagnosis

Invasive investigations, such as a catheterisation, always imply a certain risk to the patient. The overall mortality, including angioplasty is about 1%. The mortality for investigative catheterisations is lower, at an estimated 0.2%.

Presently there are three main diagnostic procedures available, namely X-ray angiography, Doppler-ultrasound scanning and MRI. Their advantages, disadvantages and capabilities are described briefly.

X-ray angiography is the most common diagnostic procedure for the investigation of diseased coronary arteries. A catheter is pushed up from the left femoral artery all the way to the beginning of the coronary artery of interest. An iodinated contrast medium is released, and the angiograph records the distribution in the vessel. A typical picture of a diseased coronary artery taken with an angiograph can be seen in figure 2-2. This procedure shows only the outline of the artery of interest. The advantages of this procedure are its high resolution and its well known performance. The disadvantages are the risks and costs of any invasive procedure. Furthermore, it is not always possible to get accurate information about the reduced lumen as only the outline of the artery is detected. Atheroma shaped like the one in figure 2-1c would show an outline that implies a much larger lumen than is in fact the case.

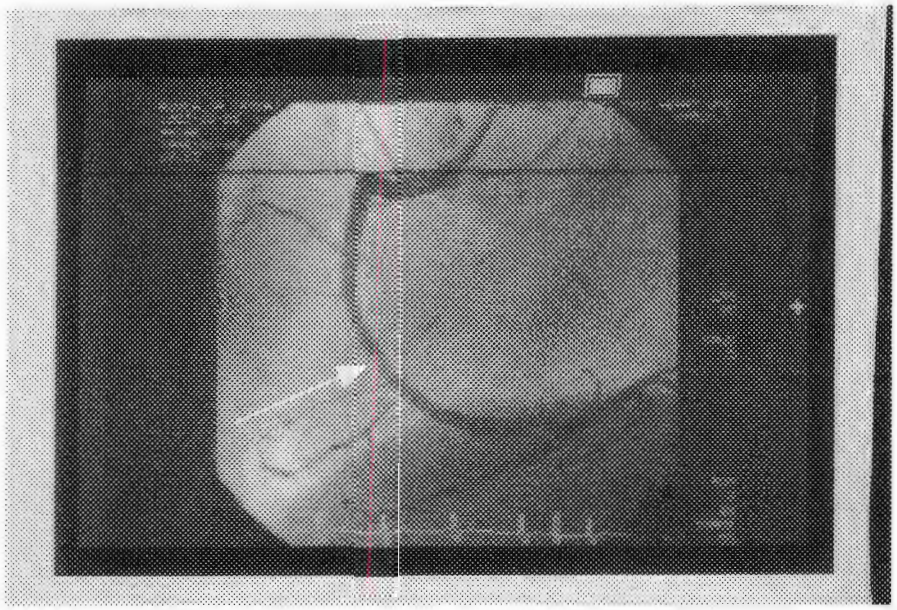

Figure 2-2: angiogram of coronary artery; blocked section indicated by arrow

Doppler-Ultrasound (US) scanning is a rather new technique. A catheter with a Doppler-ultrasound probe at its tip is inserted into the artery of interest. The actual inside of the vessel can be imaged. Figure 2-3 is a typical picture taken from the inside of a coronary artery. This method is occasionally used if the suspicion arises that the angiogram gives insufficient or misleading (see above) geometrical information for a decision on the treatment. The results of an angioplastic catheterisation can be controlled with Doppler US as well. The advantage of this method is once again the high resolution and particularly the possibility of seeing the actual inside of the vessel. But the cost is even higher than with angiography, as special catheters must be used.

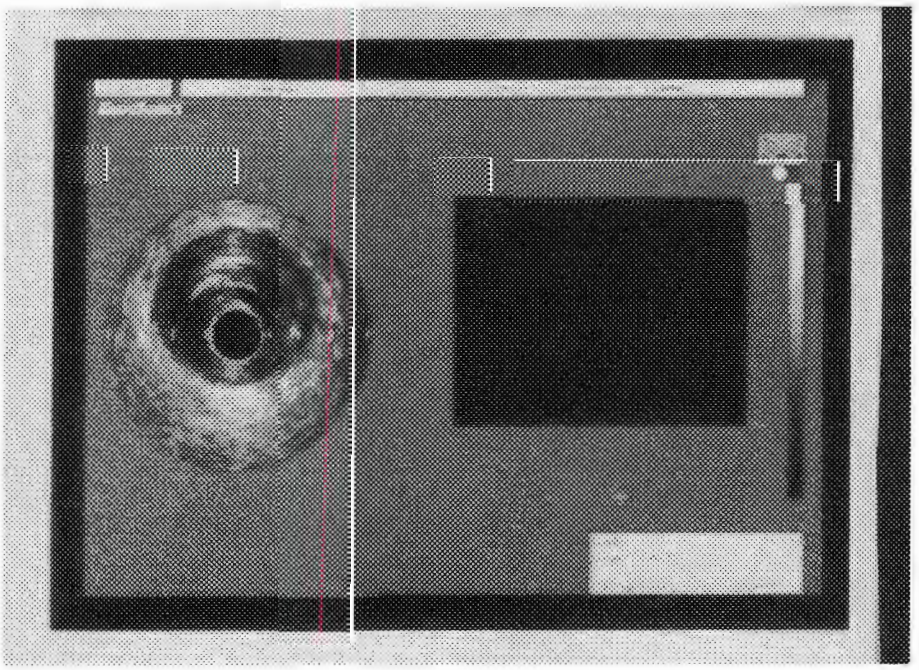

Figure 2-3: Doppler-ultrasound picture from the inside of an artery; free flow area is the inside of the circle only

The most recent, and still developing, technique for investigations of coronary arteries is Magnetic Resonance Imaging MRI. The physics of MRI as well as the possibilities are explained in detail in section 2.2. This completely noninvasive procedure is without any known side-effects to the human body (unlike the cancerogenic risks of X-rays for example). Another advantage is the possibility of measuring the velocity of the blood. As pictures can be taken in any plane, misleading information due to atheroma as in figure 2-1c can be avoided. Opposing the main advantage of MRI being non-invasive is the comparably low resolution. To give an example of geometrical resolution, a coronary artery might be indicated by a row of one pixel width, while the diseased section is indicated by a missing pixel. The same resolution applies to the velocity measurement: the corresponding velocity field would be the mean velocity over the entire cross-section of the blood vessel.

2.1.3. Treatment

The decision of whether or not surgical treatment is necessary, is made after one of the above-mentioned investigation methods. It is notable that only about 50% of the patients investigated do not get treated surgically. The grade of the blockages is not severe enough. Atheroma that blocks less than half of the flow area is usually treated with medication only. If one coronary artery is blocked by more than 50% a catheter with an inflatable balloon at its tip is inserted into the blocked section and blown up with a pressure of up to 18 bar. The plaque is squashed onto the arterial walls. Additionally, a stent (a metallic mesh) can be placed inside the artery to prevent the soft plaque from reforming or moving inwards again. If all three coronary arteries are blocked, a by-pass of the blocked section is done. This is a major surgical procedure. Pieces of vein are taken from the patient's leg and fixed at the aorta and beyond the blocked sections of the coronary artery.

2.2. Magnetic Resonance Imaging MRI

The following section about the physical principle of MRI is a paraphrase of the MR-tutor by Siemens Medical Systems [18].

2.2.1. Physical Principle

Atoms have a nucleus consisting of neutrons and positively charged protons. The hydrogen atom is the most common atom in the human body and the most sensitive to magnetic resonance. That's why MRI is almost exclusively a study of the hydrogen proton.

The heart of an MRI-scanner is a very strong magnet. Modern scanners have a superconducting magnet with a magnetic field of up to 3 Tesla.

Hydrogen protons have randomly orientated magnetic spins. The magnetic spin of any atom will be orientated if inserted into a strong magnetic field. The spins align themselves parallel or anti-parallel to the magnetic field. The energy level of the parallel spin is lower, thus this position is more numerous. The spins precess with a certain frequency, described by the Larmor equation 2-1:

$$w_0 = G \cdot B_0 \tag{2-1}$$

where w_0 [Hz] is the precessional frequency, G the gyromagnetic ratio and B_0 [T] the external magnetic field strength.

The precession of the protons is random in the x-y plane, given a magnetic field in the z-direction (see figure 2-4). The atoms do not precess in phase. The resulting transverse magnetization in the x-y plane is zero. The resulting longitudinal magnetization, in the z-direction, has the same orientation as the external magnetic field.

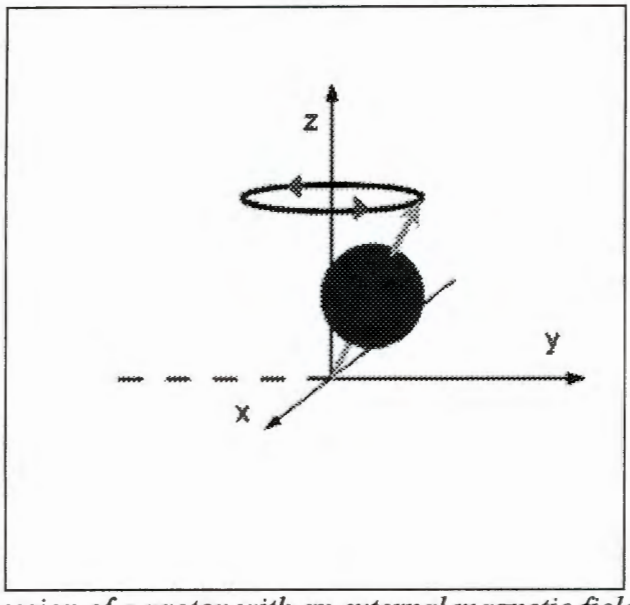

Figure 2-4: precession of a proton with an external magnetic field in z-direction

An RF-pulse is emitted at the precession frequency causing the atoms to precess in phase (they point in the same direction at the same time). The ~~transversal~~ transverse magnetization is not zero anymore and some of the spins gain energy. These atoms are orientated anti-parallel to the magnetic field now, resulting in a decreased longitudinal magnetization.
After the RF-pulse is switched off, the whole system goes back to its original random state. The transverse magnetization disappears, while the longitudinal magnetization returns to its original magnitude.
This return to the random state is a continuous process. The return to the original longitudinal magnetization is represented by the T1-curve, the characteristic time constant is called T1. The return to the original transverse magnetization is represented by the T2-curve, and the corresponding time constant is called T2. Different tissues have different values of T1 and T2, e.g. the T1 and T2 for water is a lot longer than for fat.
The stronger the energy of the stimulating RF pulse, the greater the angle of deflection for the magnetization. A 90° pulse flips the magnetization into the x-y plane, a 180° pulse inverts the magnetization and flips it into the opposite direction.
A characteristic value in MRI is the time of repetition of 90° pulses, TR. This time is the time between two emitting pulses. After the second pulse, protons emit an MR signal. The signal is dependant on the characteristic times, T1 and T2, and the chosen TR. A long TR allows all the protons to relax. The emitted signals of the different tissues ~~is~~ are similar.
With a short TR, protons relax more in tissue with short T1 than in a tissue with long T1. The emitted signal of the first tissue type is stronger.
When a 180° pulse is emitted, it makes the protons turn around, so that they precess in the opposite direction. The faster precessing protons are now behind the slower ones.

They are nearly in phase again. The resulting signal is called echo or spin echo. A combination of 90° pulses and 180° pulses is usually applied for MRI scans. The sequence shown in figure 2-5 is called spin echo sequence.

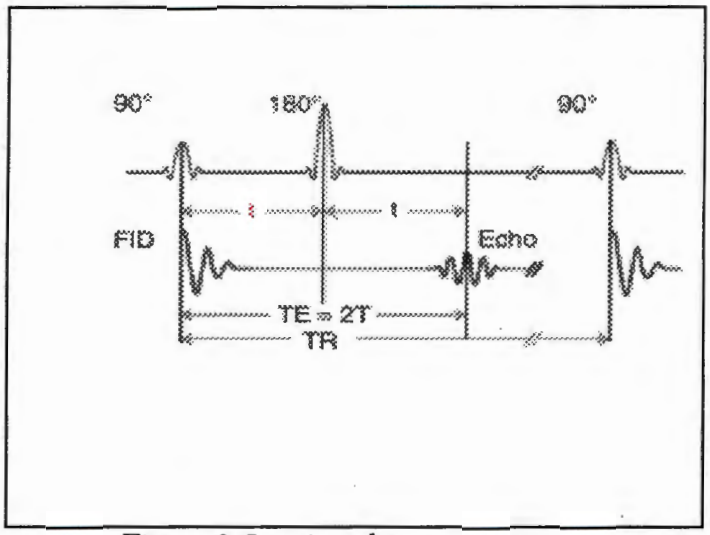

Figure 2-5: spin echo sequence

After the first 90° pulse the spins start falling out of phase as they relax. After the run time *t*, a 180° pulse is applied. The spins turn around and are forced again into phase. The spin echo increases steadily and reaches its peak after the full run time of 2t, also known as the echo time TE. If several 180° pulses are applied one after another, the echo amplitude gets progressively smaller because of the random interactions between the spins.

The following three figures show the qualitative signal emitted by two different tissues. Sequences, as shown in figure 2-6, with a short TR and a short TE are called T1 weighted.

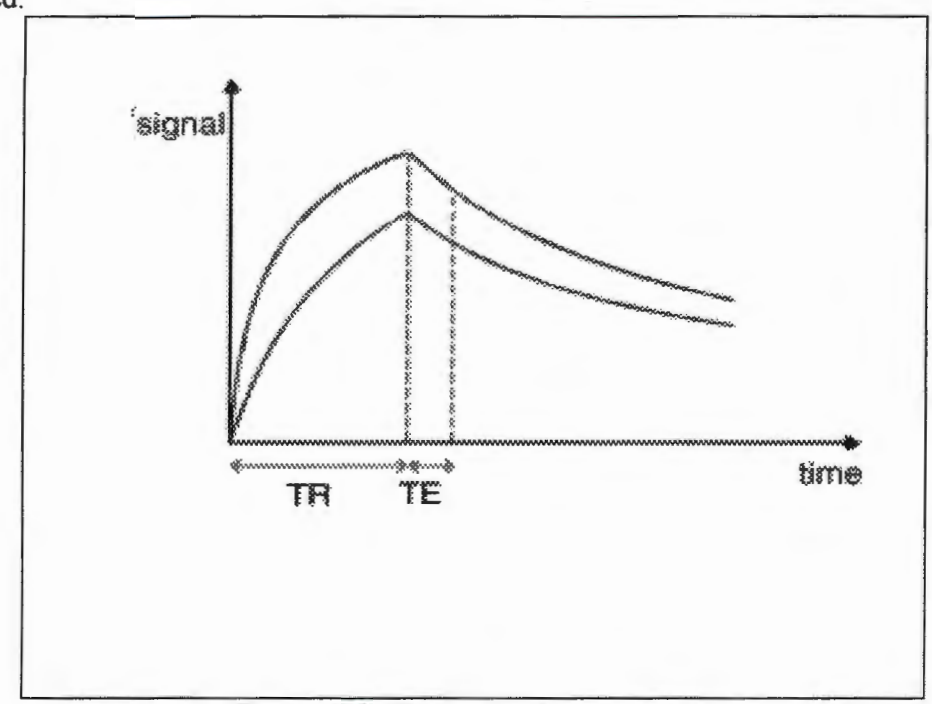

Figure 2-6: T1 weighted sequence

The difference in T1 will show up in signal intensity. With a short TE though, differences in T2 are negligible. To receive a good contrast, TR's are chosen that lie between the T1 times of the two tissues.
Sequences, as shown in figure 2-7, with a long TR and a long TE are called T2 weighted.

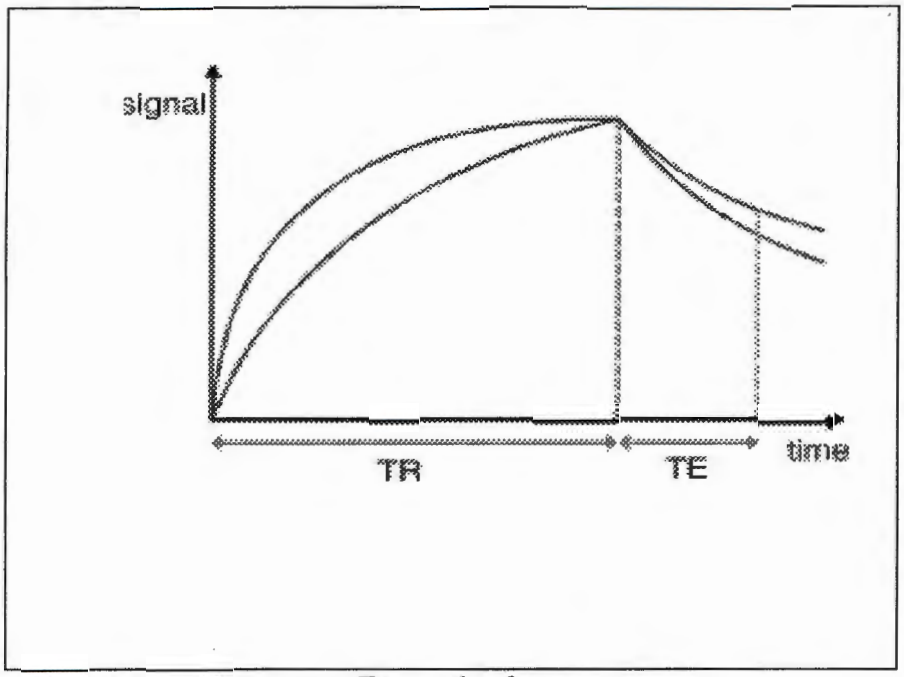

Figure 2-7: T2 weighted sequence

Due to the long TR, all the tissues recover their longitudinal magnetization. With a long TE the differences in T2 become pronounced.
Sequences, as shown in figure 2-8, with a long TR and a short TE are called PD (proton density) weighted.

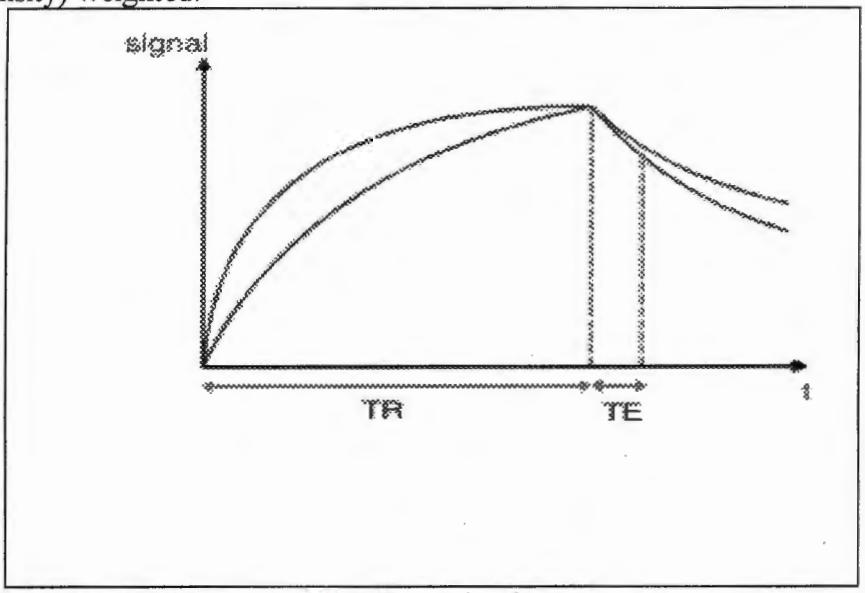

Figure 2-8: PD weighted sequence

The signal emitted is influenced mostly by differences in protons or spins density. The more protons present, the stronger the signal gets.

Only slices of the material are of interest. To visualize only a particular area, a second magnetic field is superimposed on the primary magnetic field. This additional field is a gradient field and is produced by the gradient coils during the RF pulse. This gradient field modifies the strength of the original field which now has different strengths at various locations. Since the protons also have different precessional frequencies, an RF pulse is sent that contains only the frequencies that excite the protons in the slice to be examined. This gradient field is called a slice selecting gradient field. It can be superimposed in any direction.
The thickness of the slice is determined by two parameters. The first is the bandwidth of the frequency of the RF pulse. The wider the range, the thicker the slice. The second parameter is the slope of the gradient field. A steeper gradient produces a thinner slice.
A second gradient field is superimposed to produce a two dimensional picture. This gradient is called a frequency encoding gradient. If the frequency encoding gradient decreases from left to right, the frequency of the protons that were precessing with the same frequency also decrease from left to right. To get enough spatial information, another gradient field is superimposed, this time a phase encoding gradient. This magnetic field is applied along the column for a short time. As the strength of the magnetic field decreases from top to bottom, protons speed up their frequency according to this varying strength. When this short magnetic field is switched off, they have the same frequency again, but they are out of phase.
The signals with different frequencies and phases are finally analyzed with a Fourier Transformation. This enables the assignment of a specific signal to a certain location in the slice and the image can be reconstructed.
Different advanced pulse sequences with varying flip angles are used in the medical application of MRI. The advantages include higher resolution and shorter acquisition times. Obtaining 3D data in acceptable time is possible with Gradient Echo Sequences.

2.2.2. Present Possibilities

Imaging of the *arterial walls* can be done with spin echo sequences. Blood appears black, while the vessel wall is clearly shown and atherosclerotic plaque shows as areas of wall thickening. This technique can be applied for sufficiently large vessels only.
One of the methods available to image the *vessel lumen* is the time-of-flight TOF method. The principle of TOF is based on gradient echo sequences. In TOF, repeated RF pulses with a short repetition time, magnetically saturate the volume of tissue imaged, causing decreased signal intensity (SI). Flowing blood entering from outside the volume is not subjected to the saturation pulses, so the blood maintains its signal intensity. Images can be generated in which flowing blood shows high SI, and tissue shows relatively low SI. TOF MR angiograms can be obtained by 2D or 3D acquisition techniques. In the 2D approach the imaging volume is limited to a thin slice (~1.5mm). As the slices are thin the blood does not become saturated and remains bright throughout the slice. In the 3D approach, the imaging volume is a relatively thick slice (~4cm). Data is acquired from the entire volume and then divided into thin (0.7mm) partitions. It is possible to select blood flowing in a specific direction. Either arteries or veins can be imaged. TOF methods actually depict the flowing blood.
Velocity measurement is done with "marking" a short volume of blood with a specific frequency and phase. The time required to pass two points gives an average velocity of this blood volume.
A more elegant method of measuring the velocity is the phase sensitive angiography. Each gradient pulse causes a change in the Larmor frequency, whereby this change

depends on the gradient and the position of the spin. If a second gradient pulse with the opposite sign is used after a given time, the phase shift can be compensated if the individual spin has not changed its position. Stationary spins always have the same magnetization as before, following the bipolar gradient pulse. A moving spin, for example the spin of a blood molecule, causes an entirely different situation. In this case, the phase shift of the first pulse cannot be fully compensated for since the spin is located at a different position. This phase shift is dependent on the spin velocity. With knowledge about that dependency, the velocity of blood flow can be determined by measuring the phase of the MR signal.
Scanning coronary arteries requires a triggering of the slice with a specific phase in the cardiac motion. This is usually done with measurements of the pulse and a corresponding adjustment of the scanning area.

2.2.3. Future Development

MRI cannot yet match the spatial resolution of conventional angiography. This applies to both the measurement of a velocity field, and the scanning of geometries. The development in MRI is towards shorter acquisition times and higher resolution. These two contrary objectives require new pulse sequences and improved gradient performance as well as advanced software for the post-processing of the data.
A problem encountered when imaging small vessels, especially the coronary arteries, is the respiratory movement, which degrades the images. A relatively new technique is called navigator monitoring. Navigator echoes are used to monitor the diaphragm position. The images can be gated to breathing motions. This technique is relatively new and not applied in routine medical applications yet. It allows the elimination of most respiratory noise in the images. This is expected to improve visualization of the arterial wall and the lumen of small arteries (smaller than 5mm), such as the coronaries, considerably.

2.3. Diagnostic Parameters for medical application

Diagnostic Parameters for medical application have one main objective; they must be brief. One or two significant numbers are acceptable, as well as a significant graph. A whole list of numbers and a long analysis are impractical and would not be accepted.
Up to now, the judgement of atheroma is made only by its geometry. The presence of a reduced lumen inside the blockage is established and with this information, the decision on a treatment is made.
An improvement of this diagnostic method could be the consideration of the actual parameters. Of particular interest concerning the atherosclerotic potential before and especially after a treatment are two flow parameters.
The first one is the shear stress. High shear stress is believed to be a possible cause for vessel damage. Shear stress also seems to play a role in the deposit of plaque. There are opposing views. Some say atheroma occurs in areas of intense shear stress [9]. In a more recent publication, it is stated that low shear stress is believed to be a haemodynamic risk factor [22]. The second flow parameter is the turbulence. Atherosclerotic plaque is often found at sites of turbulent flow [10]. The destruction of blood cells might be caused by high turbulence intensities. Damage of the arterial wall can be another consequence of high turbulence intensity.

3. Fluid Dynamic Aspects

3.1. Arterial Blood Flow

The fluid dynamics of arterial blood flow is very complex. A lot of research has been done in this field and a wide variety of literature is available [1] [10] [11] [13]. This chapter gives a brief overview to understand the consequences of the assumptions made in the modeling.

Arterial blood flow is an *unsteady pulsed flow*, driven by the contraction of the heart. Each pulse is divided into two sections, the systole or the active part of the cardiac cycle, and the diastole, the resting phase. Figure 3-1 shows a typical cycle of arterial blood flow rate as a function of time.

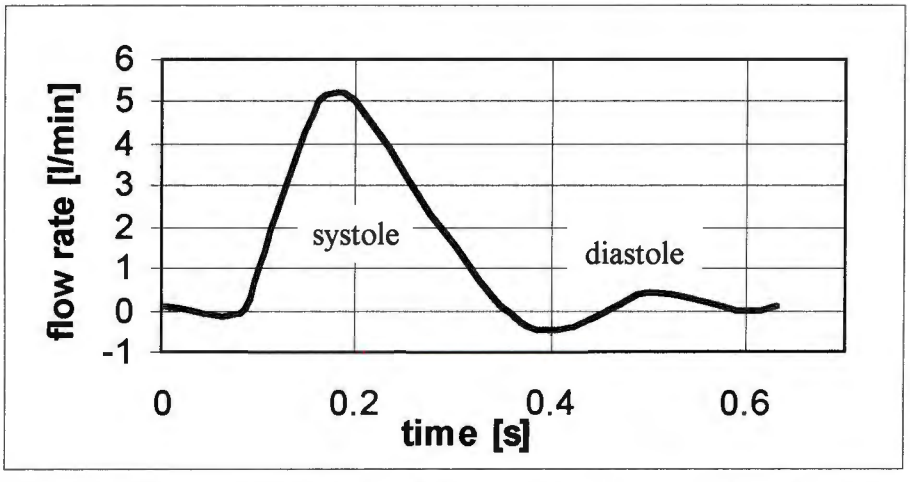

Figure 3-1: qualitative arterial flow cycle at a normal heart rate

The arteries are not ideal stiff tubes but organic vessels with *non-linear elasticity*. The arteries have a characteristic wave speed dependant on several factors, such as wall thickness, wall material and surrounding material, that influence the blood distribution.

The arteries *branch* into smaller arteries. The branching sections, or bifurcations, cause local disturbances in the blood flow. Usually the critical Reynolds number for turbulence is lowered in these sections. Boundary layer separation is possible at low Reynolds numbers. The resulting high wall shearing stress, trailing vortices and scouring effects can locally injure the arterial wall. Other flow phenomena such as backflow can occur during a heart cycle. It is not known in detail what kind of influence bifurcations have on the deposit of atheroma, but high local shear stresses seem to have some influence.

Arterial blood flow is *laminar* in general, as shown in Table 3-1. *Turbulent* flow is possible in large vessels close to the heart, at certain points of the circulating system, mainly points of complex geometry, at branchings, and beyond blockages.

vessel	Diameter [mm]	Mean velocity [m/s]	Corresponding Reynolds number [-]
Aorta	25	0.22	2000 - 4000
Internal carotid artery	4	0.5	750
Femoral artery	5	0.26	500
Renal artery	4	0.5	750

Table 3-1: characteristic parameters of arterial blood flow in the human body

The fluid blood is a suspension of blood cells in plasma. At rest, the cells form a continuous structure. When a finite stress is applied to blood, the continuous structure breaks down. The stress required to disrupt the standing structure of blood is referred to as the yield stress. After disruption, the structure appears as a cluster of cell aggregates suspended in plasma. The aggregates are in turn made up of smaller units of cells called rouleaux or flocs. As additional stress is applied, the rouleaux and aggregates become smaller. A dynamic equilibrium exists between the size of aggregates and the stress applied. When aggregates and rouleaux are under sufficiently high stress that they are reduced to individual cells, further increases in stress cannot cause changes of aggregate size. As a result, the shear stress - shear rate relationship becomes a straight line at sufficiently high shear stresses. This can be seen in figure 3-2 for shear rates greater than $50s^{-1}$.

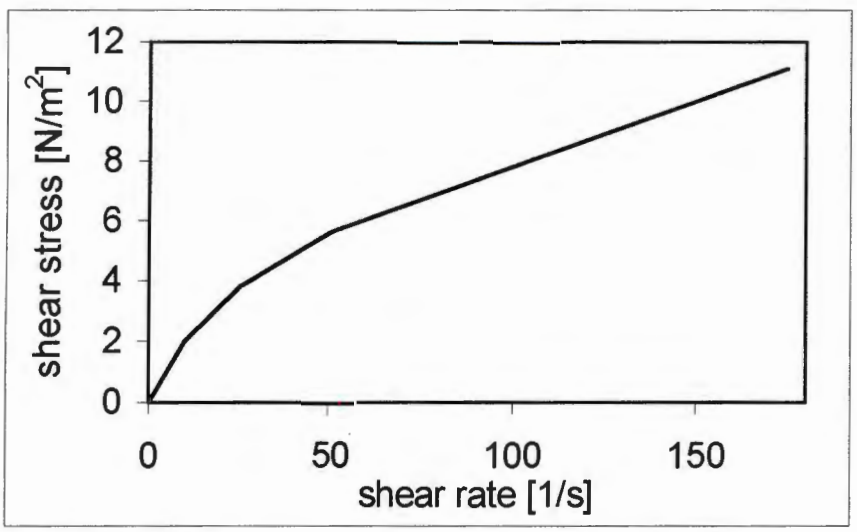

Figure 3-2: shear stress-shear rate relationship for blood in dynamic equilibrium

Fluids with the quality of shear stress versus shear strain rate forming a linear function passing through the origin are called *Newtonian* fluids. The slope of this function is the dynamic viscosity. In other words, the viscosity is constant for a Newtonian fluid.
The viscosity of the blood varies with the rate of shear strain in the flow. Under sufficiently high shear stress blood behaves like a Newtonian fluid. This depends not only on the shear stress, but also on parameters like the protein concentration of the plasma, the deformability of the blood cells, and the tendency of the blood cells to aggregate. The viscosity increases when the shear strain rate decreases. The viscosity also increases when the haematocrit increases, and when the temperature is decreased. Aggregation and hardening of the cells increase the viscosity. These factors are all affected by various states of health and disease.

3.2. Conceptual Model

The assumptions and simplifications made in both the numerical and the experimental modeling are explained with respect to the resulting accuracy. There are three main assumptions which impose clear restrictions on the models, and three more which have a minor influence.

- The modeling is done with a laminar flow regime. This first main assumption is very close to reality, as the arterial blood flow is laminar in most parts of the circulation. This simplification is quite restrictive in respect to this thesis, as most of the turbulent flow develops in zones of arterial diseases like atherosclerosis. Furthermore, the turbulence intensity is a potential parameter of interest, as stated in section 2.3.
- The blood flow is assumed to be steady in the model. This simplification places quite a heavy restriction concerning general fluid dynamic effects. With regards to this thesis, the consequences are believed to be not that drastic. The unsteady effects are not believed to have a major influence on the qualitative results of this research, as mainly the maximum velocity in the velocity field and the pressure loss is used in the analysis.
- The non-Newtonian behaviour of the blood is not considered. Blood is modelled as a Newtonian fluid. This is the third main assumption. Plasma alone is often modelled as a Newtonian fluid with good accuracy. Blood, as a suspension of red cells in plasma, certainly does not have a Newtonian behaviour for low shear rates. For higher shear rates, however, the assumption made is close to reality. The consequences of this simplification on this thesis are believed to be minor. Final certainty will only be achieved with a corresponding experiment.
- The branching and bending of the arteries is not considered. The arteries are modelled as single and straight pipes. This assumption is reasonable for the corresponding zones of interest in the circulatory system, such as single arteries which are only slightly bent. The flow at bifurcations, which are potential atherosclerotic risk zones, is especially influenced by unsteady flow effects.
- The complex and individual geometry of each single atheroma can not be considered. Characteristic, simple geometries are used as blockages in the models.
- The flexible walls of the arteries are not considered. The walls are modelled as rigid walls. This assumption is believed to have no further influence, as the flexibility of the walls only has an influence on the flow in the unsteady case.

Both approaches to model the arterial blood flow use the same assumptions. To achieve comparability of the results of both models the boundary conditions, fluid parameters and geometrical dimensions are kept as similar as possible.

3.3. Model Validation Problem

Two different approaches to model arterial blood flow are done, an experimental investigation and a numerical simulation. These two were unfamiliar to both, the author and the Department of Mechanical Engineering of the University of Cape Town. The accuracy and reliability of the two models must therefore be checked thoroughly.

A comparison of the results from the two models will give some evidence about their accuracy but errors in both models can not be excluded. Further comparison with analytical data can help with this task.

3.3.1. Laminar Velocity Profile

The problem of steady, incompressible, laminar pipe flow in a circular straight pipe of constant diameter with a constant pressure gradient is also known as the Hagen-Poiseuille problem. The setting is shown in figure 3-3.

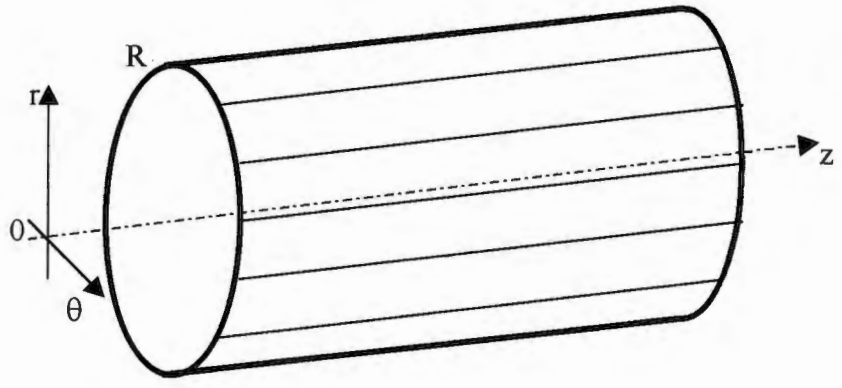

Figure 3-3: setting of Hagen-Poiseuille problem

The velocity has components in the axial direction only, radial and circumferential components do not occur. Gradients in the circumferential direction are zero due to the symmetry of the problem. The pipe is considered to be infinitely long, transient effects do not play any role. Therefore gradients in the axial direction are also zero.
The Navier-Stokes equations take the following form:

$$\begin{aligned} 0 &= \mu \cdot \Delta v_z - \frac{\partial p}{\partial z} \\ v(R) &= 0 \\ v(0) &= v_{max} \end{aligned} \tag{3-1}$$

This reduces in cylindrical coordinates to:

$$\mu \cdot \frac{1}{r} \cdot \frac{\partial}{\partial r}\left(r \cdot \frac{\partial v}{\partial r} \right) = \frac{\partial p}{\partial z} = const. \tag{3-2}$$

Integration under consideration of the boundary conditions finally leads to the velocity profile in a crossection of the pipe:

$$v_z(r) = v_{\max}\left(1 - \frac{r^2}{R^2}\right) \tag{3-3}$$

This parabolic profile is shown in the figure 3-4. The mean velocity for such a velocity is exactly half of the maximum velocity:

$$v_{mean} = \frac{1}{2} \cdot v_{\max} \tag{3-4}$$

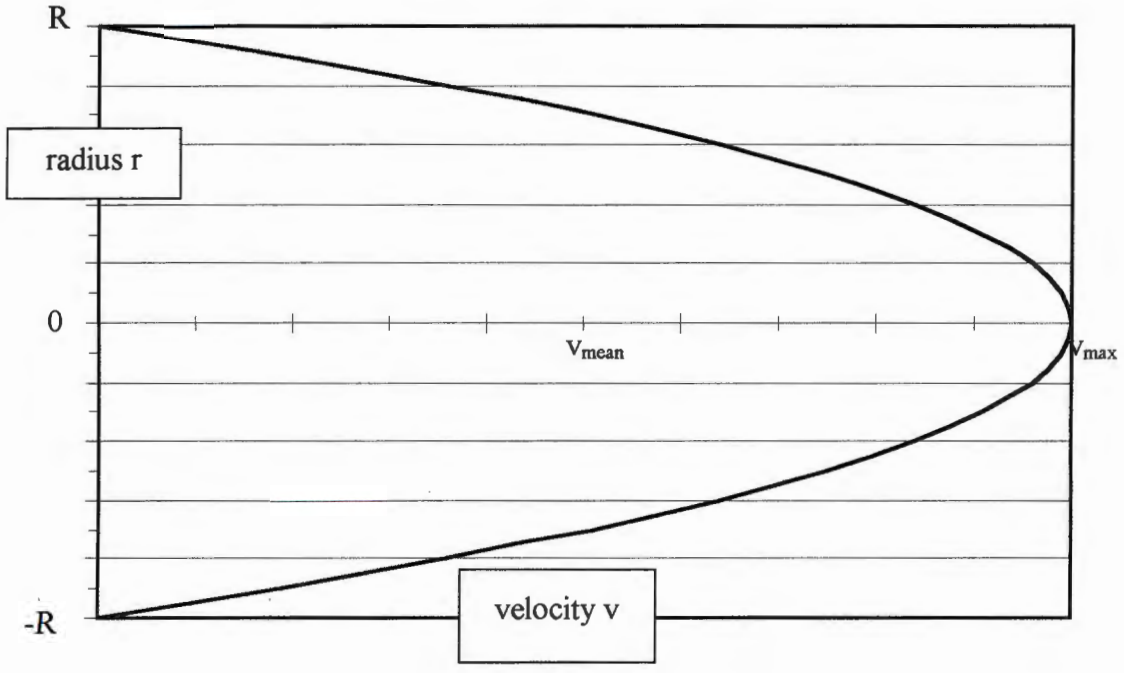

Figure 3-4: parabolic velocity profile

The comparison of this ideal laminar velocity profile with both, the experimental and numerical results will give more evidence about the functionality and the accuracy of both. It is not expected, that the models give exactly the same velocity profiles, as some assumptions, like the one of an infinitely long pipe, are definitely not fulfilled. How well the measured and calculated profiles match this ideal profile is an indicator for the accuracy of the models.

3.3.2. Mean velocity

The continuity equation gives some, rather trivial, information about the mean velocity in a pipe. Assumptions are that the entire mass flow with a density ρ has its mean velocity $\mathbf{v_{mean}}$ normal to the area **A**. This setting, for a straight pipe with variable diameter is shown in figure 3-5.

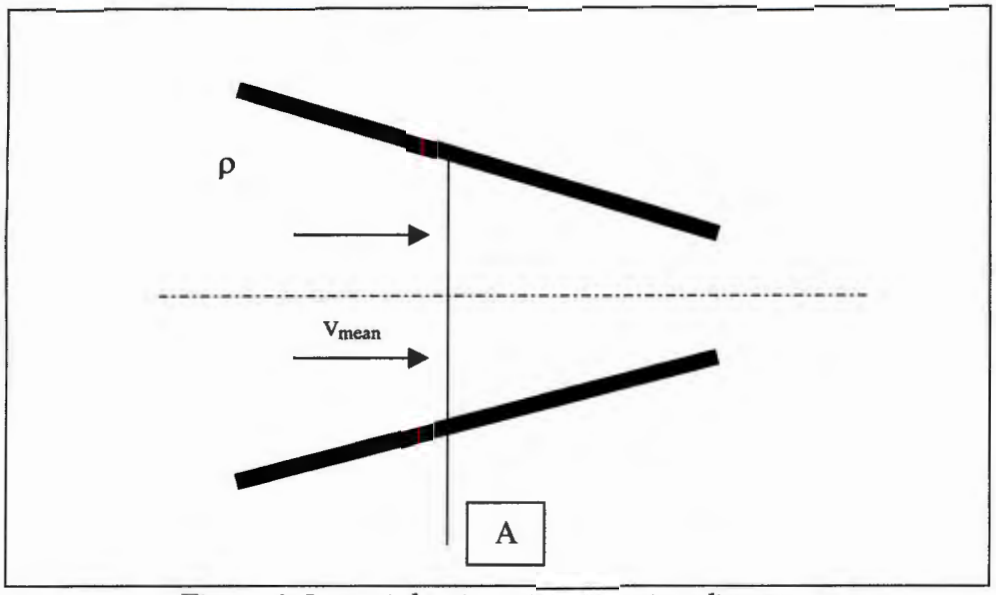

Figure 3-5: straight pipe with changing diameter

With a constant density ρ the continuity can be written as:

$$\dot{m} = A \cdot v_{mean} \cdot \rho = const. \tag{3-5}$$

This simple expression gives a mean velocity for known mass flow rate, density and flow area. From equation 3-4 (laminar velocity profile), an expression for the maximum velocity is found:

$$v_{max} = 2\frac{\dot{m}}{A \cdot \rho} \tag{3-6}$$

This parameter is easy to calculate and the comparison with the experimental and numerical results will give indications about accuracy of the numerical formulation, accuracy of the measurement equipment, leakage of the experimental test-rig and build up of the laminar velocity profile.

4. Experimental Modeling

4.1. Experimental Apparatus

4.1.1. Design

The design of the experimental test-rig is a vital part of the experimental modeling. Therefore, the design process and the fundamental considerations are presented in the following section.

The objective of *finding of a good compromise between the need for reliable, accurate data and the limitations of a low financial budget and limited time* is the fundamental aim applied in the design process. The necessary technical capabilities of the experimental apparatus are more specific:

- The flow parameters required to set up a numerical simulation must be measured.
- For good correspondence with the numerical simulation, the flow has to be steady with a constant velocity in the entry of the pipe.
- Measuring of the required flow parameters must be done with the smallest possible influence on the flow.
- The handling of the test-rig, especially the exchange of the blockages and the measuring of the velocity has to be as simple as possible without loss in accuracy.
- The laminar boundary layer must be fully developed at the test section.

Some theoretical research is done concerning the last requirement. The length of the pipe is the relevant parameter for the development of the boundary layer. The parabolic velocity profile (for the laminar flow regime) is theoretically reached only after an infinite distance from the beginning of the pipe. It is standard to regard the so-called *entry length* as the distance along the pipe to the point at which the maximum velocity is only 1% different from the final value. Langhaar [14] gives a simple expression for this entry length:

$$l_{entry} = 0.057 \cdot \mathrm{Re} \cdot d \tag{4-1}$$

with the Reynolds-number $\mathbf{Re} = v_{mean} \cdot d/\nu$,
the mean velocity v_{mean},
the viscosity ν
and the pipe diameter **d**

The length of the pipe required to ensure the full development of the laminar velocity profile is therefore a function of the pipe diameter and the Reynolds-number.

The process of designing the test-rig starts with the decision on a specific fluid – pipe – probe combination. The requirements of a large enough diameter, to enable measurements at several points across the flow, a high enough velocity to obtain high accuracy at the point of velocity measurement, and of a low Reynolds-number to ensure a laminar flow are self contradictory. Taking the fluid viscosity into account, there are only two possible cheaply available fluids, air and highly viscous oil. The decision to use air is made due to its easier handling. The idea of modeling blood with air seems slightly far fetched, but it has to be kept in mind that both air and blood are fluids, and that the Reynolds-number is the significant parameter and the phase of material. Air does not have to be circulated, an open system can be used. The problem

of sealing is also far less difficult to solve with air than with oil. The pipe diameter is finally chosen by the easiest commercially available. The next step is to find a fan that creates a sufficiently high volume flow rate. Measuring the flow rate is slightly problematic, as the low flow rate requires a small rotameter, which in turn causes a high pressure loss in the system. Measuring of velocities this low (mean velocity around 0.5m/s) is slightly problematic as well, as most of the commercially available probes are recommended for a minimum velocity just slightly above the expected mean velocity in this test rig.

4.1.2. Test-rig

A schematic drawing of the experimental test-rig is shown in figure 4-1.

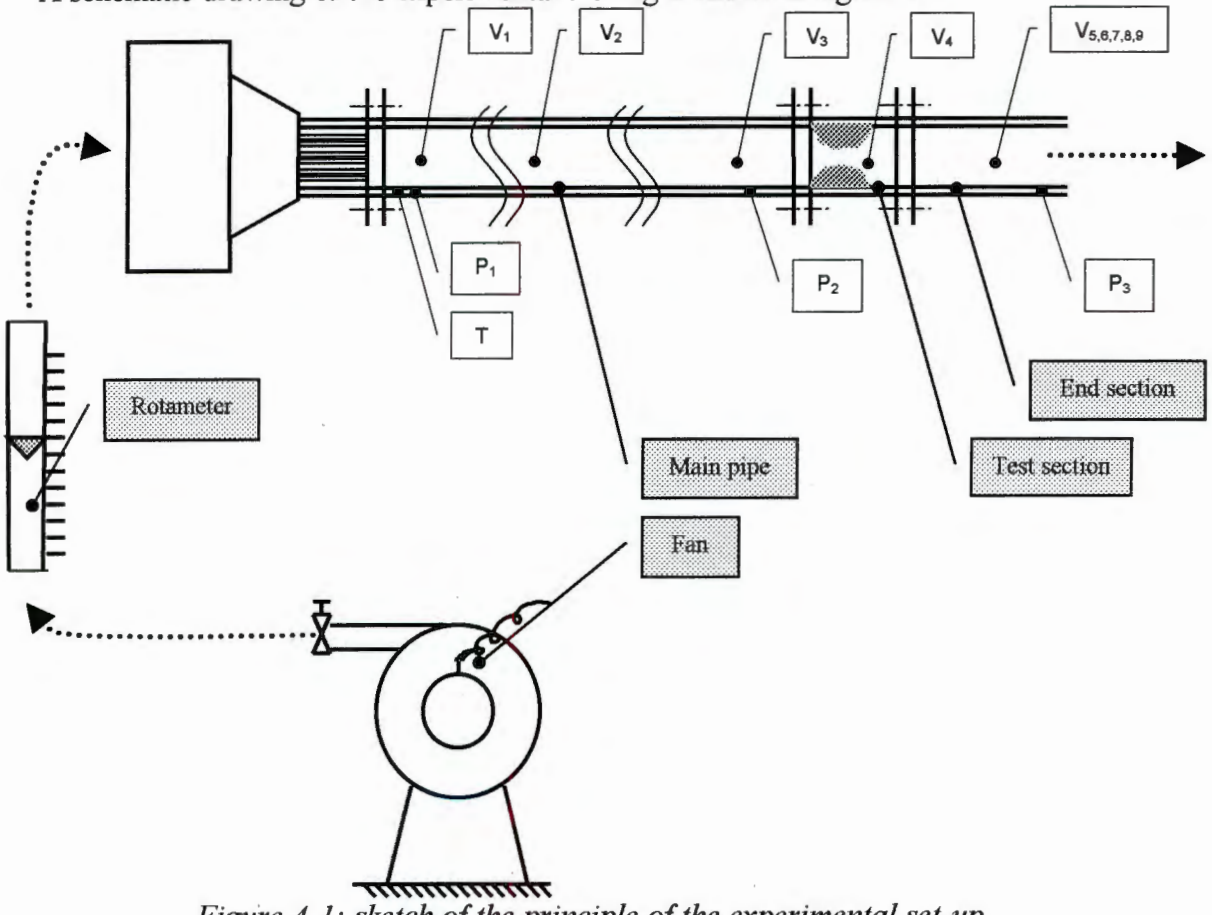

Figure 4-1: sketch of the principle of the experimental set-up

The elements of the experimental test-rig are described in order of the direction of the air flow.

Fan

The centrifugal fan, a disc of ~90cm diameter, is driven by an electrical motor manufactured by Brook Motors Ltd. The engine has a power input of 7.5hp and turns at a constant speed of 2900rpm. The fan and the motor are shown in figure 4-2. Air is blown into a flexible pipe from the fan and the volume flow rate is adjusted by a gate valve at the exit of the fan. This valve enables the flow to be regulated continuously in the range between 0% and 100%. An 8mm internal diameter flexible pipe connects the valve to a downstream rotameter, which measures the volume flow rate of the air.

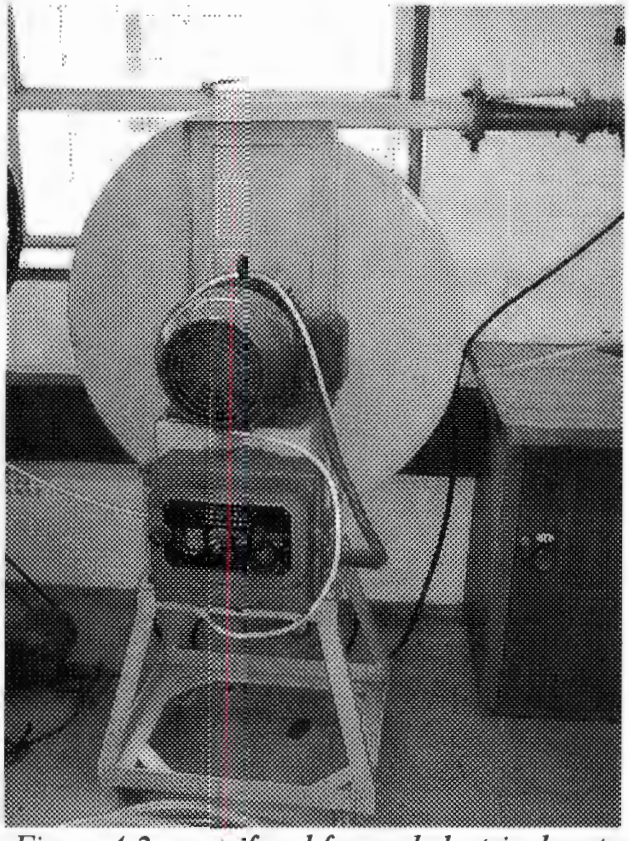

Figure 4-2: centrifugal fan and electrical motor

Settling chamber and straightening section

The settling chamber, a modified paraffin-can, and the flow straightening section, a pipe segment filled with straws, are attached to the beginning of the main pipe with a flange. The settling chamber and straightening section are connected to a diffuser made of cardboard. Settling chamber, diffuser and straightening section are shown in figure 4-3, together with the rotameter and the fan.

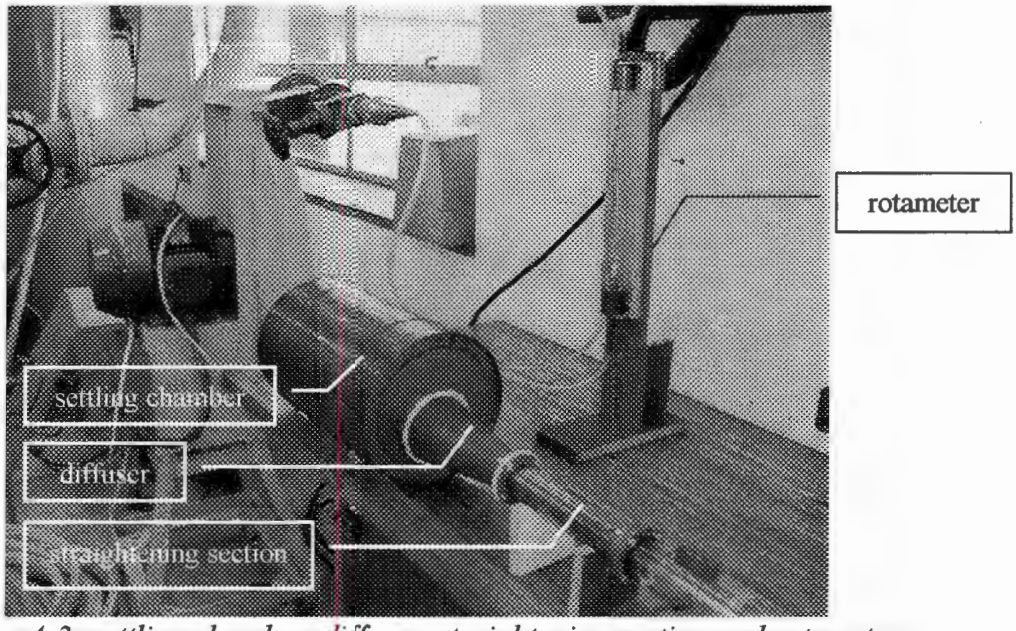

Figure 4-3: settling chamber, diffuser, straightening section and rotameter

The area ratio between the settling chamber and flexible pipe is about 960, while the ratio between the flow area in the settling chamber and the test pipe is about 29. Inside the settling chamber, the mean air velocity drops down to 0.015m/s (for a volume flow rate of about 47litres/min), an almost negligible speed. The straightening section, the first part of the main pipe, is filled with straws to suppress radial and circumferential velocity components.

Main pipe section

Flanged to the straightening section is a 5m length of PVC pipe to enable the build up of the laminar velocity profile. The inner diameter of the transparent pipe is 46mm, the outer diameter is 50mm. Both ends of the pipe are equipped with 70mm flanges each, that are attached with four 6mm bolts. The entire pipe, including test section and end section, is shown as seen from the end in figure 4-4.

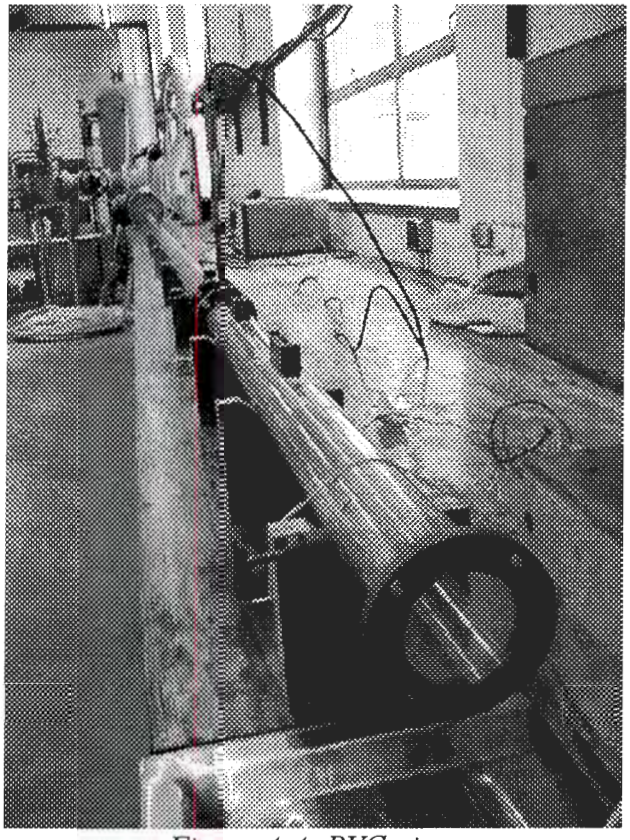

Figure 4-4: PVC pipe

Test section

The various blockages are inserted into a 0.12m length of PVC pipe. This pipe section can easily be changed by unbolting the connecting flanges. Four test sections are built to make the process of measuring and building a blockage more convenient. Both ends of the pipe are equipped with 70mm flanges that are attached with four 6mm bolts.

End section

The last section of the pipe system is 0.8m long. Both ends of the pipe are equipped with 70mm flanges that are attached with four 6mm bolts.

Pipe support

All the pipe sections are mounted on wooden supports. Square pieces of a 20mm wood block have a "V"-cut at the top into which the pipe is laid. They can be seen in figure 4-4.

4.1.3. Instrumentation

The locations of the measuring points for the different flow parameters are shown in figure 4-1. The dotted arrows indicate the direction of the air flow. All the measuring points inside the pipe are included. The letter *v* indicates a measuring point for velocity, the letter *p* indicates a measuring point for the pressure and the letter *T* indicates a measuring point for temperature. Their coordinates are given in the following tables 4-1 and 4-2. Z indicates the distance from the beginning of the pipe in mm and L indicates the distance from the downstream end of the blockage in mm.

Measured value	T	P1	P2	P3
Z [mm]	40	100	4900	5820
L [mm]	-5060	-5000	-200	720

Table 4-1: location of the pressure and temperature tappings

Measured value	V1	V2	V3	V4	V5	V6	V7	V8	V9
Z	50	2500	4950	5105	5135	5195	5255	5315	5515
L	-5050	-2600	-150	5	35	95	155	215	415

Table 4-2: location of the velocity measuring points

The instrumentation used to measure the different flow variables is now described.

Pressure

The ambient pressure is measured with a mercury manometer manufactured by F. Darton & Co. Ltd. The difference between ambient pressure and static pressure is measured with an electronic micromanometer FCO11, manufactured by Furness Controls Ltd. The pressure ranges from 0 to 20Pa .

The pressure difference between the inside and outside of the pipe is very small, less than 10Pa. Therefore, the fluid pressure is considered to be equal to the ambient pressure for the velocity measurements.

Temperature

The temperature is measured with a microprocessor-based, digital thermometer designed to use external thermocouples as temperature sensors. A K-type chromel-alumel thermocouple is used as a sensor. The temperature range for this type of thermocouple is from –270°C to +1370°C. The thermometer, as well as the thermocouple, are manufactured by Fluke. The name of the thermometer is FLUKE 52.

Several measurements showed that the temperature inside the pipe is almost exactly the same as outside the pipe (±0.1°C). For reasons of convenience and less flow disturbance, the temperature is measured outside of the pipe.

Several measurements showed that the temperature inside the pipe is almost exactly the same as outside the pipe (±0.1°C). For reasons of convenience and less flow disturbance, the temperature is measured outside of the pipe.

Volume flow rate

The flow-meter chosen is a rotameter series Metric 18. This device is a vertical, conical glass tube with a special float inside. Depending on the volume flow rate, the float stabilises at a certain height.

Calibration of the rotameter

With the help of the *Calibration Data for Metric Series rotameters* the calculation of the flow calibration is done. This booklet contains families of curves, expressing the relationship between the variables involved. Using the known meter and fluid constants, the parameters of the curves are evaluated and from these the calibration for the required fluid is established. The procedure is described in detail in this booklet.
The resulting chart of flow rate versus scale reading, is shown in the following figure 4-5. A fourth order polynomial curve is fitted to the calibration curve and this equation is used to calculate the volume flow rate from the rotameter reading.

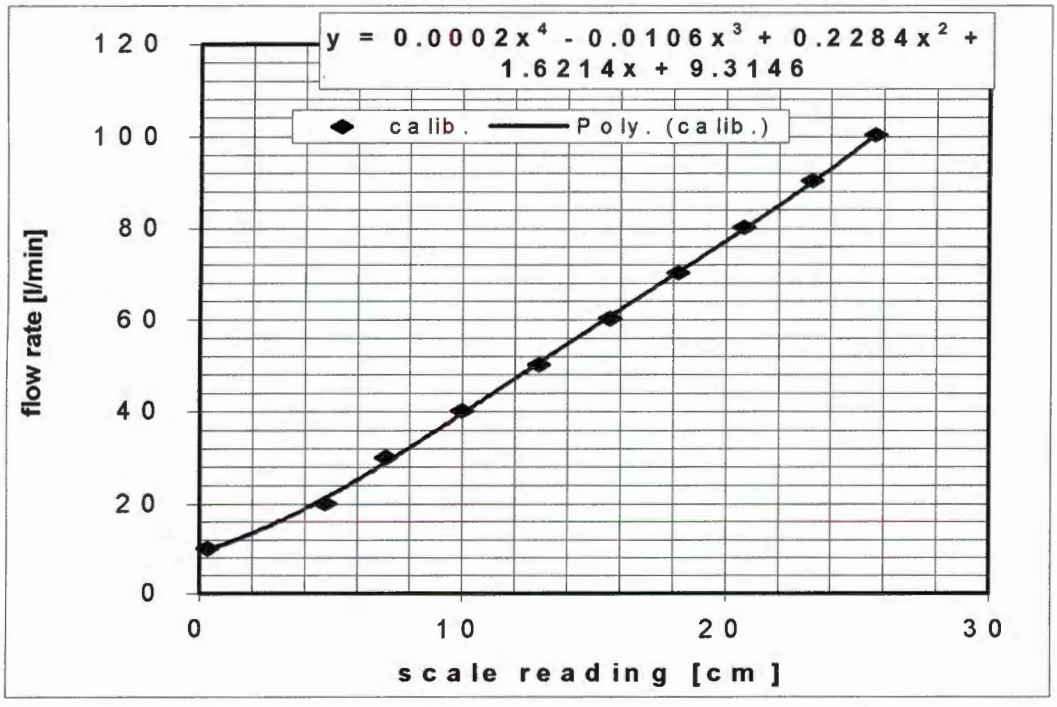

Figure 4-5: calibration chart for rotameter Metric18

The mean velocity calculated from the flow rate did not correspond very well with the maximum velocity measured in the pipe in the first experiments (the maximum velocity should have the double value of the mean velocity for laminar flow). The suspicion that the calibration of the rotameter is not accurate, urges the design of a calibration unit for the rotameter. A large, sealed container is filled with water at different flow rates. The flow rate is established with the volume marks on the outside of the container and a stop watch. The displaced air leaves the container through an opening at the top and is fed into the rotameter.
This new data corresponds well with the original calibration.

Velocity

The air velocity is measured with a hot-film probe manufactured by TSI Inc. This ruggedized metal clad probe has the model number TSI-1266. The principle of operation of this kind of sensor is as follows is that a small resistance element, the film, is heated and then controlled at the elevated temperature. The amount of electrical energy dissipated in the sensor is a measure of the cooling effect of the fluid flowing past the heated sensor. The probe is shown in figure 4-6.

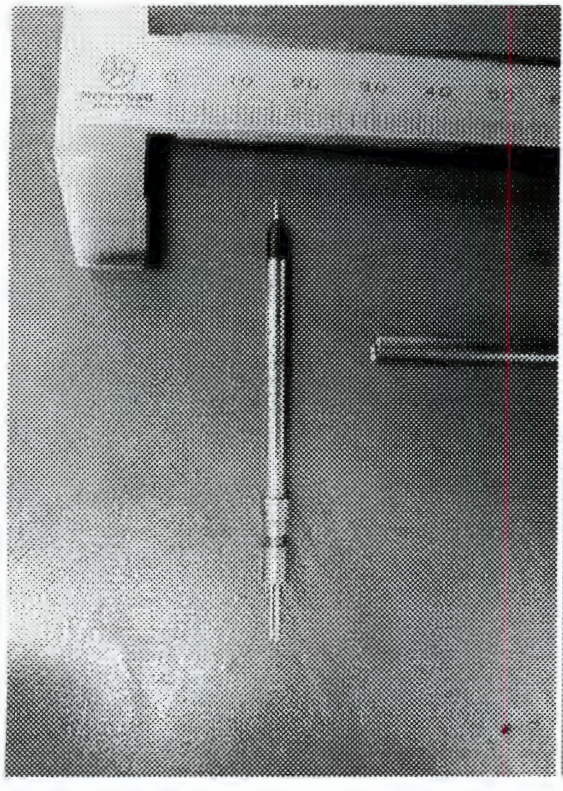

Figure 4-6: hot film probe TSI-1266

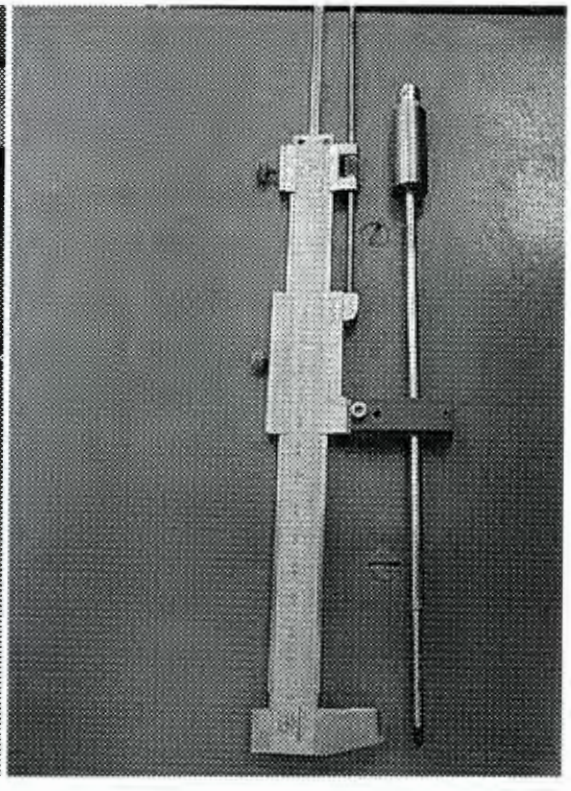

Figure 4-7: support for hot film probe

Support of the hot-film probe

The design of the support for the probe allows easy handling and accurate measuring. The heart of this design is a modified vernier held by PVC-blocks glued onto the outside of the pipe. Nine of these blocks are distributed over the length of the pipe, and holes for the probe are drilled next to the blocks at the desired axial position (see table 4-2). This device allows one to adjust and measure the vertical position of the probe.

Calibration of the hot-film probe

A low-speed wind tunnel is used to generate the reference air flow. This wind tunnel has a settling chamber and an open test section. The ratio of the flow area of the settling chamber to that of the open test section is 10 to 1. To satisfy the law of conservation of mass, the ratio of velocity between settling chamber and open section is 1 to 10.

The velocity is measured with a pitot static tube in the open test section in combination with an inclined manometer. The hot film probe is placed in the settling chamber of the wind tunnel. As the minimum required velocity for the inclined manometer is 1m/s, reference velocities as low as 0.1m/s ~~ca~~ can be ~~adjusted~~ obtained.

The scale reading of the inclined manometer $h_{scale,incl.man.}$ or h, is a function of the velocity v at the pitot static tube, of the static ambient pressure p_{stat}, of the density of the air ρ_{air} and of the density of water ρ_{water}:

$$p_{stat} + \frac{v^2}{2}\rho_{air} = p_{stat} + \rho_{water} g \cdot h_{scale,water} \tag{4-2}$$

$$h_{scale,water} = \alpha_{factor} \cdot h_{scale,incl.man.}$$

$$\Rightarrow v = \sqrt{2 \cdot \alpha_{factor} \cdot h_{scale,incl.man.} \cdot g \cdot \frac{\rho_{water}}{\rho_{air}}}$$

or

$$\Rightarrow h = v^2 \frac{1}{2 \cdot \alpha_{factor} \cdot g \cdot \frac{\rho_{water}}{\rho_{air}}}$$

The required height on the scale is evaluated for every velocity with the ambient temperature, the ambient pressure and the chosen α_{factor}.
The following figure 4-8 shows the final calibration chart as well as the polynomial curve fit of fourth order, used to calculate the velocity from the measured voltage.

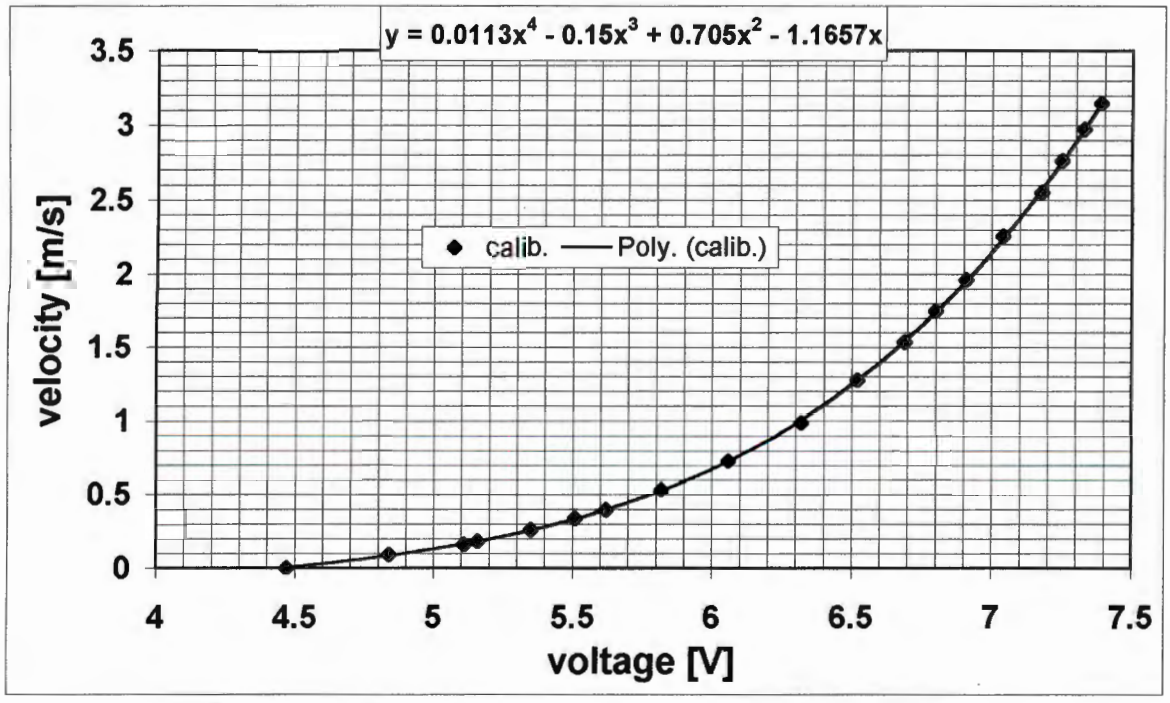

Figure 4-8: calibration chart for hot-film probe TSI 1266

4.2. Experimental Results

The 22 experiments performed are categorised according to their aim. Six experiments are done to improve the design of the test-rig. These can be seen as the final design stage. Three experiments are done to check the performance of the test-rig. One experiment is performed with the so-called reference configuration. Changes in the set-up always refer to this reference case later on. Two experiments are done to evaluate the influence of the roughness of the blockage on the downstream velocity profiles. Two experiments are compared to evaluate the influence of the length of the blockage. Four experiments are done to establish the influence of the diameter of the blockage. Four experiments are done to evaluate the influence of the position of a semi-circular blockage. One final experiment is performed to measure the pressure losses caused by the various blockages.

The flow rate is kept constant for all experiments, except for the six experiments to finalize the design. The fan and the electronic measurement equipment are heated up for at least 20 minutes before beginning each measurement. The dimensions of the blockages are given in dimensionless numbers. The two significant dimensions are the dimensionless length L* and the reduced flow area A*, defined as:

$$L^* = l_{blockage} / d_{pipe} \qquad (4\text{-}3)$$

$$A^* = A_{blockage} / A_{pipe} = d^2_{blockage} / d^2_{pipe}$$

The corresponding figure 4-9 shows a cut through the main pipe and the blockage.

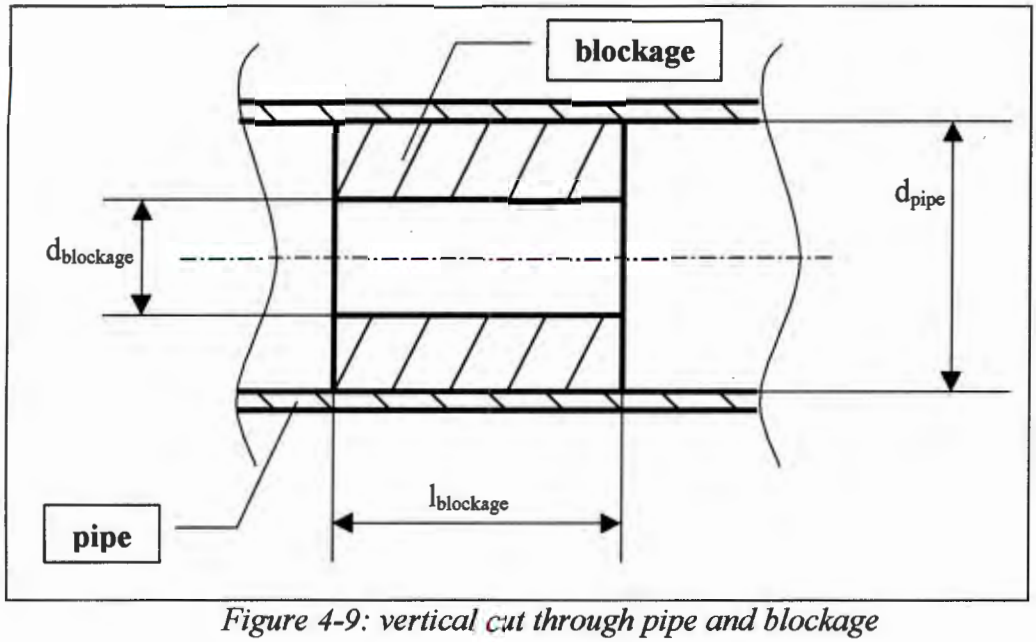

Figure 4-9: vertical cut through pipe and blockage

4.2.1. Final Design

To start with, six experiments without blockages are performed to finalize the design of the experimental set-up. These experiments show that a settling chamber is necessary. Without the settling chamber the flow is decelerated at the entrance of the main pipe. This flow is not stable; the bending of the flexible pipe upstream has a strong influence on the inlet velocity profile so that reproducibility can not be guaranteed.

The settling chamber stagnates the air, and accelerates it into the main pipe again. This flow condition is stable and reproducibility is achieved.

4.2.2. Reference Configuration

In the following, the configuration used in experiment N° 1-1 will be referred to as the standard or reference configuration. No blockage is used, the volume flow rate of 47.4l/min corresponds to a scale reading of 0.12m on the rotameter and the settling chamber and the straightening section are inserted into the system. The mean velocity in the main pipe is w=0.48m/s. The Reynolds-number in the main pipe has the value of Re=1444. This is definitely in the range of laminar pipe flow. There are several notable aspects of the result shown in figure 4-10.

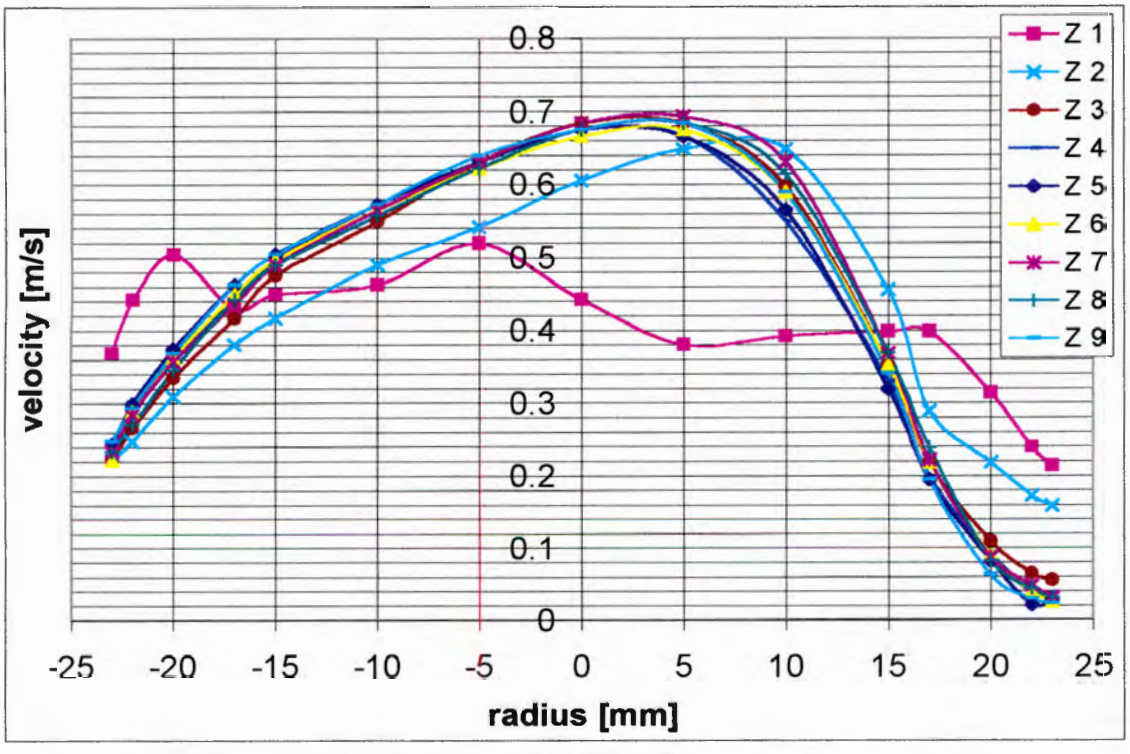

Figure 4-10: velocity profiles for reference configuration

The boundary layer seems to be entirely built up at the third measuring point z3, as the velocity profiles do not change significantly further along the pipe. This is an expected result. Furthermore, the boundary layer is not yet fully developed at the second measuring point z2, 2.5m after the beginning of the pipe. The velocities measured seem however to be too low. The peak velocity in a laminar pipe flow should be double the value of the mean velocity. The mean velocity, calculated from the flow rate, is 0.48m/s while the peak velocity is only about 0.7m/s.

4.2.3. Performance Test

In experiment N° 1-2 the settling chamber is absent. This is the only parameter changed in comparison with the standard configuration. The resulting velocity profiles directly after the straightening section (z1) are compared with those of other experiments with settling chamber (exp.1-1, exp.1-3 to exp.1-6). The corresponding velocity profiles are shown in figure 4-11.

Clearly, the influence of the settling chamber can be seen. It ensures similar inlet flow conditions. The velocity profile at z1 in experiment 1-2 has a different shape without the settling chamber.

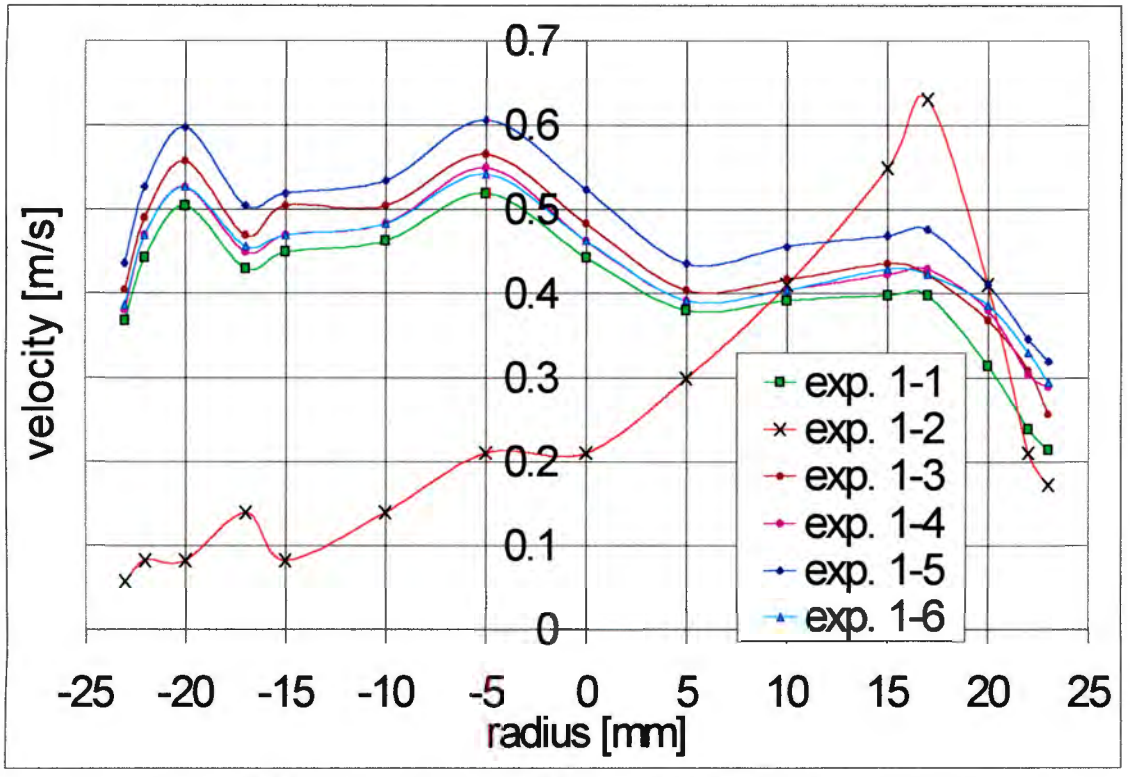

Figure 4-11: inlet velocity profiles (z1) for different experiments; only experiment 1-2 without settling chamber

Two experiments are performed to establish the influence of the velocity probe on the velocity profiles obtained with this probe. The test-section of the pipe is inserted such that the probe is measuring in the horizontal plane (instead of in the vertical plane like in all the other experiments). The axial measuring coordinate is z4, just behind the blockage. One experiment measures the probe insertion from the left, while the other experiment measures the probe insertion from the right side of the pipe. If the probe has no influence on the measured values, the results should be identical. If the probe is the only disturbing influence, the measured values should be symmetrical about the pipe centerline. The comparison of these two velocity profiles at z4 for both experiments is shown in figure 4-12.

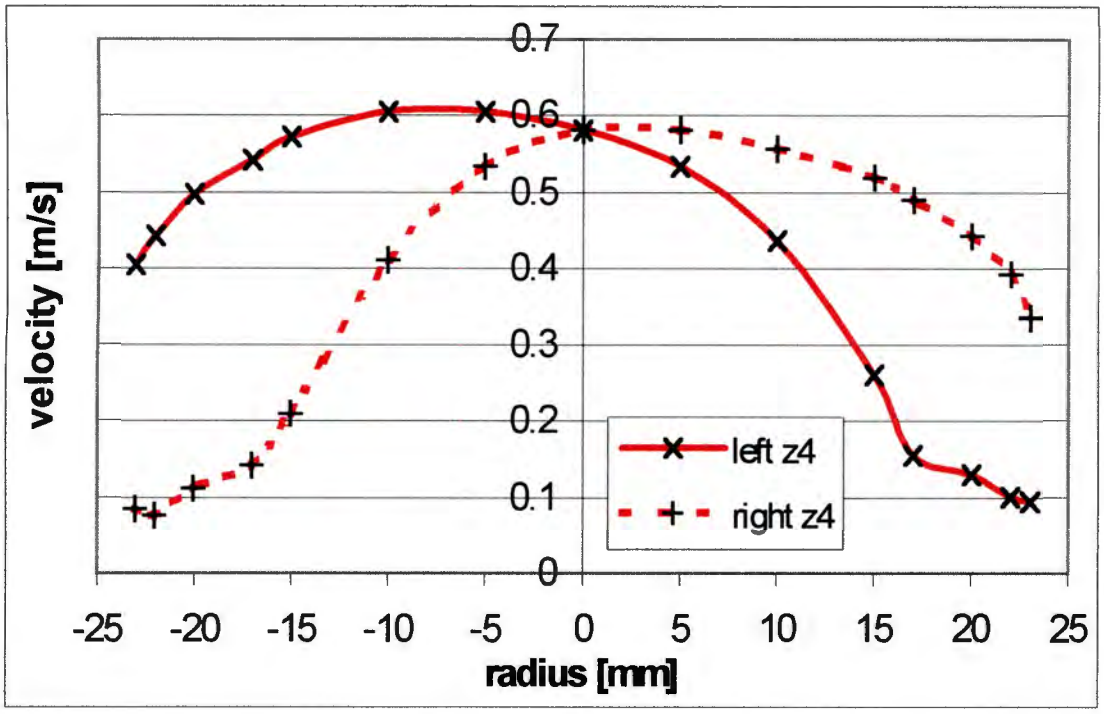

Figure 4-12: influence of the probe on the airflow

The velocity profiles at the test section are almost perfectly symmetrical about the pipe centerline; therefore showing the strong influence the probe has on the airflow.

4.2.4. General Blockage

The influence of a blockage on the velocity profiles at the different axial measurement points is shown with an example. The dimensions of the blockage are L*=0.11 and A*=0.48 (experiment N° 1-3). The mean velocity inside the blockage is calculated to be w=0.99m/s, which corresponds to a Reynolds-number of Re*=2084. This is an interesting case, as a pipe flow would still be laminar at this Reynolds-number. The blockage is made out of PVC. This experiment shows a significant change of the velocity profiles at the measurement locations z4 to z9 compared to experiment 1-1, which is done without a blockage. The velocity fluctuations become strong, especially close to the wall, which indicates a wake, but there is no reliable way to quantify these fluctuations. They are in the range of ±0.1V. The upstream profiles are almost identical to the reference case, which is to be expected.

Close behind the blockage the peak velocity is high and the profile is narrow. Further downstream the profile broadens while the peak velocity decreases. The laminar boundary layer is building up again. The velocity profiles measured behind the blockage are shown in figure 4-13.

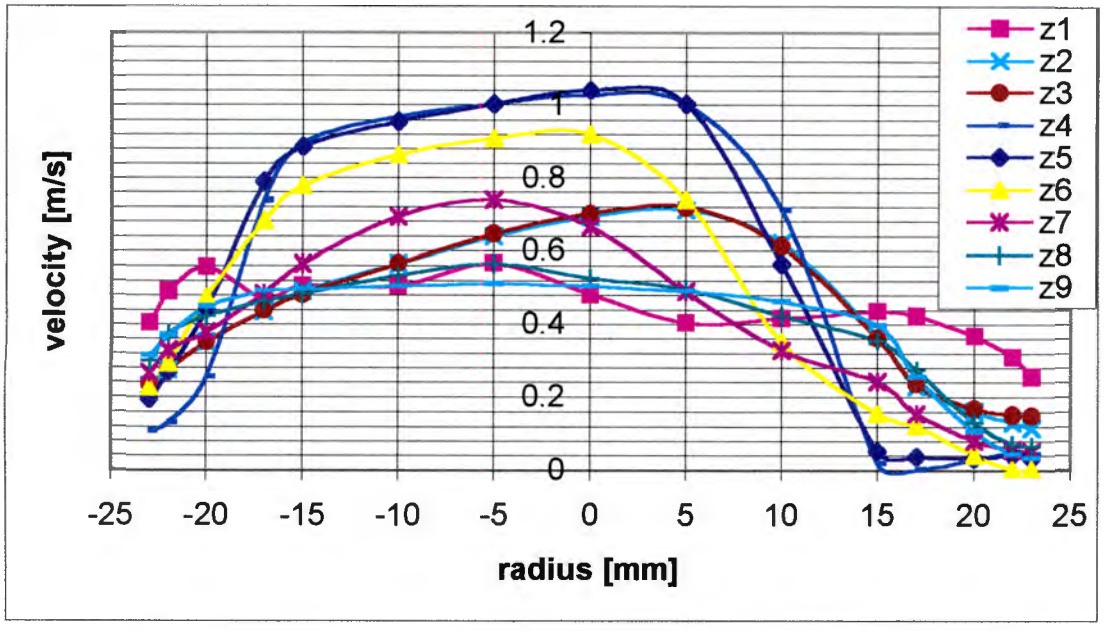

Figure 4-13: velocity profiles with blockage L=0.11, A*=0.48*

4.2.5. Surface Roughness

The influence of the surface roughness of the blockage is investigated with two experiments. Blockages with identical geometry, L*=2 and A*=0.48 are made out of two different materials. One blockage is drilled out of a block of PVC, which gives a very smooth surface (experiment N° 1-4). The other blockage is made out of Prestik, a putty-like material (experiment N° 1-5). The surface of this blockage is rather irregular and uneven. The influence of the material on the velocity profile is observed in figure 4-14.

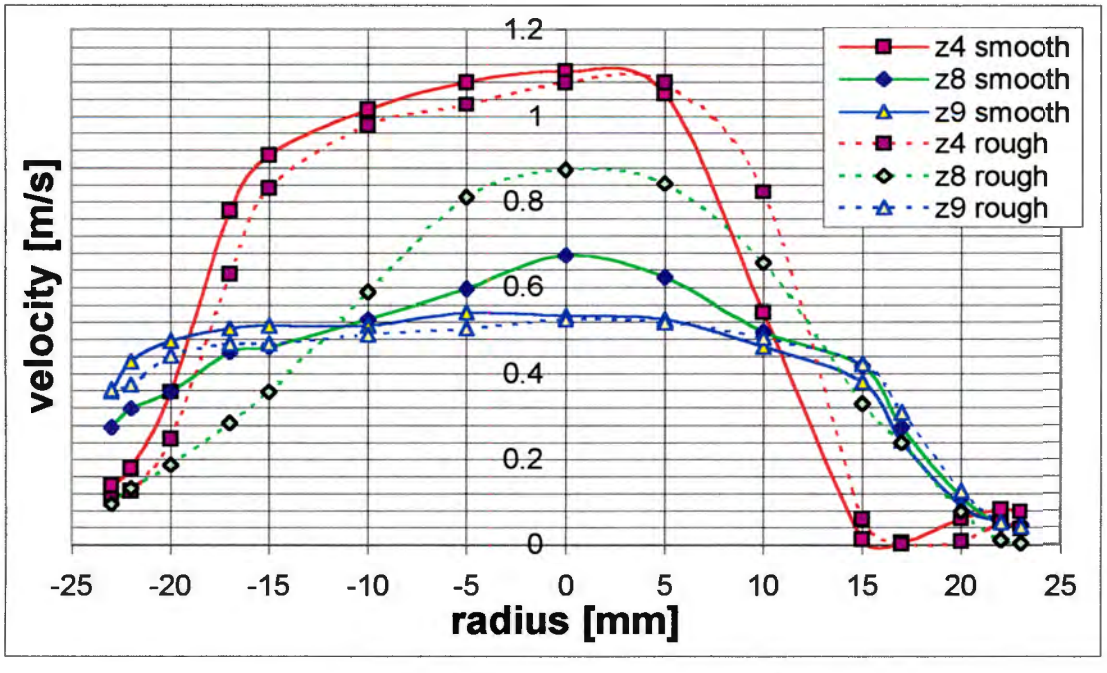

Figure 4-14: influence of surface roughness

This shows the profiles of each experiment directly behind the blockage (z4) and the two profiles furthest downstream (z8, z9). The profiles of the two experiments are almost identical at the measuring points z4 and z9. The profiles at z8 indicate that the flow with the Prestik blockage returns to a laminar flow regime further upstream, as the profile at z8 is fairly close to the one at z9. It is not possible to state if this is due to the material roughness or due to the geometrical accuracy, which is lower for the Prestik blockage.
Overall, the influence of the material is not very strong.

4.2.6. Length of the Blockage

The length of the blockage is expected to have an influence on the downstream flow field. A long blockage might not change the flow regime to a turbulent flow, while a short blockage could produce a turbulent area behind the blockage, before the flow stabilizes and the laminar pipe flow builds up again. Two blockages with different lengths (L*=2 and L*=0.11) and similar reduced flow area (A*=0.48) are compared in figure 4-15.

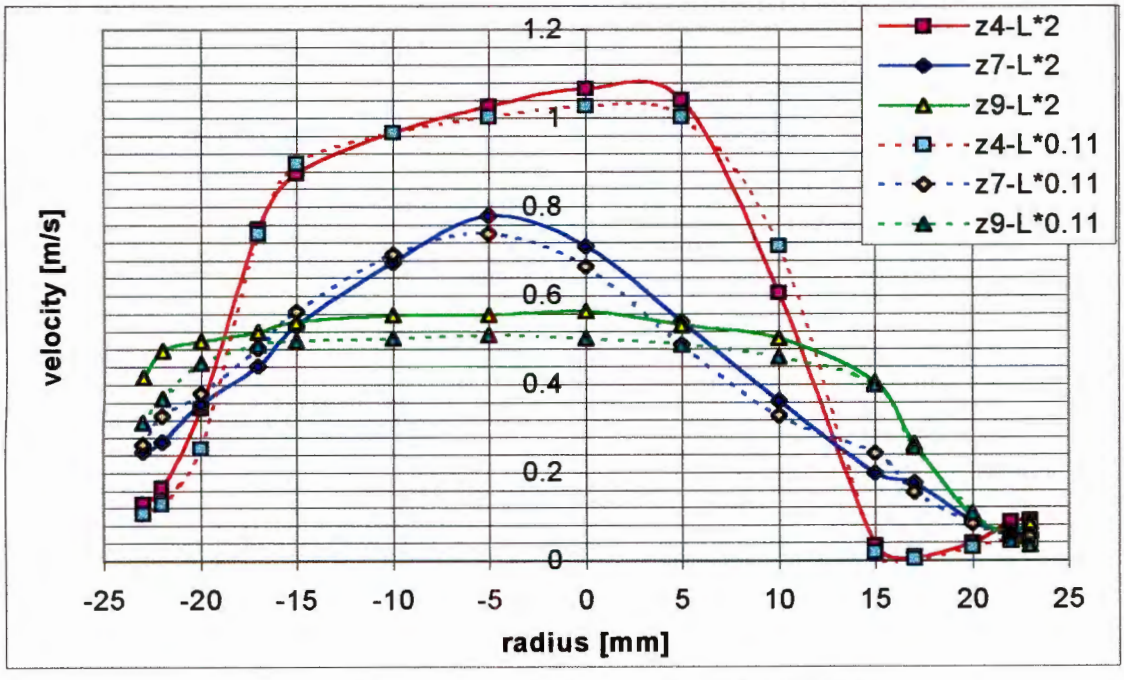

Figure 4-15: influence of the length of the blockage

The differences in the velocity profiles are not huge. The profile for the shorter blockage is slightly wider and has a lower peak velocity.
The difference in length is in the order of one magnitude. The difference in the velocity profiles is only slightly larger than the uncertainty of the results. The length does not seem to have a strong influence on the velocity profiles.

4.2.7. Diameter of the Blockage

Four experiments are aimed at showing the influence of different reduced areas on the velocity field. All the blockages are made out of Prestik and have the dimensionless length L*=1. The reduced areas of the blockages applied in these four experiments are shown in the following brief overview.

Experiment N° 2-1:	A*=0.76	(d*=40mm)
Experiment N° 2-2:	A*=0.48	(d*=32mm)
Experiment N° 2-3:	A*=0.32	(d*=26mm)
Experiment N° 2-4:	A*=0.19	(d*=20mm)

The similarity of the velocity profiles at the first three measuring points z1 to z3 of the different experiments is acceptable to make a comparison of the velocity profiles downstream of the blockages.
These are shown in the following figure 4-16.

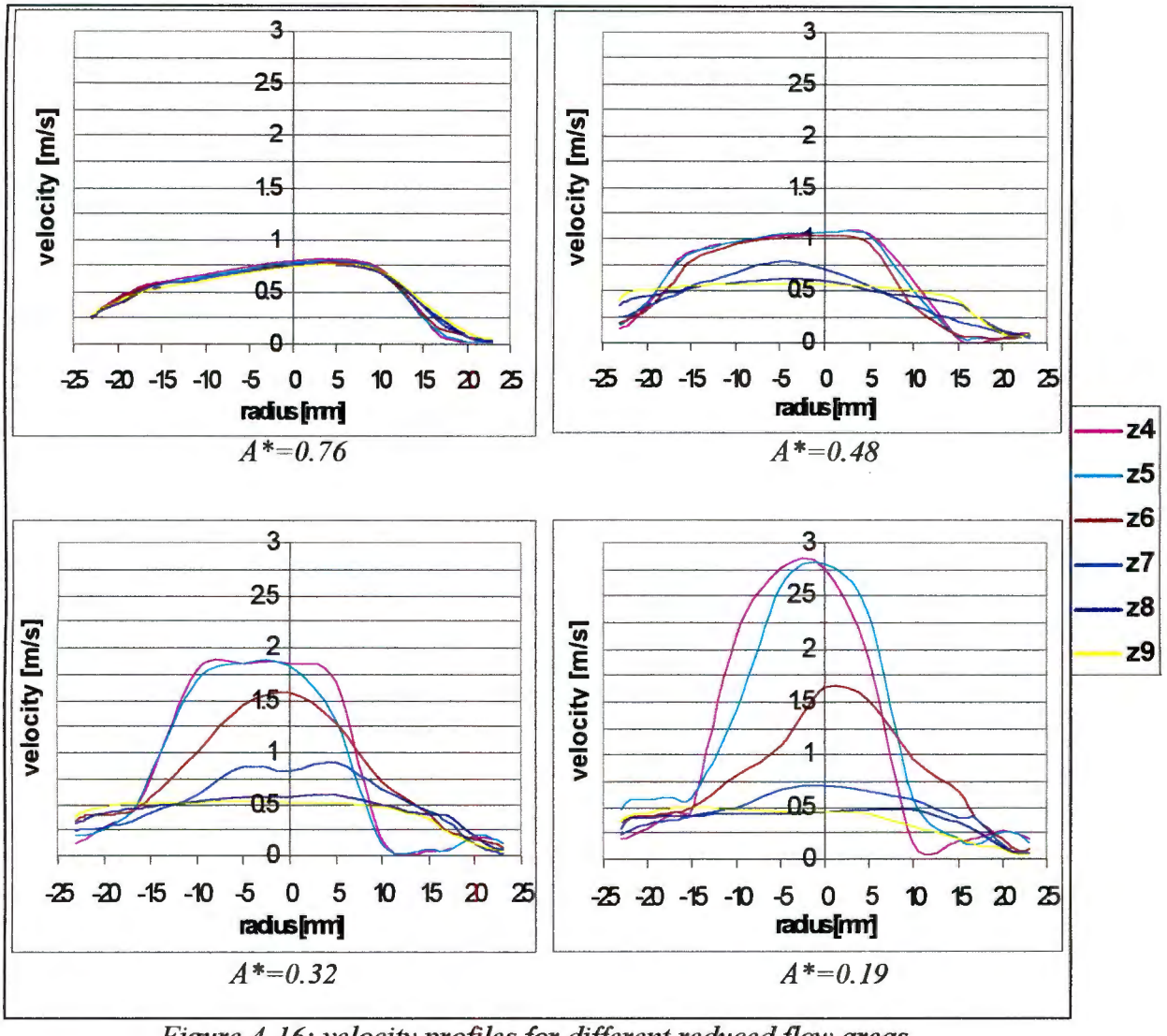

Figure 4-16: velocity profiles for different reduced flow areas

The blockage with A*=0.76 (experiment N° 2-1) has almost no influence on the velocity profiles downstream of the blockage. The mean velocity inside the blockage is 0.63m/s, and the corresponding Reynolds-number inside the blockage is Re*=1661. The peak velocity behind the blockage reaches w=0.81m/s. The fluctuations of the velocity in this case do not exceed those of the reference configuration without blockage.
The reduced flow area in experiment N° 2-2 is A*=0.48. As can be seen in figure 4-16, this reduction does have a notable influence on the velocity profiles. The mean velocity

inside the blockage is calculated to be 0.99m/s, and the corresponding Reynolds-number inside the blockage is Re*=2084. The peak velocity behind the blockage reaches w=1.07m/s. The fluctuations are stronger than in the reference case, up to ±0.15V, while the flow could be laminar or turbulent depending on the Reynolds-number. The fluctuations indicate that the flow is turbulent in certain areas behind the blockage, especially close to the wall.
The reduced flow area in experiment N° 2-3 is A*=0.32. As can be seen in figure 4-16, this reduction has an even stronger influence on the velocity profiles. The mean velocity inside the blockage is calculated to be 1.49m/s, and the corresponding Reynolds-number inside the blockage is Re*=2553. This indicates a turbulent or transitional flow regime. The peak velocity behind the blockage reaches w=1.84m/s. The fluctuations are stronger than in the reference case, up to ±0.15V.
The reduced flow area in experiment N° 2-4 is A*=0.19. As can be seen in figure 4-16, this reduction has an even stronger influence on the velocity profiles. The mean velocity inside the blockage is calculated to be 2.50m/s, and the corresponding Reynolds-number inside the blockage is Re*=3314. This indicates a turbulent flow regime. The peak velocity behind the blockage reaches w=2.8m/s. The fluctuations are stronger than in the reference case, up to ±0.2V.

4.2.8. Position of a Semi-Circular Blockage

Four experiments are performed to evaluate the influence of the position of a semi-circular blockage with the characteristic dimensions L*=1 and A*=0.5. The blockage is moved to the four general positions DOWN, UP, RIGHT and at 90° to each other in the four experiments. Position DOWN is shown, as an example, in figure 4-17.

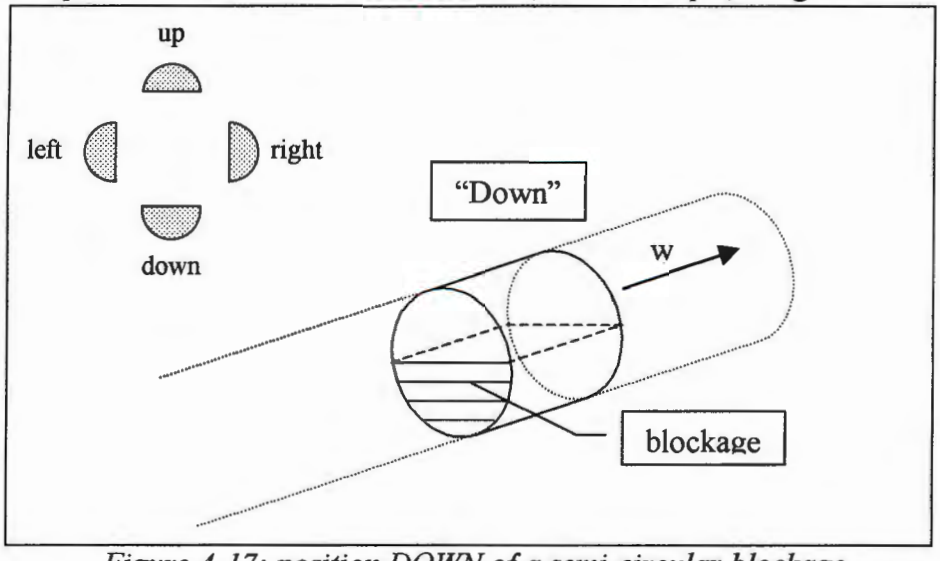

Figure 4-17: position DOWN of a semi-circular blockage

Ideally, the velocity profiles for the position DOWN and UP should be symmetrical about the pipe axis and the profiles for the positions LEFT and RIGHT should be identical. The results are shown in figure 4-18.
The symmetry of the airflow is achieved in the positions UP and DOWN, however the velocity distributions for the two configurations LEFT and RIGHT are not similar. The first measurement point behind the blockage, at z4, is particularly different. The following measurement points show better agreement, up to z9, where the velocity profiles are almost identical again. The question, whether this deviation from the

expected result is caused by asymmetrical flow or by errors in the geometry of the pipe or the blockage remains open.

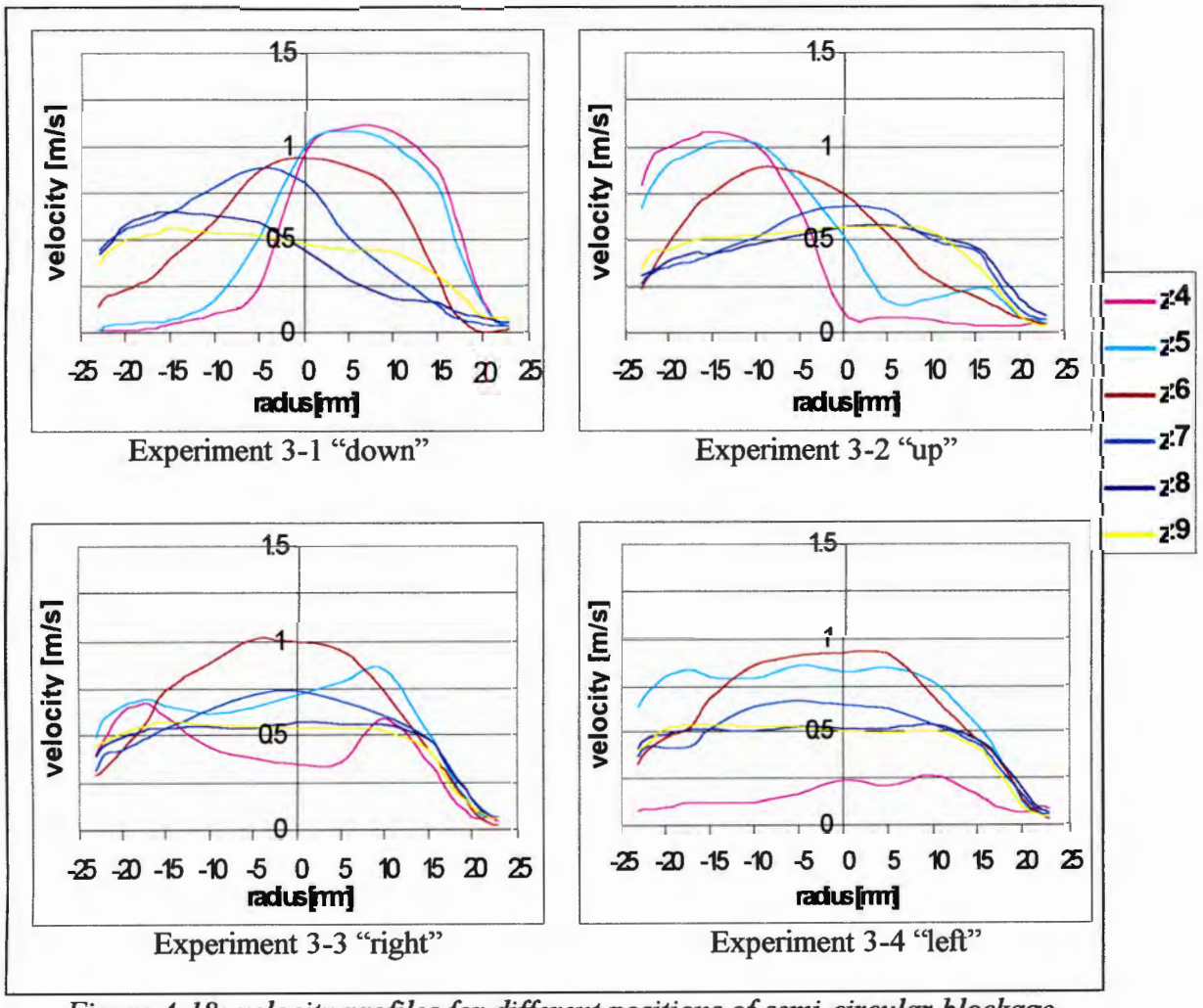

Figure 4-18: velocity profiles for different positions of semi-circular blockage

4.2.9. Pressure Loss

In the last experiment the pressure loss caused by the various blockages is measured. This experiment has the main purpose to deliver another parameter to be compared with the results of the numerical simulation.

The three pressure tappings at the pipe, p1 just after the straightening section, p2 before the test section and p3 just before the end of the pipe are used to measure the pressure change from the ambient pressure with the different blockages. The pressure loss between p1 and p2 should be similar for every blockage. The pressure loss over the blockage, between p2 and p3, should increase with decreasing A*.

The following table 4-3 shows the numerical data for the pressure loss.

Blockage type	Pressure loss pipe, p1-p2 [Pa]	Pressure loss blockage, p2-p3 [Pa]
No blockage	0.61	0.08
Wood	0.6	0.37
Smooth PVC L*=2, A*=0.48	0.61	0.31
Ring L*=0.11, A*=0.76	0.61	0.1
Ring L*=0.11, A*=0.48	0.61	0.3
Ring L*=0.11, A*=0.32	0.63	1.04
Ring L*=0.11, A*=0.19	0.62	3.89
Prestik L*=1, A*=0.76	0.63	0.1
Prestik L*=1, A*=0.19	0.64	3.74

Table 4-3: pressure loss for different blockages

The pressure loss across the blockage is shown as a function of A* in figure 4-19.

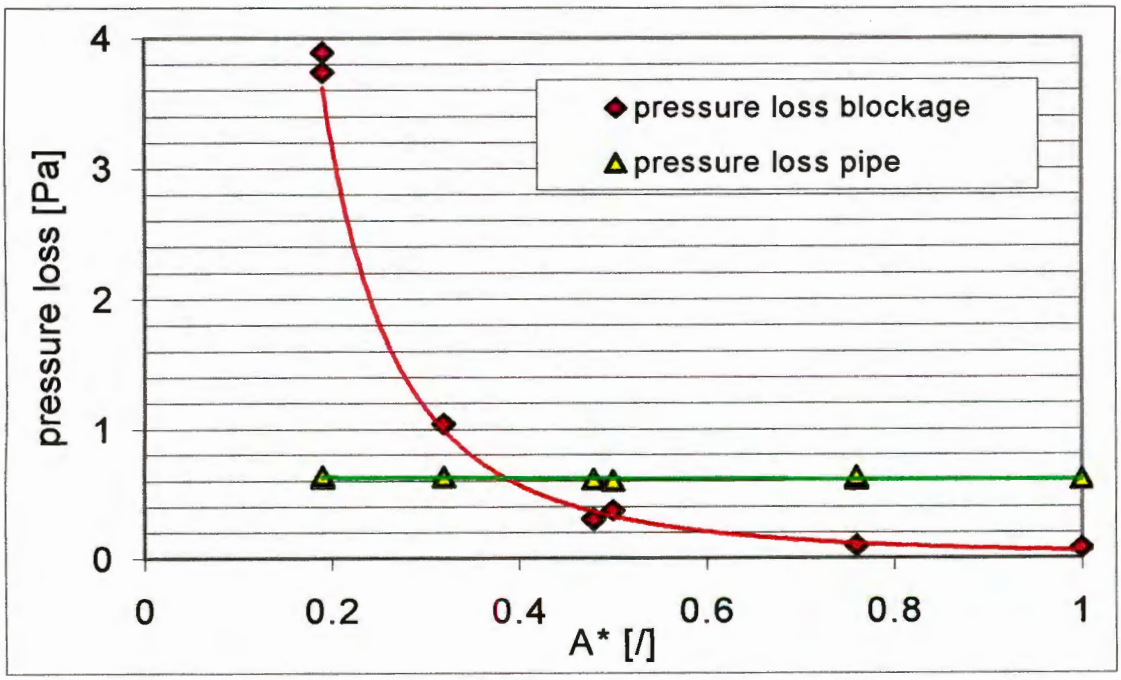

Figure 4-19: pressure loss as function of A (approximation with power series)*

The results correspond to those expected. The pressure loss in the pipe is similar for the different grades of blockages. The pressure loss over the blockage increases with decreasing A*.

4.3. Errors and Uncertainty

The results obtained with the experimental test-rig only gain value with the knowledge about the accuracy. The errors in the test-rig, in the measurement equipment and in the measurement procedure are analysed to gain this knowledge.

4.3.1. Test-rig

The performance of the entire system is checked with several experiments on the reproducibility and the ability to produce a homogeneous laminar air flow in the test section. The reproducibility is high, but the measured flow field does not entirely correspond to the laminar profile expected in section 3.2. This is believed to be largely caused by the errors made in the measurements.

4.3.2. Hot film probe

The hot film probe is believed to have significant influence on the flow. The measured velocity is not zero at the bottom side of the pipe. This could be due to the measurement principle of the hot film probe. The heat transfer could be influenced by the proximity of the wall. The offset of the peak velocity from the centre line of the pipe is caused by the probe, as can be seen from experiments 1-7 and 1-8. The value of the maximum relative decrease of the flow area due to the inserted probe is in the range of 12%.

The calibration-procedure of the hot film probe is another source of errors. The inaccuracy due to reading the scale of the inclined manometer and thus adjusting the air velocity, is estimated to be at least 0.5mm. This is equivalent to a velocity of 0.2m/s for the smallest inclination angle and 0.6m/s for the largest. The relative error decreases for higher velocities since the velocity is proportional to the square root of the scale reading. To eliminate this error, as well as the influence of the ambient conditions, the whole procedure of calibration was repeated 20 times. These twenty calibrations were made on two different days with slightly different ambient conditions. The average data is taken to draw the final calibration chart.

In all the experiments the peak velocity is lower than expected from the theoretical considerations. This is also caused by the presence of the probe. The probe is calibrated in the wind tunnel, a highly turbulent environment, but the measurement is largely done in laminar flow. As the TSI-1266 probe is larger than practically any other sensor, it is slower to respond to flow changes. As such, turbulent flows tend to have a higher average cooling effect than laminar flows of the same basic velocity. In other words: the heat transfer in a turbulent flow is a lot better than the heat transfer in laminar flow. The discrepancy between expected and obtained peak velocity may be caused by this fact.

To summarise, the hot film probe is a serious source of uncertainty for the experiments. Some aspects of the uncertainty can be quantified. The decrease of the flow area theoretically causes a proportional increase in the mean velocity of up to 12% at the bottom of the pipe. The uncertainty in the calibration due to reading of the inclined manometer should be eliminated by the repeated calibration procedure. The greatest uncertainty due to the calibration in a turbulent flow is very difficult to quantify. It is assumed to be the cause for the discrepancy between expected and real peak- (and therefore also mean-) velocity.

4.3.3. Rotameter

The accuracy of the volume flow rate determined with the rotameter depends on three factors.

The first is the accuracy of the calibration. This was checked in two ways which confirmed the accuracy of the data given by the manufacturer, even though the rotameter is quite old. The limiting factor in the calibration is the reading from the manufacture's graphs in [4]. The error is estimated to be approximately ±1mm of scale reading which corresponds to a maximum flow rate variation of ±0.4l/min.

The second factor is the reading from the scale of the rotameter, which can be done with an estimated accuracy of ±1mm, which again corresponds to a maximum deviation of ±0.4l/min.

The third factor is the error in the approximation of the calibration curve with a polynomial fourth order. The error is estimated to smaller than ±1l/min.

This sums to an uncertainty in the volume flow rate of ±1.8l/min, which corresponds to an uncertainty in the mean velocity of ±0.018m/s. This is considered sufficiently accurate.

4.3.4. Further Error Sources

Further errors are caused by the uncertainty of the location of the measuring point. The accuracy in axial direction is estimated to be around ±1mm and the accuracy in radial direction is estimated to be around ±0.1mm. In the worst case of high velocity gradients, these correspond to an uncertainty in the velocity of ±0.2m/s (one order of magnitude higher than the uncertainty caused by the rotameter). This is still considered accurate.

The errors in the test-rig are considerably small except for two. One is the decrease of the flow area that causes an increase of the mean velocity of up to 12% for a fully inserted hot film probe. The other is the decrease of velocity due to calibration in a turbulent flow while measuring in a laminar flow. This error, which is assumed to be significant, can not be quantified, as no calibration in a laminar environment can be made.

5. Numerical Modeling

5.1. Theory

This section explains the procedure of the numerical simulation of flows. This is done with respect to the given fluid and flow conditions in this work, as well as to the specific methods applied in the software that is employed. A more general description can be found in the related literature [25].

The physical aspects of any fluid flow are governed by three fundamental principles:

- Mass is conserved
- Momentum is conserved
- Energy is conserved

These basic principles are expressed in the form of mathematical equations, known as the Navier-Stokes equations NSE. This set of equations can only be solved analytically in very small number of special cases. Therefore, numerical methods are used to approximate the exact results of the NSE.

The Navier Stokes equations are expressed in various mathematical formulations. The most general case, written in the conservation form is shown in (5-1).

$$\frac{\partial \underline{U}}{\partial t} + \frac{\partial \left(\underline{F} - \underline{F}^d\right)}{\partial x_1} + \frac{\partial \left(\underline{G} - \underline{G}^d\right)}{\partial x_2} + \frac{\partial \left(\underline{H} - \underline{H}^d\right)}{\partial x_3} = \underline{f} \tag{5-1}$$

With:

- the vector of the conservation variables: $\underline{U} = \left(\rho, \rho u, \rho v, \rho w, \rho E\right)^T$
- the convective flux in x_1: $\underline{F} = \left(\rho u, \rho u^2 + p, \rho uv, \rho uw, \rho uH\right)^T$

  x_2: $\underline{G} = \left(\rho v, \rho v^2 + p, \rho vu, \rho vw, \rho vH\right)^T$

  x_3: $\underline{H} = \left(\rho w, \rho w^2 + p, \rho wu, \rho wv, \rho wH\right)^T$
- the diffusive flux in x_1: $\underline{F}^d = \left(0, \tau_{11}, \tau_{21}, \tau_{31}, \sum_{k=1}^{3} u_k \tau_{k1} - q_1\right)^T$

  x_2: $\underline{G}^d = \left(0, \tau_{12}, \tau_{22}, \tau_{32}, \sum_{k=1}^{3} u_k \tau_{k2} - q_2\right)^T$

  x_3: $\underline{H}^d = \left(0, \tau_{13}, \tau_{23}, \tau_{33}, \sum_{k=1}^{3} u_k \tau_{k3} - q_3\right)^T$

This general and complex formulation simplifies with the following assumptions:

- Steady state flow $\frac{\partial}{\partial t} = 0$
- Newtonian fluid $\underline{\underline{\tau}} = \mu\left(\nabla \underline{v} + (\nabla \underline{v})^T\right) - \frac{2}{3}\mu \cdot div\underline{v}\,\underline{\underline{I}}$

  $\mu = const.$
- Incompressible fluid $\rho = const.$
- No heat transfer $\underline{q} = 0$
- No external volume-forces (gravitational force is neglected) $\underline{f} = 0$
- Cylindrical coordinate system (r,θ,z)

The Navier Stokes Equations can then be expressed as an set of elliptic partial differential equations:

- r-direction:

$$\rho\left(v_r\frac{\partial v_r}{\partial r} + \frac{v_\theta}{r}\frac{\partial v_r}{\partial \theta} - \frac{v_\theta^2}{r} + v_z\frac{\partial v_r}{\partial z}\right) = -\frac{\partial p}{\partial r} + \mu\left(\frac{\partial}{\partial r}\left(\frac{1}{r}\frac{\partial}{\partial r}(rv_r)\right) + \frac{1}{r^2}\frac{\partial^2 v_r}{\partial \theta^2} - \frac{2}{r^2}\frac{\partial v_\theta}{\partial \theta} + \frac{\partial^2 v_r}{\partial z^2}\right)$$

- θ-direction:

$$\rho\left(v_r\frac{\partial v_\theta}{\partial r} + \frac{v_\theta}{r}\frac{\partial v_\theta}{\partial \theta} + \frac{v_r v_\theta}{r} + v_z\frac{\partial v_\theta}{\partial z}\right) = -\frac{1}{r}\frac{\partial p}{\partial \theta} + \mu\left(\frac{\partial}{\partial r}\left(\frac{1}{r}\frac{\partial}{\partial r}(rv_\theta)\right) + \frac{1}{r^2}\frac{\partial^2 v_\theta}{\partial \theta^2} + \frac{2}{r^2}\frac{\partial v_r}{\partial \theta} + \frac{\partial^2 v_\theta}{\partial z^2}\right)$$

- z-direction:

$$\rho\left(v_r\frac{\partial v_z}{\partial r} + \frac{v_\theta}{r}\frac{\partial v_z}{\partial \theta} + v_z\frac{\partial v_z}{\partial z}\right) = -\frac{\partial p}{\partial z} + \mu\left(\frac{1}{r}\frac{\partial}{\partial r}\left(r\frac{\partial v_z}{\partial r}\right) + \frac{1}{r^2}\frac{\partial^2 v_z}{\partial \theta^2} + \frac{\partial^2 v_z}{\partial z^2}\right)$$

- conservation of mass:

$$\frac{1}{r}\frac{\partial}{\partial r}(rv_r) + \frac{1}{r}\frac{\partial v_\theta}{\partial \theta} + \frac{\partial v_z}{\partial z} = 0$$

(5-2)

This expression can be written in a more compact form by using mathematical terms from vector analysis. The momentum equation can be written for any coordinate x_i as follows:

$$\rho \cdot div(v_i \cdot \underline{v}) = -\frac{\partial p}{\partial x_i} + \mu \cdot \Delta v_i$$

And the conservation of mass:

$$div(\underline{v}) = 0$$

(5-3)

The numerical method applied in this thesis is a finite volume method. The key step is the integration of the equations over a three dimensional control volume CV.

$$\rho \int_{CV} div(v_i \underline{v}) dV = -\int_{CV} \frac{\partial p}{\partial x_i} dV + \mu \int_{CV} div \cdot grad(v_i) dV \tag{5-4}$$

With Gauss' divergence theorem one obtains integrals over the entire bounding surface A of the control volume:

$$\rho \int_{A} \underline{n} \cdot (v_i \underline{v}) dA = \mu \int_{A} n \cdot grad(v_i) dA - \int_{CV} \frac{\partial p}{\partial x_i} dV \tag{5-5}$$

where $\underline{n}$ is the vector normal to the bounding surface element dA.

The left hand term is the net rate of decrease of the velocity component v_i of the volume due to convection. The first right hand side term is the net rate of increase of the velocity component v_i due to diffusion. The second right hand term is the rate of the increase of the velocity component v_i as a result of pressure gradients inside the element CV.

The equations, which describe the exact physical reality in the entire flow domain, cannot be solved analytically. Therefore, the flow problem is defined in a discrete formulation. The flow domain is subdivided into discrete control volumes that form the basic building blocks of a computational grid or mesh. Two basic cell shapes are available, namely hexahedra and triangular prisms. There are different mesh structures: a *regular mesh* arises from one-to-one correspondence between adjacent faces of neighbouring cells; a *structured mesh* is a regular mesh which has a structured vertex and cell-numbering character, i.e. there is a specific pattern in the numbering system. An *unstructured mesh* is a regular mesh which has no clearly identifiable numbering structure for vertices and cells.

The governing equations are approximated with a differencing scheme. There are numerous differencing schemes, each one with certain qualities and disadvantages. To give a simple example for a differencing scheme, the following one-dimensional convection and diffusion problem is treated:

$$\rho \frac{\partial}{\partial x}(u \cdot \phi) = \Gamma \frac{\partial^2 \phi}{\partial x^2}$$
$$\frac{\partial(\rho \cdot u)}{\partial x} = 0 \tag{5-6}$$

where u is the velocity of the flow field, ϕ is a general flow variable and Γ is the diffusion coefficient. This problem is applied to the one-dimensional discretized flow area, shown in figure 5-1.

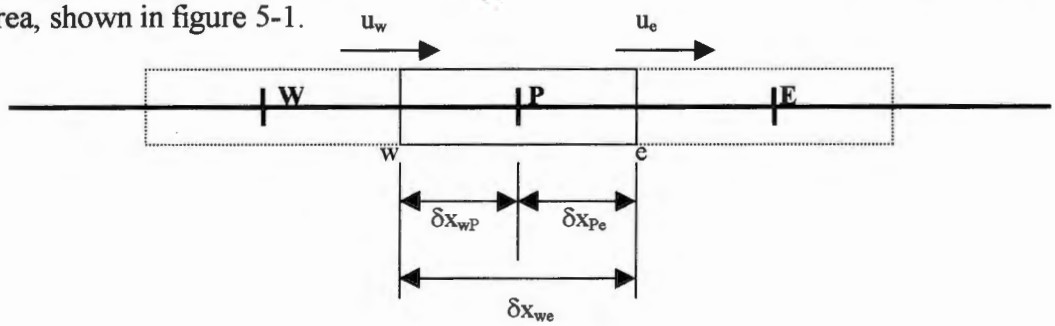

Figure 5-1: 1-D finite volume discretization of flow area

The attention is focused on the centre of the control volume, the node **P**. The neighbouring nodes are identified by **W** and **E** and the control volume faces are identified by w and e.
Integration of equations (5-6) over the control volume gives:

$$\begin{cases} F_e\phi_e - F_w\phi_w = D_e(\phi_E - \phi_P) - D_w(\phi_P - \phi_W) \\ F_e - F_w = 0 \end{cases} \tag{5-7}$$

where $F_w = (\rho \cdot u)_w$

$F_e = (\rho \cdot u)_e$

$D_w = \dfrac{\Gamma}{\delta x_{WP}}$

$D_e = \dfrac{\Gamma}{\delta x_{PE}}$

In the central difference scheme, the cell face values of the property ϕ are approximated with:

$$\begin{aligned} \phi_e &= (\phi_P + \phi_E)/2 \\ \phi_w &= (\phi_W + \phi_P)/2 \end{aligned} \tag{5-8}$$

This approximation, substituted into equation (5-7) yields

$$a_P\phi_P = a_W\phi_W + a_E\phi_E \tag{5-9}$$

where $a_W = D_w + \dfrac{F_w}{2}$

$a_E = D_e - \dfrac{F_e}{2}$

$a_P = a_W + a_E + (F_e - F_w)$

Equation (5-9) applied to all nodes leads to a set of algebraic equations that can be written in Matrix form:

$$\begin{bmatrix} \ddots & \ddots & & & \\ \ddots & a_P & a_E & 0 & \\ & a_W & a_P & a_E & \\ & 0 & a_W & a_P & \ddots \\ & & & \ddots & \ddots \end{bmatrix} \begin{bmatrix} \vdots \\ \phi_W \\ \phi_P \\ \phi_E \\ \vdots \end{bmatrix} = \begin{bmatrix} \vdots \\ 0 \\ 0 \\ 0 \\ \vdots \end{bmatrix} \tag{5-10}$$

It should be noted that the boundary conditions still have to be considered in the formulation of this system.
This system of algebraic equations becomes very large for three dimensions and several flow variables. These systems are solved with iterative algorithms. There is a wide variety of algorithms, often created for a specific type of problem. A commonly used algorithm for steady flows is the Sem-Implicit Method for Pressure-Linked Equations SIMPLE. This algorithm enables the solution of the discretized system of the originally used equations (5-3), shown again for convenience.

3 momentum equations (in the 3 dimensions i): $\rho \cdot div(v_i \cdot \underline{v}) = -\dfrac{\partial p}{\partial x_i} + \mu \cdot \Delta v_i$

continuity equation: $div(\underline{v}) = 0$ (5-3)

This system presents two main problems: the non-linear terms on the left hand side of the momentum equations and the coupling of all four equations. The most complex issue is the role of the pressure. It appears in all of the momentum equations but there is evidently no equation for it. The link between pressure and velocity introduces a constraint on the solution of the flow field: if the correct pressure field is applied in the momentum equations, the resulting velocity field should satisfy continuity.
To initiate the SIMPLE algorithm a pressure field over the computational grid is estimated. The discretised momentum equations are solved using the estimated pressure field to yield the three velocity components. The result is a velocity field based on the estimated pressure. This flow field and the continuity equation enable the calculation of a pressure correction field, the difference between the estimated pressure field and the correct pressure field required to fulfil continuity. Velocity corrections are calculated using the pressure correction. The original pressure and velocity components are adjusted with an under-relaxation to ensure stability. Now the convergence is checked. If the convergence level is not reached, the algorithm starts again with the new pressure field.

5.2. Software

5.2.1. General Information

The software used for the numerical simulation is a commercial software package, called FLO++, version 2.30. This Computational Fluid Dynamics CFD program is developed, distributed and supported by SOFTFLO cc, a South African company. FLO++ is a finite volume computational fluid dynamics program for the solution of fluid flow and heat transfer problems. It solves the basic conservation equations of fluid dynamics and produces results in the form of pressures, temperatures and other flow variables.
The most important capabilities of FLO++, as stated by the ~~producer~~ manufacturer, are shown in a brief overview:

- Incompressible to highly compressible transonic flows
- Laminar and turbulent flows
- Steady and unsteady flow
- Convection and conduction heat transfer; also combined fluid-solid heat transfer.
- Multiple fluid streams
- Mixtures of gases or liquids containing different individual chemical species
- Thermal buoyancy
- Dispersed multiphase flow model

5.2.2. Hardware

The software runs on a Personal Computer PC with the operating system Windows NT. The PC is equipped with a PentiumII 233MHz Processor and with 64MB RAM.

5.2.3. Procedure

A typical numerical simulation with a commercial CFD package consists of three parts, the pre-processing, the solving and the post processing.
The *pre-processing* includes several steps. The first step is the definition of the geometry of the flow domain. It is then subdivided into a number of cells, to form the basic building blocks of a computational grid or mesh. To achieve good numerical behaviour of the grid several aspects should be ~~regarded~~ considered. The inner angles of the (hexahedra) cells should be close to 90°, the ratio of the different faces should be close

to the value of 1, as should the ratio of the volume of neighbouring cells.
After the grid generation the conditions at all boundaries of the grid must be defined.
The next step is to specify the properties of the fluid flowing through the domain. Further, the parameters for the solving procedure must be specified. The two main parameters which are used to control the iterative solution are the number of iterations to perform and the overall convergence level. The pre-processing is the most work-intensive part.
The *solving* process is mainly done by the computer, the implemented numerical code is solving the CFD problem. If the error level in the solution decreases below the overall convergence level the solution stops, else it completes the number of specified global iterations. During each global iteration a system of linear algebraic equations is solved for each flow variable involved, e.g. U-, V-, W-velocities, pressure, temperature, turbulence, etc. The solution of each individual system involves a series of inner iterations called sweeps. Other parameters involved are global convergency, relaxation and residual values. The following framework shows the solution process, and the roles of the different parameters.

```
Global iterations
        Solution of U-velocity:
                Relaxation applied
                Decrement in residuals for stopping solution
                otherwise stop when Inner iterations (sweeps) to solve U-velocity are completed

        Solution of V-velocity:
                Relaxation applied
                Decrement in residuals for stopping solution
                otherwise stop when Inner iterations to solve V-velocity are completed

        Solution of W-velocity:
                Relaxation applied
                Decrement in residuals for stopping solution
                otherwise stop when Inner iterations to solve W-velocity are completed

        Solution of ...
        .
        .
        .
Check global convergency;
stop if convergence criteria are met;
otherwise stop when global iterations are completed
```

Figure 5-2: general solution process

The results for every cell are written into a result file periodically.
The *Post-processing* involves manipulation of the huge amount of numerical values obtained during the solution stage, into forms which are easy to interpret. These include colour contour plots displaying variations in flow field scalar variables, and vector plots indicating the direction and magnitude of velocity vectors. Any of the calculated parameters like velocity, pressure, temperature, concentration, density, viscosity, specific heat or turbulent kinetic energy can be used for the coloured plots. Results are printed to file or displayed on arbitrary planes intersecting the geometry.

5.2.4. Boundary Conditions

- The *Inlet* boundary condition: this boundary condition is where the mass flux over the boundary is known, and therefore the flow defined at an inlet boundary may be entering or leaving the geometry. If the flow is inwardly directed at the Inlet boundary, then an outlet, inlet or a pressure boundary may be used as the "outlet", if the flow is outwardly directed at the inlet boundary, then another inlet or pressure boundary can be used as the "inlet" boundary.
- The *outlet* boundary condition: at this boundary all flow must be outwardly directed. Zero-gradients for velocity components are imposed, while other variables are extrapolated. Inwardly directed velocity components are set to zero. If recirculation occurs over the outflow boundary, a pressure boundary could be used instead. Otherwise the mesh at the outlet should be extended to yield a physical situation where zero gradients of velocity truly exist. In the case of multiple outlets, all outlets must either be of type outlet, or all must be pressure boundaries.
- The *wall* boundary condition: The velocity of the fluid relative to the wall is always zero.
- The *pressure* boundary condition: a pressure boundary is where the pressure distribution is known, and therefore the flow may be entering or leaving the geometry at a pressure boundary.
- The *symmetry* boundary condition: a symmetrical flow field is imposed and the symmetry plane is defined in this symmetry boundary condition.
- The *cyclic* boundary condition: this boundary condition imposes a repeatable or periodic flow condition at a pair of geometrically identical boundaries. Cyclic boundaries are defined in pairs.

5.2.5. Discretization Schemes

FLO++ offers several interpolation schemes for the discretization of the partial differential equations over the computational grid:

- Upwind or Donor differencing (UD)
  The value at the surface is approximated with the upstream cell's value of the surface. This widely used first order scheme is bounded and the implicit implementation is very stable. However, it introduces large amounts of numerical diffusion.
- Central differencing (CD)
  The value at the surface is approximated with linear interpolation between the cells bracketing the surface of the control volume. This second order accurate scheme introduces unboundedness and can be unstable. In order to preserve both boundedness and the accuracy of the solution a linear weighting (k) between upwind differencing and central differencing is introduced.
- Gamma scheme
  The gamma scheme is a bounded central differencing scheme based on the normalised variable diagram of Leonard (1991). This high resolution scheme uses central differencing when the function is monotonic and switches gradually to upwind differencing based on a factor k. The default is k=0.1 with a possible range k=0.1 to 0.5 - the higher the value of k, the more diffusive the scheme will be. For small values of k the scheme may be unstable under certain conditions.

- Second order upwind differencing (SOUD)
  The value at the surface is approximated with extrapolation by using the gradient over the surface bracketing the donor cell and the upstream cell of the donor cell. This scheme is unbounded and not as unstable as CD. A linear weighting (k) between SOUD and UD is introduced in the same manner as described for CD. SOUD is represented with k=0 and UD with k=1.
- Quadratic upwind interpolation (QUICK)
  The face value is approximated with quadratic interpolation, using the donor cell, acceptor cell and the upwind cell of the donor cell. The degree of unboundedness is not as severe as in the case of central differencing. The linear weighting (k) weights between QUICK and UD, where k=0 represents QUICK and k=1 upwind differencing.
- Ultimate Quick (UQUICK)
  UQUICK is a bounded version of QUICK and approximates the value at the surface trying to maintain the monotonic behaviour of the scalar. The derivation is for explicit flow calculations, resulting in unstable solutions for the implicit implementation under certain conditions. The factor k switches linearly between UQUICK and UD, where k=0 represents UQUICK .
- Compressive scheme for interface capturing (CICSAM)
  CICSAM is a high resolution scheme specially tailored to capture a step function smoothly in multiple dimensions. The scheme switches gradually between Ultimate-Quickest and Hyper-C based on the direction of motion and spatial orientation of the step. The switch is influenced by the factor k, with default k=0.5. A small value gives preference to Ultimate-Quickest whilst a value of k=1 represent Hyper-C, the most compressive scheme which still preserves boundedness. This scheme is only suitable for the capturing of step profiles, as it tends to change any gradient into a step.

5.2.6. Turbulence Models

There are two versions of k-ε turbulence models available in FLO++. These models lead to a set of partial differential equations called the Reynolds averaged Navier-Stokes (or RANS) equations. These equations do not form a closed set so that approximations or turbulence models have to be introduced. As one is normally interested in only a few quantitative properties of turbulent flows such as frictional forces on surfaces without having to know the effect of each and every eddy in the flow the RANS give sufficient information in ~~the~~ most cases.
The models are a high Reynolds number version and a low Reynolds number version.
The high Reynolds number turbulence model is known as the 'standard' k-epsilon model with the 'law of the wall' representations for momentum, heat and mass transfer within the boundary layers.
The low Reynolds number turbulence model is based on the 'standard' k-epsilon model except in the viscosity-influenced region of the boundary layer where a one-equation low Reynolds number model is used. The model consists of a transport equation for k and an algebraic prescription for epsilon.

5.2.7. Algebraic Algorithm

An iterative method is now used by the program to solve the system of equations obtained after the discretization of the flow area and the physical laws. A modified version of the SIMPLE algorithm is used for steady flows. The PISO algorithm is applied for unsteady flows.

5.3. Numerical Results

The important results of the numerical simulations are presented in this section. All the codes of the pre-processing files are shown in the Appendix D, as well as a standard post-processing file and a table of all simulations performed, containing the most significant data.

All the simulations have several parameters in common. The fluid condition remained unchanged, with a temperature of T=20°C, a density of ρ=1.18kg/m^3, a viscosity of ν=1.85·10^{-5}Pa·s, a pressure of p=10000Pa and a constant mass flux=7.821·10^{-4} kg/s. The boundary conditions are similar as well. An inlet boundary condition with constant velocity normal to the inlet area of w=0.476m/s is applied at the beginning of the pipe, and an outlet boundary condition, where the total flow is leaving the geometry, is applied at the end of the pipe. The numerical parameters are also not changed. The convergence level, the most important parameter, has the value of 10^{-3}. The circular main pipe has the dimensions of 46mm diameter and 5.92m length. The different blockages have their downstream end at the axial coordinate z=5.1m.

16 different numerical simulations are done, two of them do not satisfy the convergence level. These two are included in the analysis for different reasons. Simulation No1 is used to illustrate the problem with a too large number of cells. Simulation No13 is included to complete the simulation of ~~the~~ all the blockages used in the experiments. This simulation, though not fully converged, shows reasonable results.

A number of simulations are done to check the performance of the new software. Three simulations investigate the flow with blockages of different lengths and same diameter. Four simulations investigate the influence of changing diameters in combination with a constant length, on the air flow. One final simulation is performed with a semi-circular blockage, similar to the one used in the experiments 3-1 to 3-4.

The velocity profile, the pressure distribution and the maximum velocity are always used in the analysis of the numerical results. The maximum velocity, as a single, significant number, is used in the rest of this chapter for the comparison of the results of different numerical simulations. If not stated differently, the variation in the velocity and pressure profiles do not give extra information and are reflected by the variation of the maximum velocity.

The flow direction in all the coloured post-processing figures is from left to right.

5.3.1. Total Number of Cells

The influence of the total number of cells in the computational grid on the result is investigated with simulations No1 (72000 cells), No2 (9000 cells) and No3 (36000 cells). Only the number of cells in axial and circumferential direction is changed. The computational grid of simulation No3 is shown in the figure 5-3.

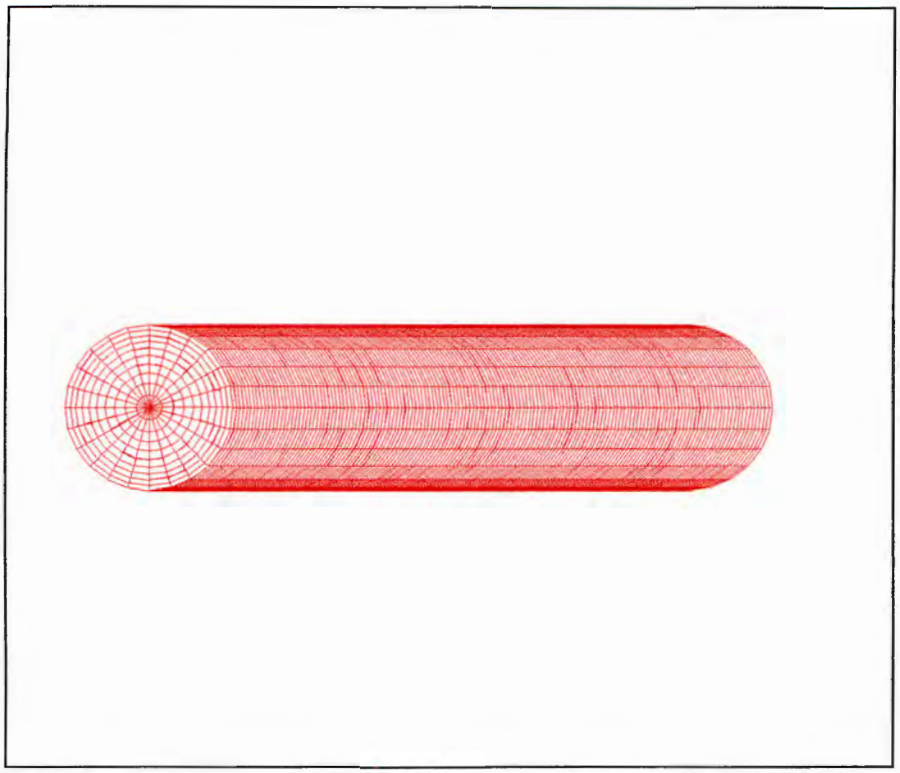

Figure 5-3: computational grid in simulation No3 (36000 cells)

Simulation No1 does not converge. The reason seems to be the large number of cells, as this is the only parameter changed to the other two simulations. Furthermore, the completion of 600 iterations took around 35 hours. The computational time invested is 24 minutes for the 114 iterations in simulation No2 and 5 hours for the 205 iterations in simulation No3.

The theoretical maximum velocity for a fully developed laminar flow in this pipe is 0.95m/s (see section 3.3). The peak velocity of the corresponding experiment 1-1 is measured to be 0.7m/s. The maximum velocity calculated with simulation No2 is 0.934m/s and the maximum velocity calculated with simulation No3 is 0.792m/s. It seems unlikely that a smaller number of cells results in a more accurate simulation, as the numerical error increases for bigger cells. A more realistic simulation is obtained with 36000 cells as the comparison of maximum velocities shows. The following experiments use a total number of cells in the order of 36000 cells. This is a good compromise between accuracy and computational time.

5.3.2. Turbulence Model

The influence of the different available turbulence models is obtained with a comparison of the simulations No3, No4 and No5. No turbulence model is used in No3, this simulation is expected to match the laminar flow the best. The standard k-ε-model is used in No4 and the low-Reynolds-number k-ε model is used in No5. The velocity distribution in the r-z-plane of all three simulations is shown in the following figures.

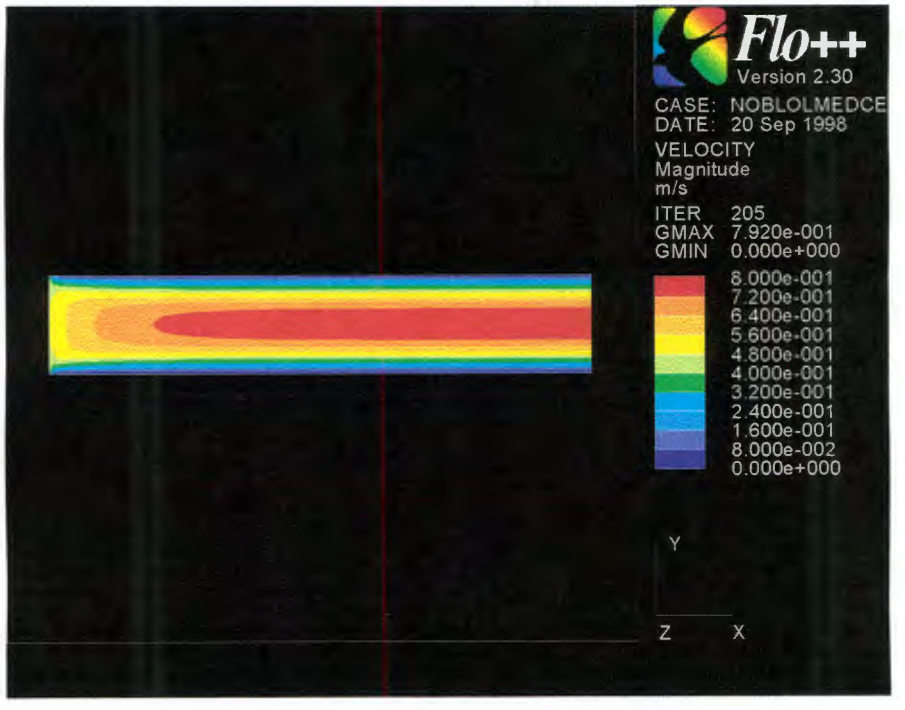

Figure 5-4: velocity in r-z-plane without turbulence model (No3)

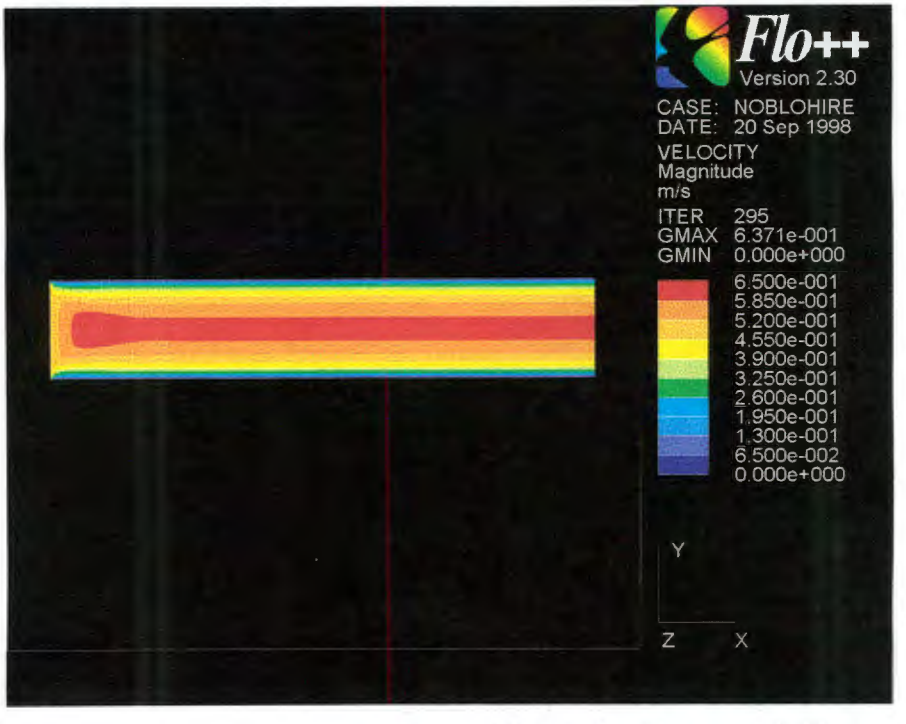

Figure 5-5: velocity in r-z-plane with standard k-ε-model (No4)

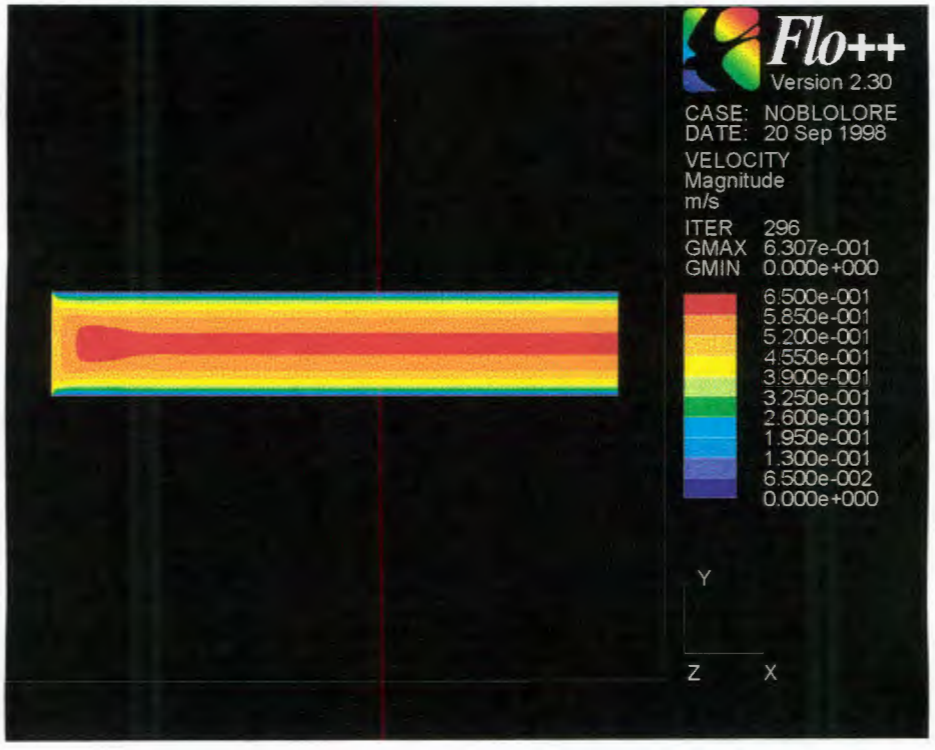

Figure 5-6: velocity in r-z-plane with low Reynolds-number k-ε-model (No5)

The shaded contour plots in figures 5-4 to 5-6 show that the simulation without the turbulence model matches the problem the best. The boundary layer takes a distance of about 100 times the pipe diameter to develop in simulation No3 (figure 5-4), as observed in the experiments and as predicted by Langhaar [14]. The difference between the two turbulence models is not significant, comparing the maximum velocity (6.37m/s and 6.30m/s), the computational time (6.48h and 6.41h) or the necessary number of iterations (296 and 295) to satisfy the convergence criteria. The velocity profiles in the radial direction give further evidence, that the simulation without turbulence model is the better choice for this problem. The profile without turbulence model is parabolic. The velocity with the k-ε model has high gradients close to the wall and a constant value closer to the middle of the pipe. The result is the comparably lower maximum velocity. The corresponding plots are shown in figure 5-7 and figure 5-8.

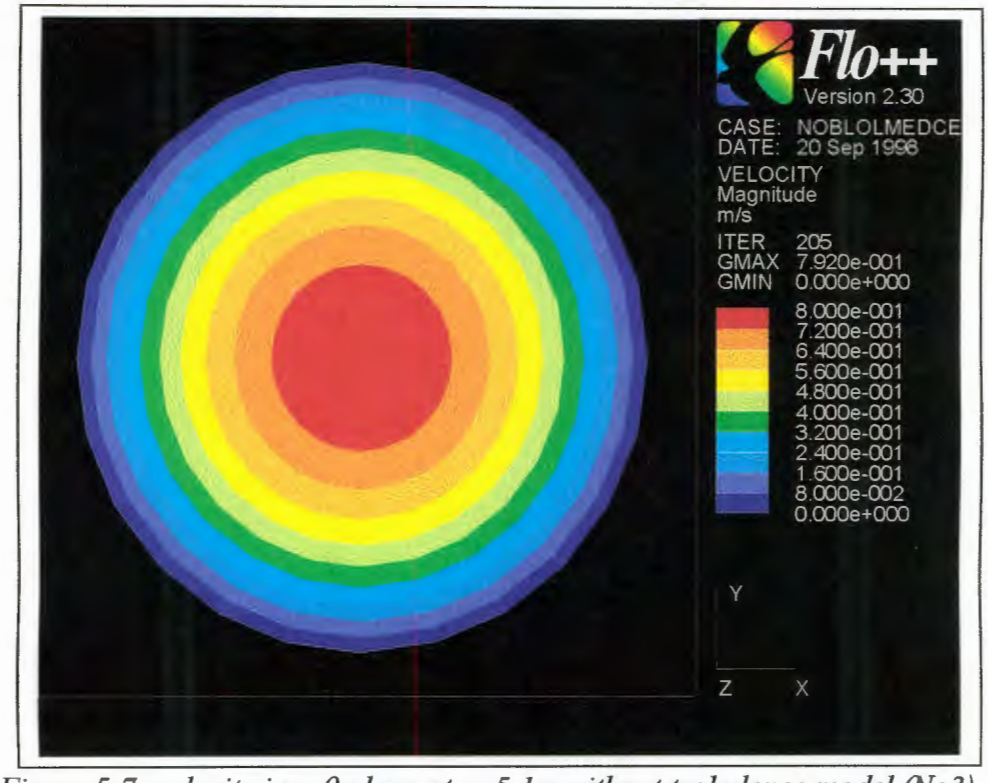

Figure 5-7: velocity in r-θ-plane at z=5.1m without turbulence model (No3)

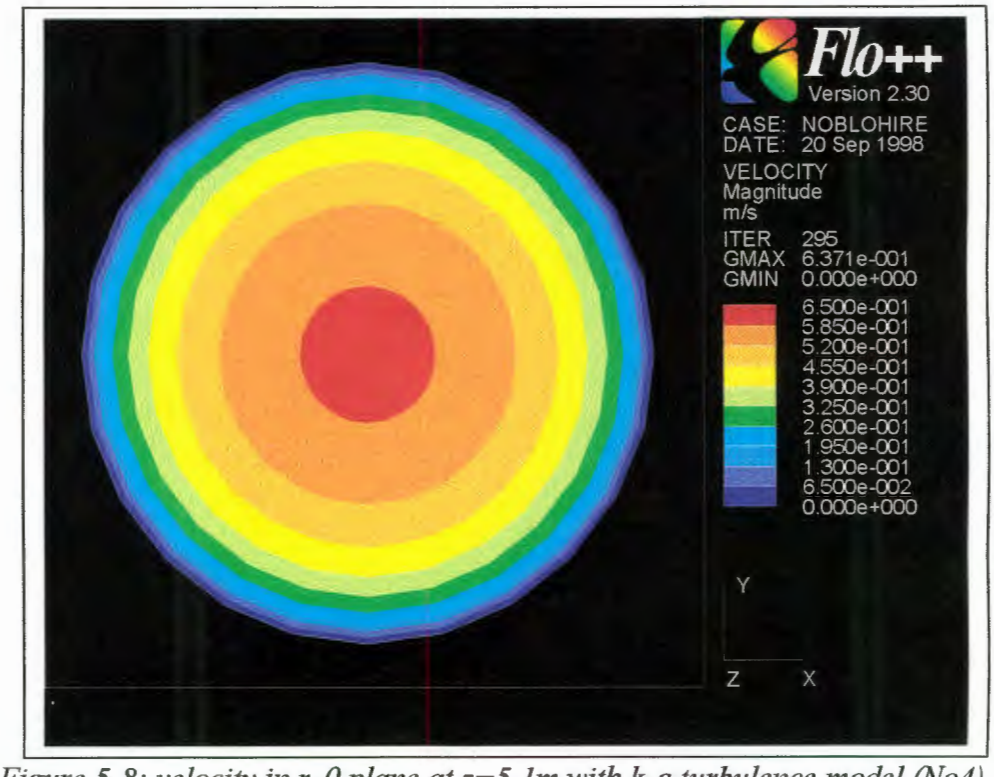

Figure 5-8: velocity in r-θ-plane at z=5.1m with k-ε-turbulence model (No4)

5.3.3. Wall Roughness

The influence of the wall roughness on the flow is investigated with the comparison between the simulations No5 and No6. The roughness, taken to its maximum value in simulation No6, only has effect when a turbulence model is applied, but no influence on the result is observable.
The following simulations do not use a turbulence model as a consequence of this analysis.

5.3.4. Number of Cells in the Axial Direction

Two pairs of simulations are performed to investigate the influence of the number of cells in the axial direction on the result. Simulations No7 and No7b are modeling a blockage of the dimensions L*=0.11 and A*=0.48. Simulation No7 uses one cell in the axial direction to model the blockage, simulation No 7b uses four cells. The grid inside the blockage only for both simulations is shown in figure 5-9a and 5-9b.

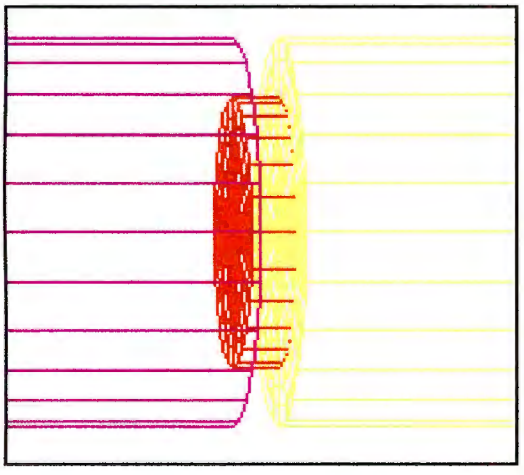

Figure 5-9a: 1 cell in z-direction (No7)

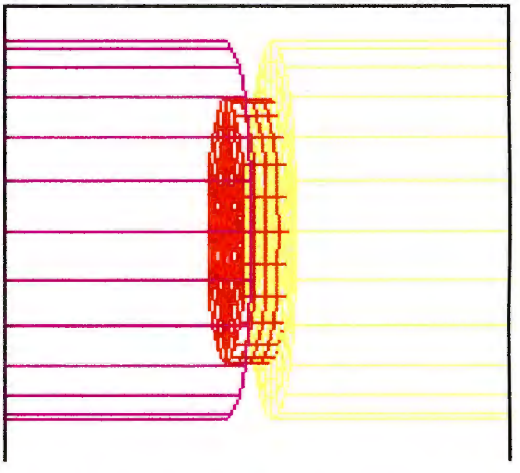

Figure 5-9b: 4 cells in z-direction (No7b)

The same comparison can be made between simulation No8 and No8b. The blockage of L*=1 and A*=0.48 is modelled with two and four cells respectively in the axial direction.
The peak velocity in simulation No7 has the value of 1.10m/s and in simulation No7b the peak velocity is 1.06m/s, which is a difference of 3.6%. The peak velocity in simulation No8 is 1.13m/s and in simulation No8b the maximum velocity is 1.12m/s, which is a change of 0.9% caused by the variation of the cell number. These differences are small, the influence of the number of cells in the axial direction is therefore not very strong.
If a varying number of cells in the axial direction is used in the modeling of blockages of different lengths, the change in the maximum velocity must be significantly larger than the above mentioned difference. Otherwise the influence of the geometrical variation can not be separated from the influence of the changes in the computational grid. In this case, a constant number of cells must be used for different geometries.

5.3.5. Number of Cells in the Radial Direction

The computational grid for the simulation of blockages is created with three blocks of cells. The first block is modeling the pipe from its beginning (z=0m) to the beginning of the blockage, while the second block is modeling the blockage and the last block is modeling the flow area from the downstream end of the blockage (z=5.1m) up to the end of the pipe (z=5.92m). These three blocks are shown in figure 5-10

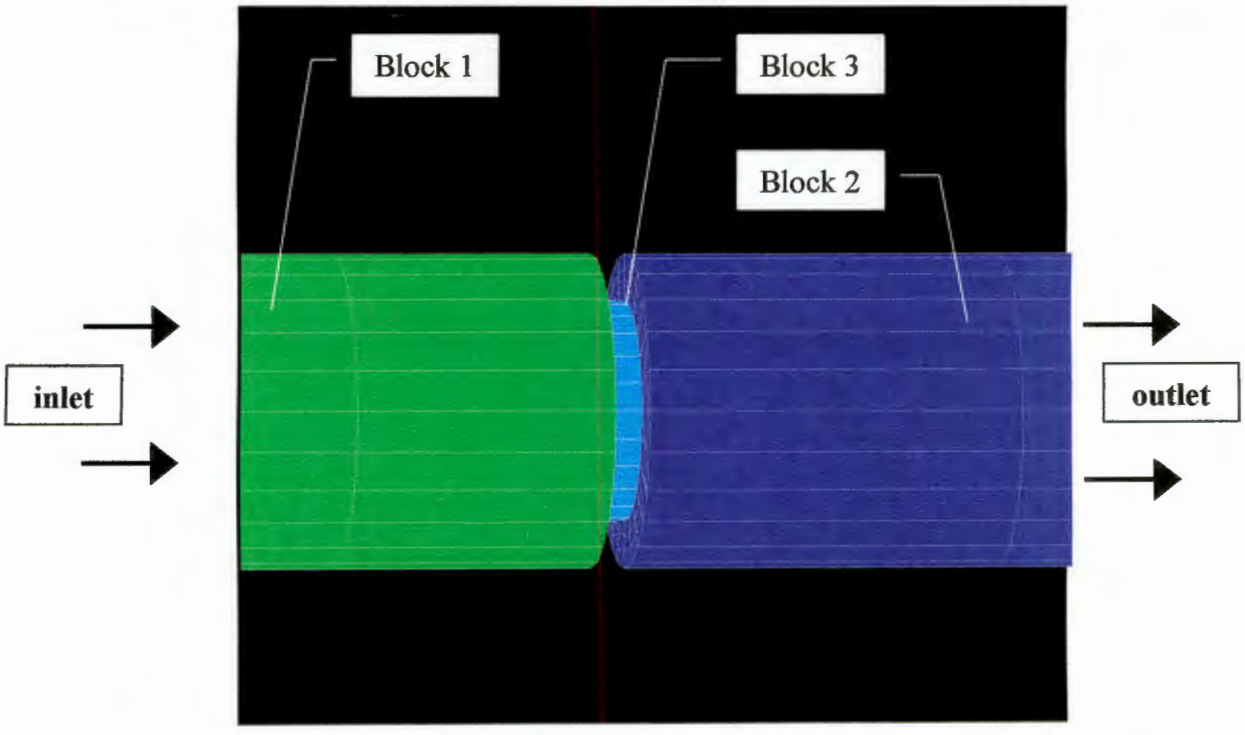

Figure 5-10: three blocks of cells for the simulation of a blockage

The three blocks are connected numerically by the pre-processor.

The influence of the number of cells in the radial direction is investigated with the comparison of two simulations for the same blockage. This is necessary as the radial cell-number cannot be kept constant for all experiments. The ratio of cells in the radial direction in the blockage and in the main pipe must be very close to the ratio of radii in the main pipe and in the blockage. Otherwise the three blocks of cells are not connected by the pre-processor of FLO++, and the air can not flow from the main pipe into the blockage and back into the last section of the pipe in the numerical model.

The simulations No10 and No10b model the same blockage with L*=1 and A*=0.76. The first uses 8 cells in the main pipe and 7 cells in the blockage. The second 15 cells in the main pipe and 13 cells in the blockage. The ratio of radii between main pipe (r=23mm) and blockage (r=20mm) has the value of 0.8696. The ratio of radial cells in simulation No10 is 7/8=0.8750, and in No10b the ratio is 13/15=0.8667. Both cell ratios are close enough to the ratio of radii, so the pre-processor can connect the block.

The two different grids are shown in figure 5-11a and figure 5-11b.

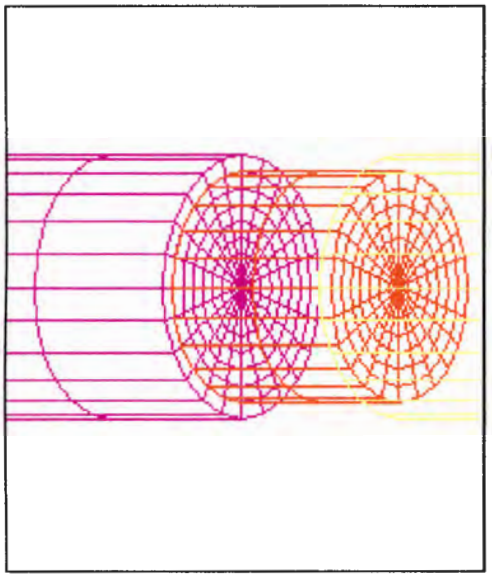

Figure 5-11a: grid in simulation No10

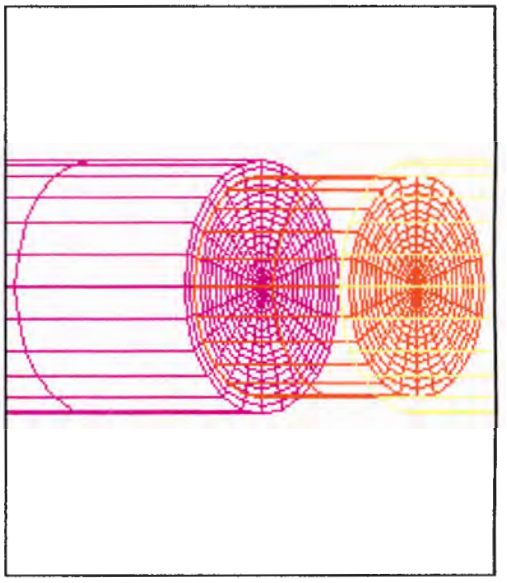

Figure 5-11b: grid in simulation No10b

The computational time required for the two simulations differs very much as the total number of cells is different. Simulation No10 with 28752 cells takes around 3.8h CPU-time and simulation No10b with 40224 cells takes around 9.2h. The maximum velocity in simulation No10 is at 0.84m/s and the one in No10b is at 0.86m/s. This is a small variation of 2.3%.
The influence of the number of cells in the radial direction is therefore also small.

5.3.6. Length of the Blockage

The influence of the length of the blockage, with constant reduced area A*=0.48, is obtained with three simulations. Simulation 7b models a blockage of L*=0.11, while simulation 8b models a blockage of L*=1, and simulation 9 models a blockage of L*=2. All three simulations use exactly the same total number of cells (35712) in the mesh. The maximum velocity is increasing slightly with increasing length of the blockage, just as experienced in the experiments. A magnification of the calculated flow in the blocked area is shown in the following figures 5-12 to 5-14.

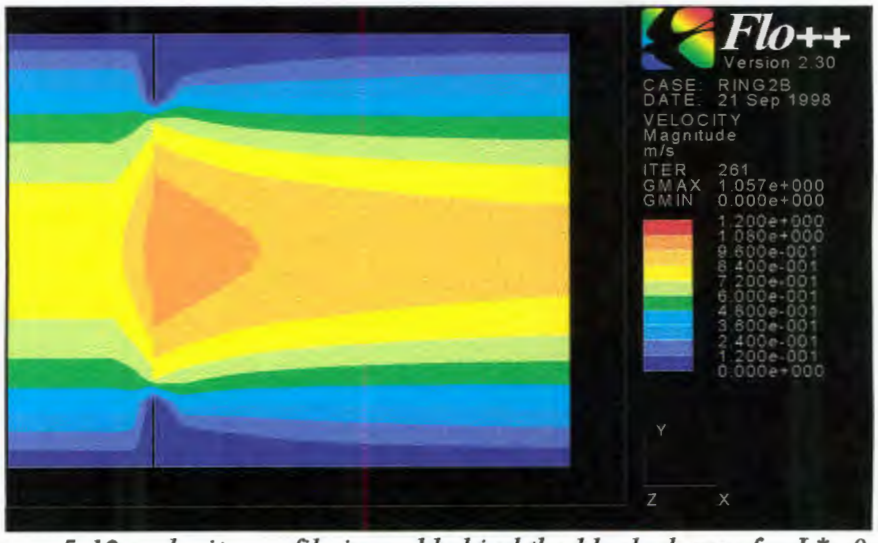

Figure 5-12: velocity profile in and behind the blocked area for L=0.11*

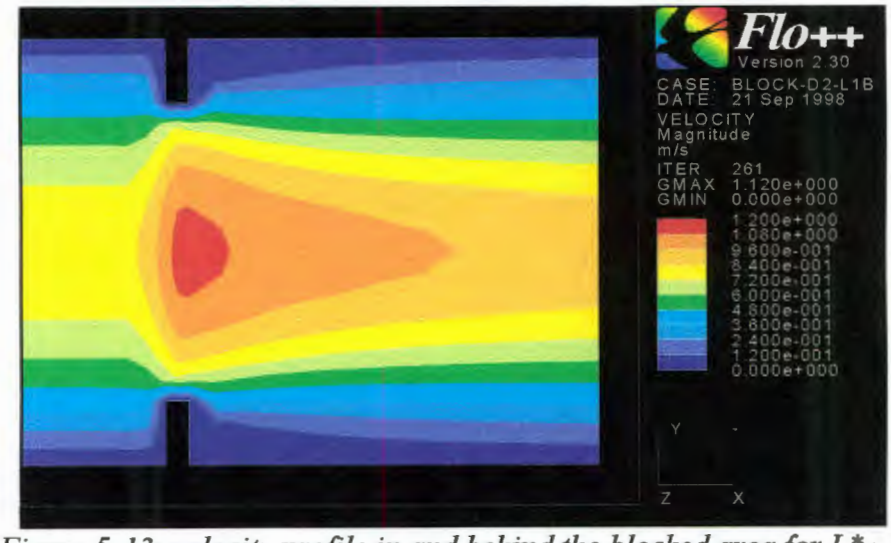

Figure 5-13: velocity profile in and behind the blocked area for L=1*

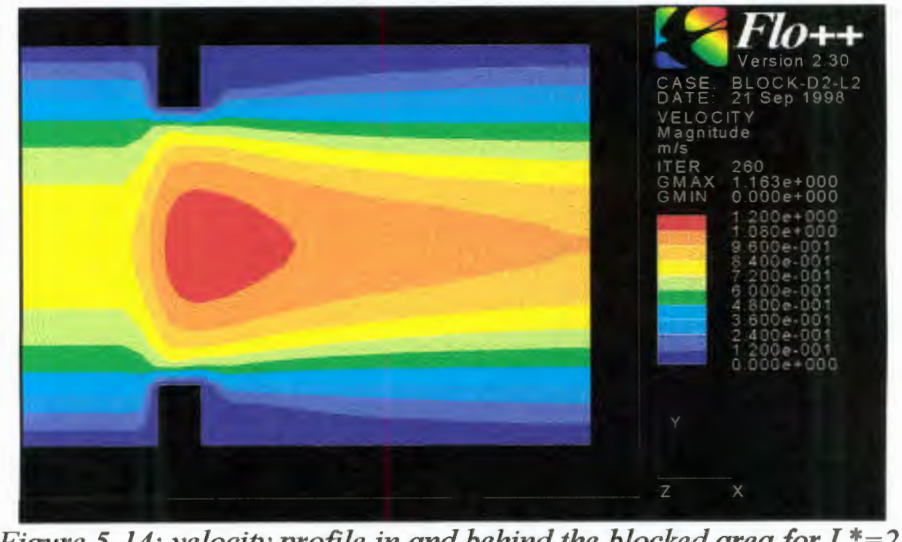

Figure 5-14: velocity profile in and behind the blocked area for L=2*

These three figures clearly show the influence of the length of the blockage. The maximum velocity is only slightly increased, from 1.06m/s for L*=0.11 to 1.16m/s for L*=2. The zone of high velocity extends with a longer blockage.
Overall, the influence of the length of the blockage on the flow is visible in the simulation and is not very strong.

5.3.7. Diameter of the Blockage

The influence of the blockage diameter, and thus the reduced area A*, on the velocity field is obtained with four numerical simulations. The blockages have all the same length of L*=1. The areas of A*=0.76, A*=0.48, A*=0.32 and A*=0.19 (similar to the corresponding experiments) are modelled in the simulations No13, No12, No8 and No10. Magnifications of the corresponding velocity distribution are shown in figures 5-15 to 5-18.

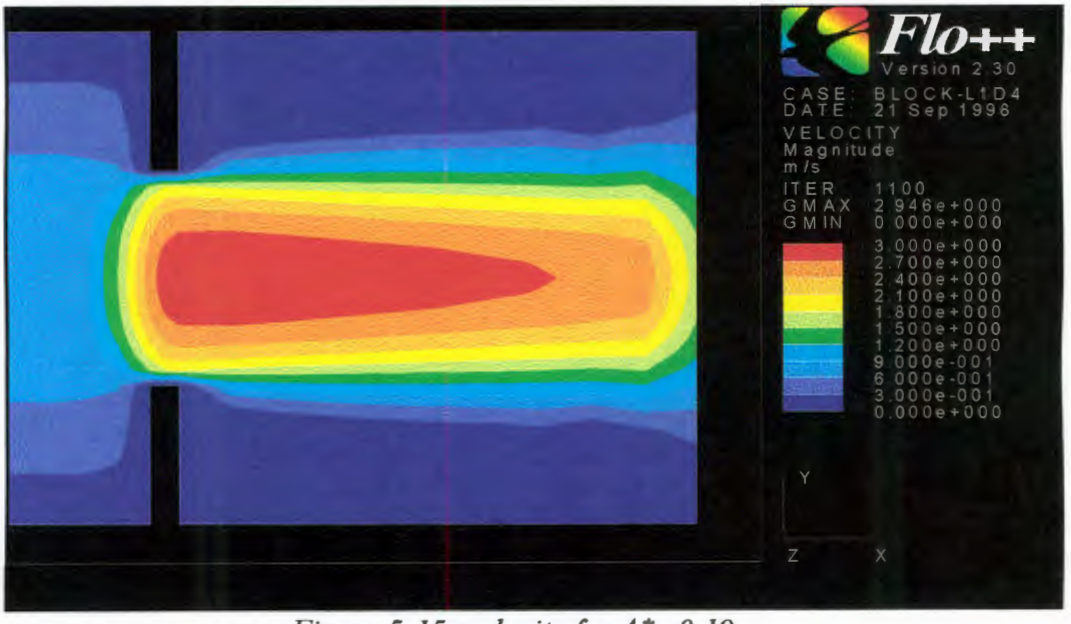

Figure 5-15 :velocity for A=0.19*

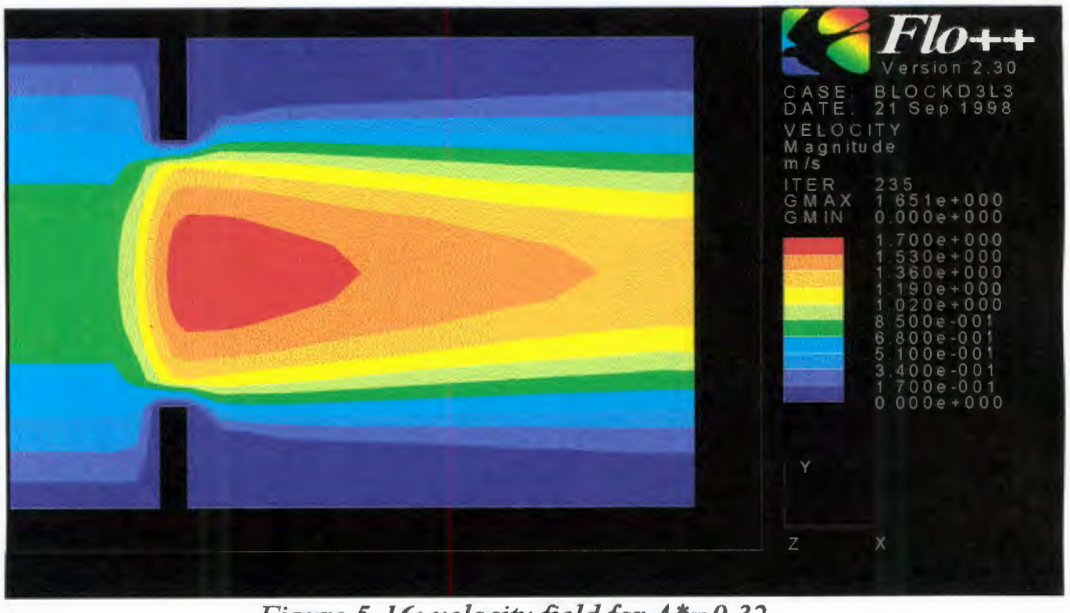

Figure 5-16: velocity field for A=0.32*

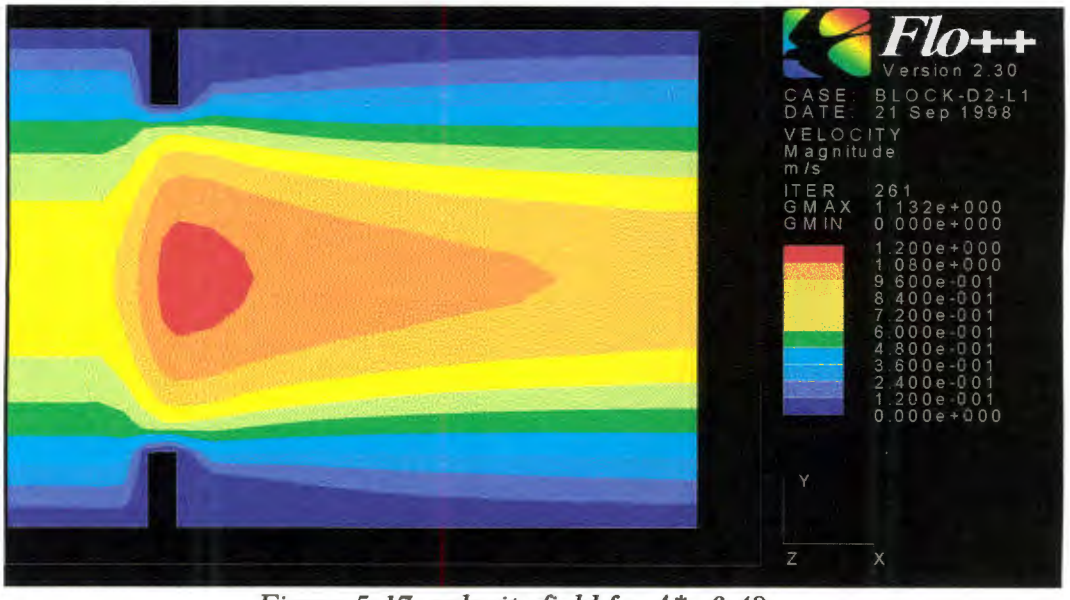

Figure 5-17: velocity field for A=0.48*

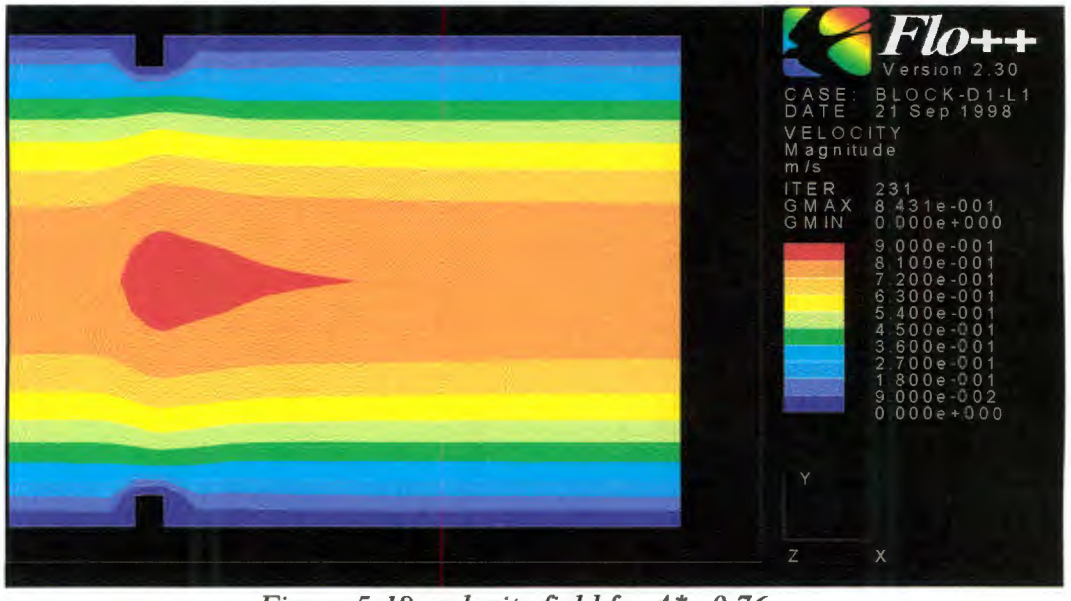

Figure 5-18: velocity field for A=0.76*

Some remarks are necessary before the results are explained. First of all it must be noted that the colour scale is different for all four plots. This is necessary, as the post-processor only offers 10 colours. Second, it must be remembered that simulation No13, the simulation of the blockage with A*=0.19, is not fully converged. The residual for the axial velocity is in the order of magnitude 10^{-2}. And third, the number of cells in the radial direction varies strongly in these simulations (8 cells for A*=0.76 – simulation No10 and 16 cells for A*=0.19 – simulation No13) .

The plots show the expected behaviour. The maximum velocity is increasing with decreasing A*. The maximum velocity for A*=0.19 is w=2.95m/s. For A*=0.76 the maximum velocity is w=0.843m/s, which is only slightly higher than without any blockage. The zone of high velocity is stretching with decreasing A*.

5.3.8. Semi-Circular Blockage

The change of the velocity field caused by a semi-circular blockage is investigated with simulation No11. The blockage dimensions are L*=1 and A*=0.5, identical to the experiment performed. The blockage section of the used computational grid is shown in figure 5-19.

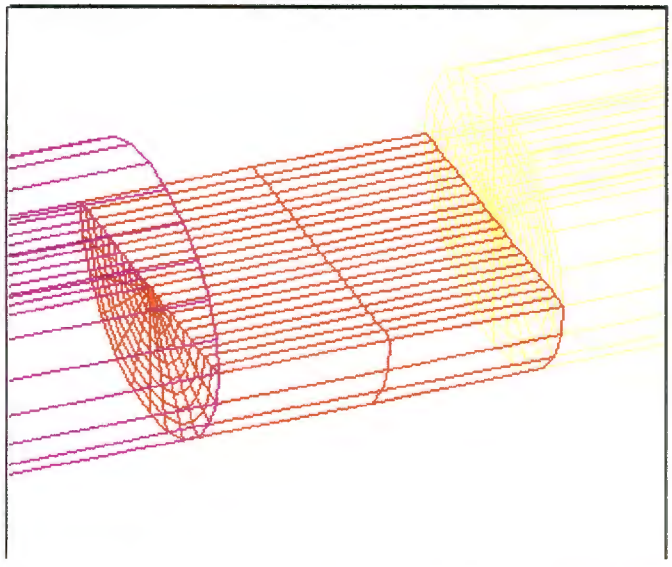

Figure 5-19: blockage section of computational grid in simulation No11

The velocity profile obtained with this simulation is shown, looking at the blockage from the side, in figure 5-20.

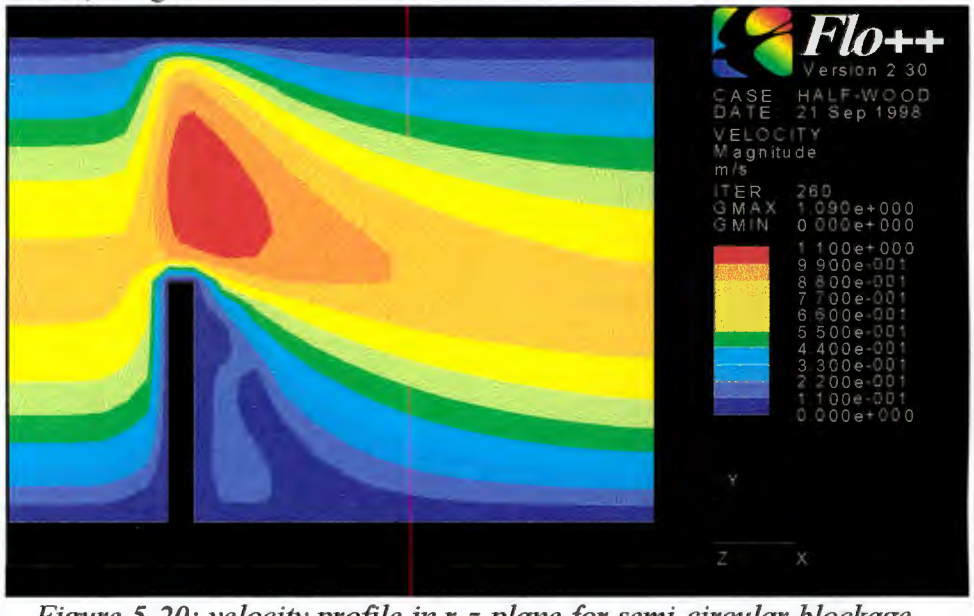

Figure 5-20: velocity profile in r-z-plane for semi-circular blockage

The same velocity field, in the r-θ-plane at the end of the blockage, is shown in figure 5-21.

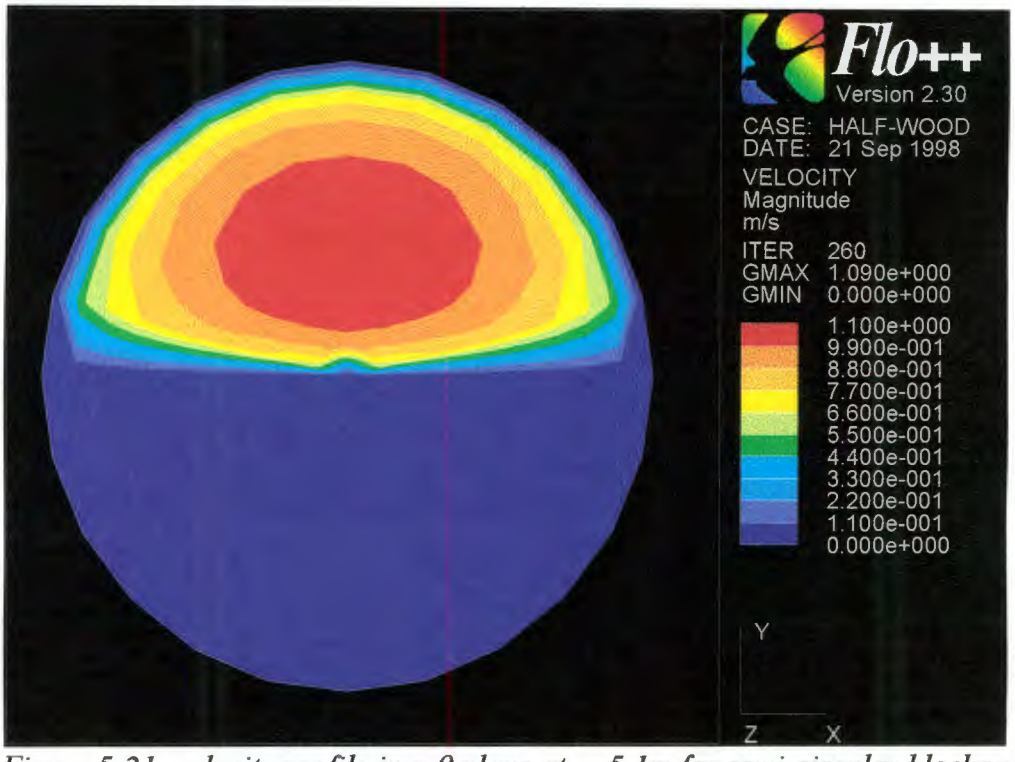

Figure 5-21: velocity profile in r-θ-plane at z=5.1m for semi-circular blockage

These two figures again show an expected result. The air is accelerated by the blockage and a wake is built up behind the blockage. Figure 5-20 shows particularly the limitations in accuracy due to the disretization of the flow area. The velocity is slightly lower in the middle of the pipe. This effect, possibly caused by the very small cells in the middle, is just contrary to the reality.

5.3.9. Pressure Loss

The pressure loss and the pressure distribution, in particular caused by the different blockages, are shown in this section.
The pressure distribution in a pipe without blockage is shown in figure 5-22.

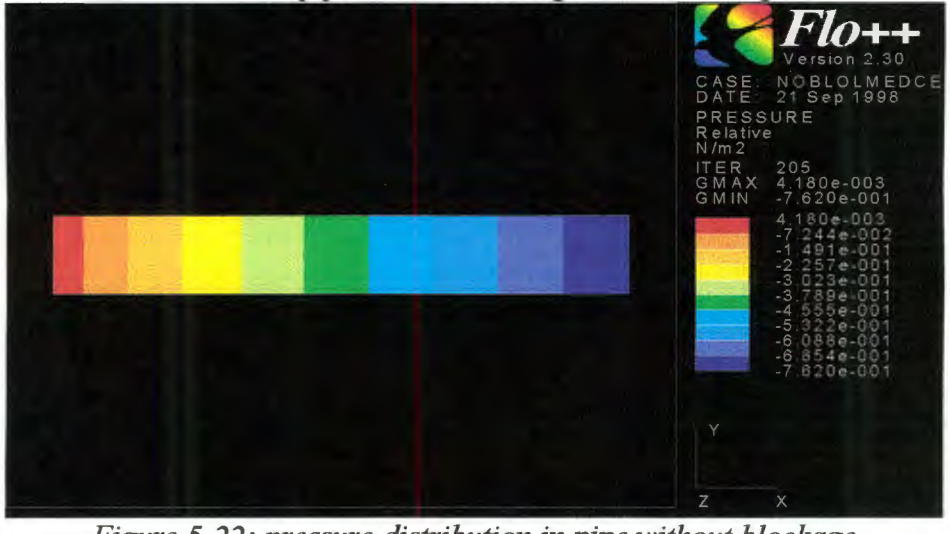

Figure 5-22: pressure distribution in pipe without blockage

Simulation No3 (the simulation corresponding to the reference experiment 1-1) without a turbulence model is chosen for the figure above.
The pressure distribution shows a constant pressure over the diameter of the pipe at every point in the axial direction. The pressure loss over the entire length of the pipe has a value of around 0.77Pa.

The pressure distribution caused by a blockage is shown, with simulation No8 (A*=0.48, L*=1), in figure 5-23. The pressure distributions in the simulations with different blockages show a similar behaviour.

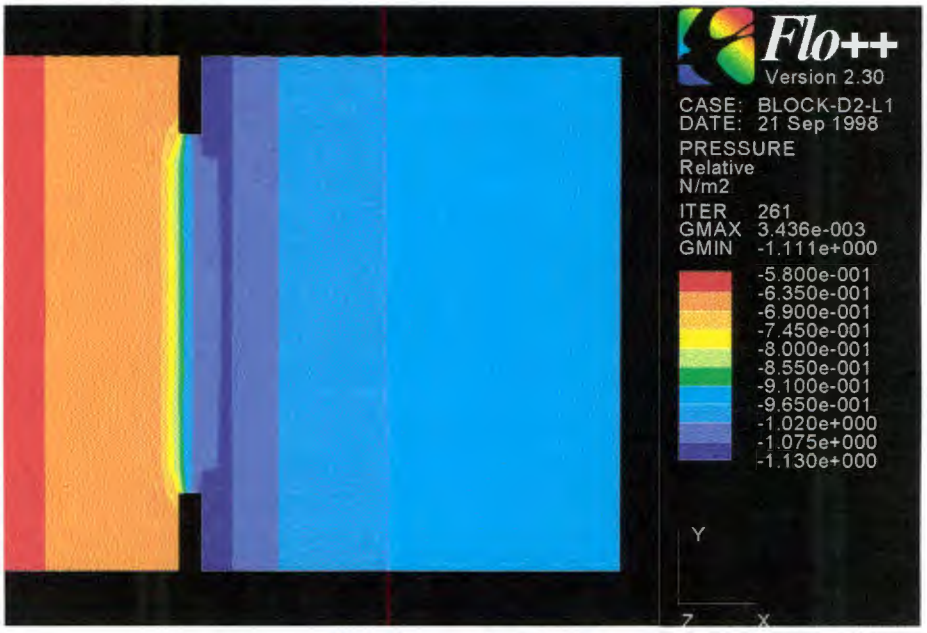

Figure 5-23: pressure distribution in blockage for simulaton No8

The pressure loss over the blockage (at the same points as measured in the experiments) has the value of 0.314Pa.

The last pressure distribution, caused by the semi-circular blockage of simulation No11, is shown in figure 5-24.

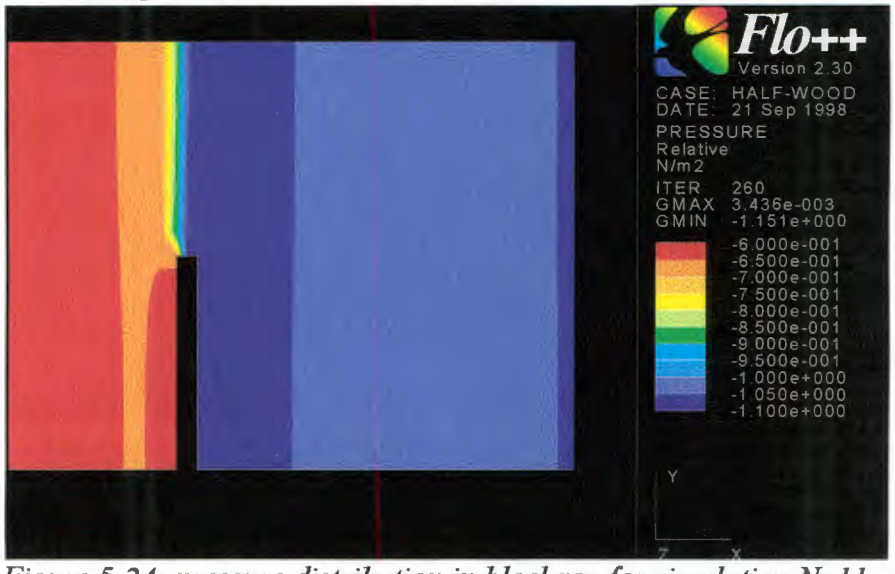

Figure 5-24: pressure distribution in blockage for simulation No11

The pressure loss, corresponding to the measuring points in the experimental test-rig, is 0.398Pa.

Table 5-1 shows the pressure loss over all the blockages, corresponding to the pressure tappings in the test-rig (shown schematically in figure 5-25), as well as the total pressure loss from the beginning to the end of the pipe. Only the relevant simulations, that are taken for comparison with the experimental results, are included. The total pressure loss is given by the post-processor, the pressure loss over the blockage is read from the shaded contour plots in the corresponding r-θ-plane.

Simulation No	Blockage	Delta p total [Pa]	Delta p1 [Pa]	Delta p2 [Pa]
1	No	1.290	1.108	0.188
2	No	0.908	0.790	0.118
3	No	0.732	0.627	0.105
4	No	1.675	1.404	0.271
5	No	1.576	1.322	0.254
6	No	1.675	1.404	0.271
7	L*=0.11; A*=0.48	0.906	0.633	0.273
7b	L*=0.11; A*=0.48	0.878	0.634	0.244
8	L*=1; A*=0.48	0.947	0.633	0.314
8b	L*=1; A*=0.48	0.935	0.633	0.302
9	L*=2; A*=0.48	0.988	0.633	0.355
10	L*=1; A*=0.76	0.761	0.637	0.124
10b	L*=1; A*=0.76	0.758	0.631	0.127
11	L*=1; (Halfcirc.) A*=0.5	1.031	0.633	0.398
12	L*=1; A*=0.32	1.689	0.633	1.056
13	L*=1; A*=0.19	5.369	0.630	4.739

Table 5-1: pressure loss of different blockages in the numerical simulation

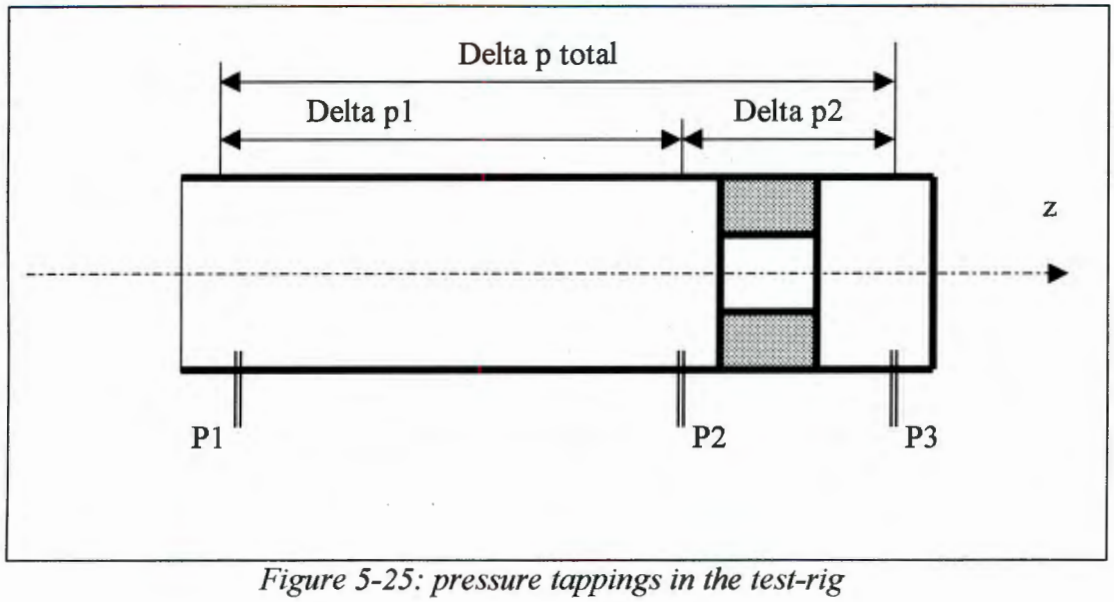

Figure 5-25: pressure tappings in the test-rig

The pressure loss obtained with the numerical simulation is shown in the following figure 5-26. Both, the data for the first section of the pipe (delta p1), and the test section with the various blockages (delta p2), are shown with an approximation by a power series.

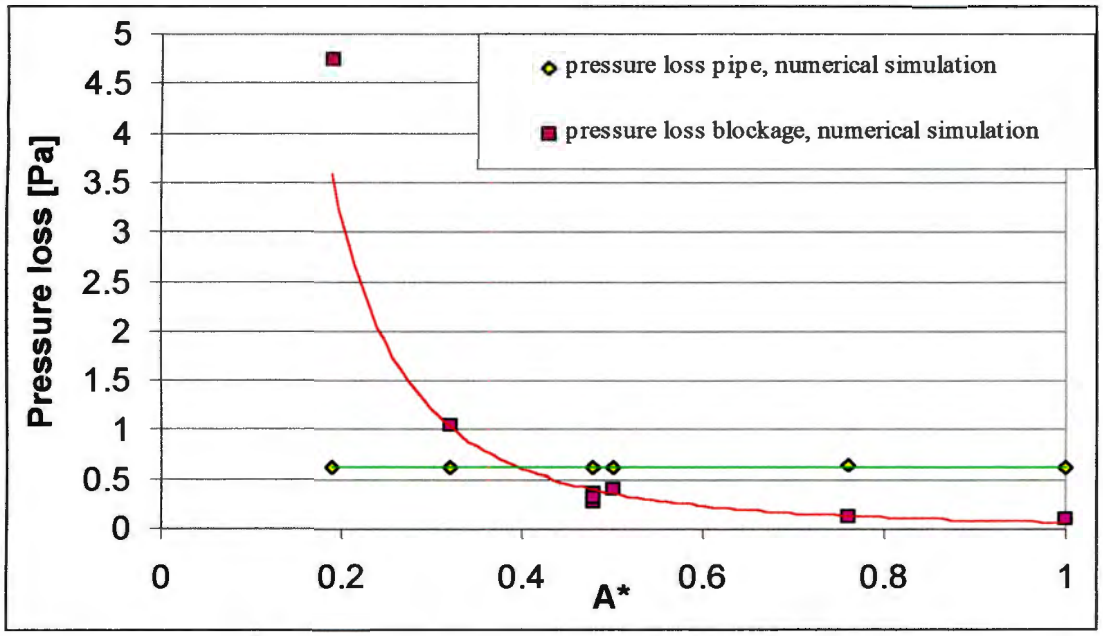

*Figure 5-26: pressure loss as function of A**

The results correspond to those expected. The pressure loss in the 5m length of the main pipe is similar for all the simulations. The pressure loss over the blockage increases with A* decreasing.

6. Conclusion

6.1. Modeling

6.1.1. Experiments

A new test-rig is built for this thesis. A large part of this work deals with the checking of the test-rig's performance, which reveals two negative aspects. Both are in connection with the hot film probe which is used.

Firstly, the calibration of the hot film probe proves to be inaccurate, as the calibration is done in the turbulent flow of a wind-tunnel, but the measured flow is laminar. This source of error cannot be eliminated with the existing installation. A laminar reference flow for the calibration is necessary.

Secondly, the hot film probe proves to have a significant influence on the air flow. The main reason is believed to be the reduction of the flow area due to the insertion of the probe into the pipe. Other effects must also play a role, otherwise the relatively high velocity measured at the bottom of the pipe cannot be explained.

Besides these two errors, the results obtained with the experiments are acceptable. The reproducibility is controlled for every experiment and proves to be high. The transitional length of the laminar pipe flow corresponds very well to the expectations. Bearing in mind the above mentioned errors induced by the probe, the laminar velocity profile is built up before the air enters the blockage. The influence of the different blockages corresponds to the expectations. Blockages with a small flow area cause a high peak velocity and a large wake. Blockages with a flow area that does not differ very much from that of the main pipe have only a very small influence on the flow. The length of the blockage has only a secondary influence on the downstream velocity distribution, while the influence of the surface roughness of the blockage is small.

The data collected poses the opportunity of direct comparison with the numerical simulation, as the test rig was designed for this purpose.

6.1.2. Numerical Simulation

The unfamiliar software is tested on its performance with the variation of different parameters. The influence of the available turbulence models and of the number of cells in the computational grid are the primary parameters which are varied. Other parameters such as boundary conditions, discretization scheme, convergence level and number of sweeps are also changed. These changes either cause the calculation to diverge (boundary conditions and discretization scheme), or they have no significant influence on the result at all (lower convergence level, number of sweeps).

Two main problems occur in the numerical simulation. The discretization of the pipe with a very high number of cells (72000) does not lead to successful convergence, with the pressure residual staying at a very high level. This simulation is done as an extreme case to check the upper limit of cells to be used in the further simulations. The grid generation for some of the blockages proves very difficult. The connectivity of the entire grid is only achieved after a lot of adjustments in the pre-processor.

The results are consistent with the expectations, except for one simulation (No12). This simulation is the only one that has a lower maximum velocity than the corresponding experiment. The reason is believed to be found in the grid-generation, but could not be positively identified.

The pressure loss and pressure distribution in the different simulations have a realistic behaviour, as do the velocity profiles.

6.1.3. Comparison of the Models

When comparing the two models, there are some significant aspects. The maximum velocities in the numerical simulations are generally slightly higher than those in the experiments. This is believed to be caused by errors in connection with the hot-film probe, which lowers the measured velocities.
The maximum velocities for different blockage diameters measured in the experiments, those obtained from the numerical simulations and those obtained from the theoretical considerations are shown in figure 6-1.

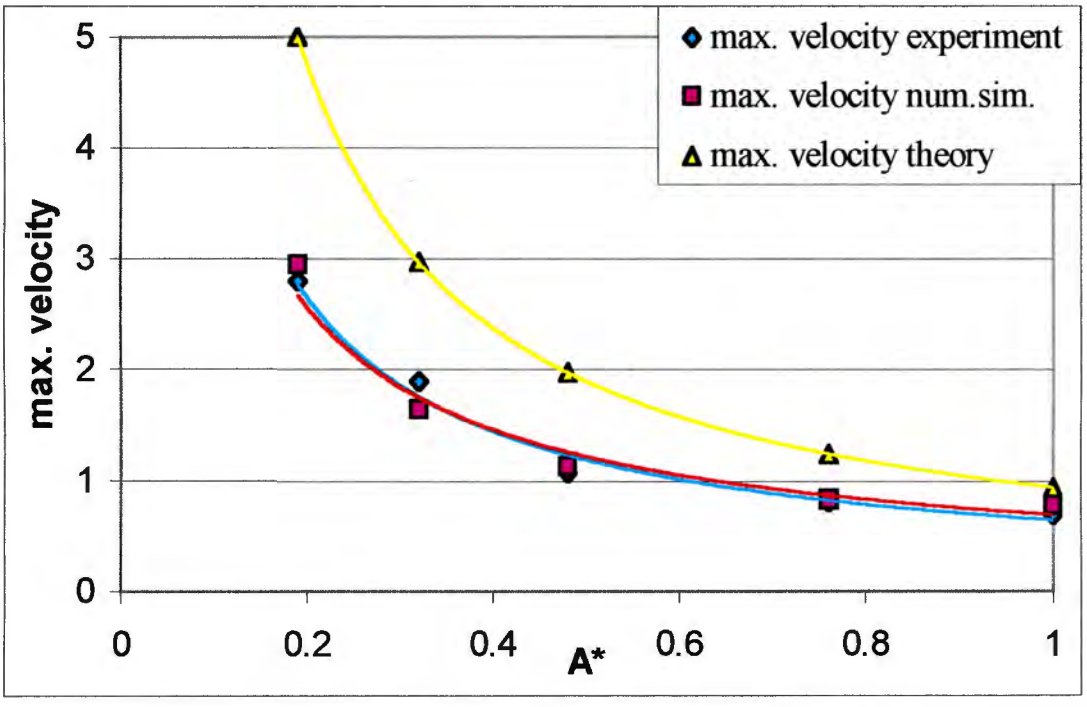

*Figure 6-1: maximum velocities as function of A**

The comparison of the experimental and numerical results with the theoretical ones show the expected discrepancy in the peak velocity. The theory assumes an infinitely long blockage with constant diameter. Therefore, the measured and the calculated peak velocity behind a blockage must be significantly lower, as is the case.

The transitional length of the laminar pipe flow in the two models corresponds very well. The qualitative laminar velocity profiles in a cross-section of the pipe are, considering the above mentioned restrictions by the probe, fairly similar. The peak velocities caused by the different blockages correspond well, too.

The good correspondence between the two models is visible when comparing the pressure loss obtained. Figure 6-2 shows the pressure loss for both models in the first, long section of the pipe, as well as the pressure loss over different types of blockages.

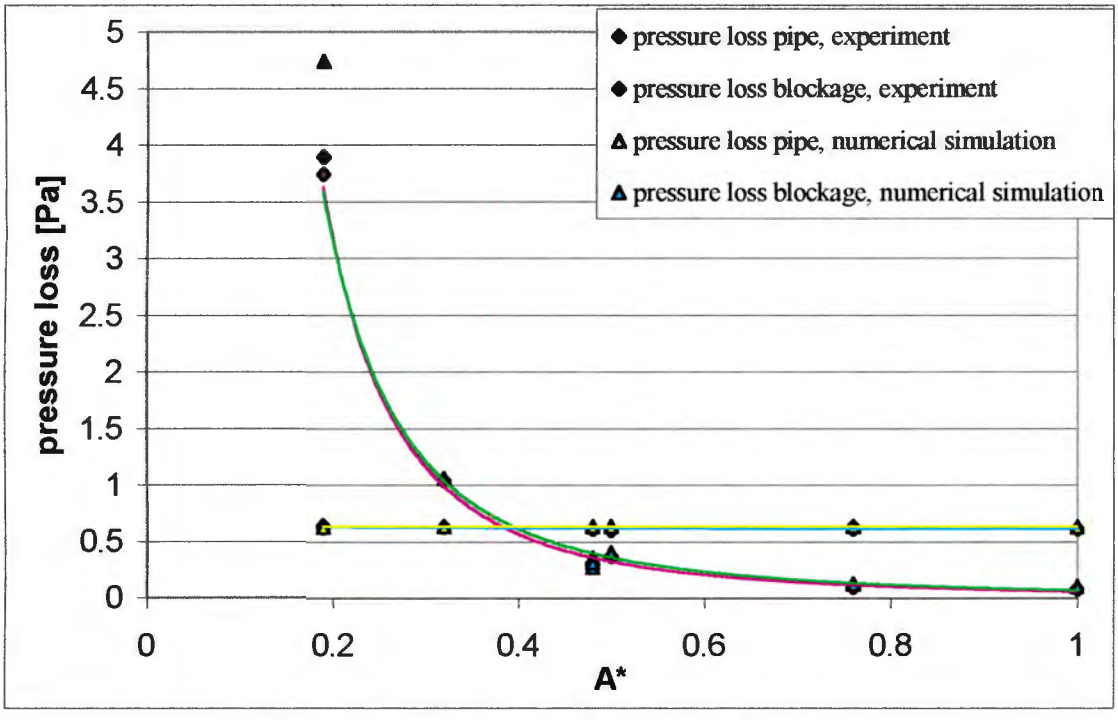

*Figure 6-2: pressure loss as function of A**

The pressure loss in the main pipe is constant at an identical level for both models. The difference in the pressure loss over the blockage is small for large values of A* and increases with A* decreasing. However, the curve fit with a power series shows an almost identical shape.

6.2. Contribution to the Medical Application

The results obtainable with the experimental simulation, as well as with the numerical simulation, do not directly contribute to the medical application of non invasive investigation of atheroma. Results of the present type do not have the necessary simplicity and brevity to be directly applied by a medical doctor.

But the prediction of the diameter of the blockage from peak velocities measured with MRI is an improvement on that which is possible from the theory only. The corresponding peak velocities as functions of the reduced area are shown in figure 6-1. In particular, the results obtained in this thesis show, that the true maximum velocities are significantly lower, than those obtained with theoretical predictions.

The change of the velocity profiles, due to angioplasty, is shown in a simplified form with the models. Typical values of reduced areas before and after such a surgery, where the atheroma is squeezed against the arterial walls, are $A^*_{before}=0.32$ and $A^*_{after}=0.76$. The influence of the latter on the flow is very small, on the other hand, the large blockage has a dominant influence. A prominent wake exists downstream of a highly reduced flow area, and high velocities occur. A wake is a potential risk area for atherosclerosis, as low shear rates and high turbulence intensities are possible. The blockage with the less reduced area has almost no influence on the flow, for a wake is hardly formed.

The influence of different shapes of atheroma, while having a similar reduced area, is also demonstrated. The perfectly symmetrical blockage has less negative influence on the flow than a highly asymmetrical blockage (seen in the extreme case of a semi-circular blockage). The asymmetrical blockage causes a larger wake and higher maximum velocities.

6.3. Recommendations for Future Work

With this thesis, a first step is taken towards obtaining results that can be applied in MRI investigations.

Systematic investigations of the velocity profiles using realistic shapes of atheroma could be performed as a direct continuation of this thesis. The present hard- and software in both experimental and numerical modeling could be used with small modifications only. The advantage would be the known performance and the accuracy of the test-rig and the numerical software respectively. The concentration of the results of this systematic study into a brief form might be challenging.

Experimental simulations with the aim of identifying and quantifying the turbulent zones require a different experimental apparatus. Different probes are necessary, two or three component hot wire probes would be a possibility. Computerized data collection, the possibility of scanning a 3D flow field behind the blockages and the possibility of creating a pulsed flow would be ideal. Investigation of the shear stress could also be included.

Numerical simulations with higher ambitions than using the present results and software could point in different directions. The emphasis could be on more realistic modeling of arterial blood flow. Several possible refinements of the numerical model include pulsed flow, non-Newtonian behavior of the blood, fluid-solid-interaction with elastic walls or branching. One of those would be the next logical step.
The emphasis could also be on the detection of the turbulent zones. This requires software capable of considering the transition from laminar to turbulent flow. Direct numerical simulation does not seem to be possible at this stage, as the corresponding hardware and the required expertise pose problems. A Large Eddy Model for the turbulence could be a possibility. This at least requires different software, and quite possibly also hardware with a higher performance.

References

[1] Bergel, D. H. (1972), Cardiovascular Fluid Dynamics, Academic Press, London and New York.

[2] British Standards Institution, Methods for the Measurement of Fluid Flow in Pipes, *British Standards 1042: Part 1: 1964.*

[3] Bronstein, Semandjajew (1991), Taschenbuch der Mathematik, Teubner Verlagsgesellschaft, Stuttgart and Leipzig.

[4] Calibration Data for 'Metric' Series Rotameters.

[5] Clinical MRI Primer, Vol. 1 (1996), Siemens Medical Systems, Erlangen.

[6] Edelman, R.R. (1992), Fast Magnetic Resonance Imaging: A Primer, Siemens Medical Systems, Erlangen.

[7] Edelman, Warren, Coronary Artery Imaging - Pioneering New Applications on the MAGNETOM, Siemens Medical Systems, Erlangen.

[8] Flow Quantification, MAGNETOM Vision - MAGNETOM Impact, Siemens Medical Systems, Erlangen.

[9] Fry, D. L. (1969), Certain chemorheological considerations regarding the blood vascular interface with particular reference to coronary artery disease, *Circulation 39, Suppl. 4, 38-59.*

[10] Fung, Y.C. (1993), Biomechanics – Circulation, Springer, New York.

[11] Fung, Y.C. (1997), Biomechanics - Mechanical Properties of Living Tissues, Springer, New York.

[12] Gieck, K. + R. (1989), Technische Formelsammlung, Gieck Verlag, Germering.

[13] Ku, David N., Blood Flow in Arteries, *Ann. Rev. Fluid Mech. 1997. 29:399-434.*

[14] Langhaar, H. L. (1942), Steady Flow in the Transition Length of a Straight Tube, *J. Appl. Mech. 1942 Vol. 9* .

[15] Laub, G. (1994), Basics of MR Angiography - Translation of reprint, *Radiologe 34: 416-422*, Springer, Berlin.

[16] Massey, B.S. (1983), Mechanics of Fluids, Van Nostrand Reinhold (UK) Co. Ltd.

[17] Meier, Maier, Boesiger (1988), Quantitative flow measurements on Phantoms and on blood Vessels with MRI, *Magn. Res. in Med. 8, 25-34.*

[18] MR_Tutor, http://www.siemens.de, Siemens Medical Systems.

[19] Patankar, S.V. (1980), Numerical heat transfer and fluid flow, Hemisphere Publishing Corporation, Washington.

[20] Prandtl, L. (1965), Fuehrer durch die Stroemungslehre, Vieweg & Sohn, Braunschweig.

[21] Taylor, Hughes & Zarins, Finite Element Modelling of Blood Flow in Arteries, *IACM Expressions 3/1997.*

[22] Taylor, Hughes, Zarins (1998), Finite element modeling of blood flow in arteries, *Comput. Methods Appl. Mech. Engrg. 158, 155-196.*

[23] Thomann, H.H. (1994), Stroemungslehre 1 & 2, AMIV-Verlag, Zurich.

[24] TSI Inc., Hot Wire / Hot Film Anemometry.

[25] Versteeg, Malalasekera (1995), An Introduction to computational fluid dynamics – The finite volume method, Longman Group Ltd, London.

[26] Walton, Conradi (1987), Flow velocity measurement with ac Gradients, *Magn. Res. in Med. 4, 274-281.*

Glossary of Medical Terms

Angiogram	X-ray picture in which the contents of the blood vessels have been rendered radio-opaque by the injection of a contrast medium.
Angioplastic surgery	Surgery of the blood vessel which increase the lumen.
Angioplasty	see *angioplastic surgery*
Aorta	see *heart*
Arteries	Vessels carrying the blood from the left or right ventricles to the tissues.
Atheroma	see *atherosclerosis*
Atherosclerosis, arteriosclerosis	Varieties of degenerative disease of the arteries; atheroma is a fatty degeneration of the inner layers of an artery; in the early stages intimal plaques of atheromatous material may be visible.
Blood	Blood is a suspension of cells in the fluid plasma. The cells comprise the red cells (erythrocytes), white cells (leucocytes) and the platelets (thrombocytes), the average number of each per mm^3 of blood being about $5{\cdot}10^6$, $1{\cdot}10^4$, and $3{\cdot}10^5$, respectively.
Cancerogene	Materials that cause the development of cancer.
Carotid arteries	Pair of major arteries and their branches that originate off the aortic arch and travel through neck and head to supply blood to the brain.
Catheter	Medical instrument in form of a pipe; is inserted in blood vessels; mostly used to release contrast medium. It can also carry surgical tools and probes
Cholesterol	A compound made in the human body (and also which composes part of certain foods, notably some animal fat, especially beef fat) which is associated with deposits within arteries (atherosclerosis) and causes heart disease if deposited in the coronary arteries.
Coronary arteries	see *heart*
Diastole	The resting phase of the heart.
Femoral artery	Main artery in the leg.
Haematocrit	The relative volume of the cells in blood, normally about 45%.

Heart	The mammalian heart consists of four chambers, left and right atria, right and left ventricles. The atria are thin walled chambers into which blood flows at low pressure from the veins. Between atria and ventricles are the tricuspid (right) and mitral (left) valves. Blood at high pressure leaves the ventricles by the pulmonary artery (right) and aorta (left); there are valves at the origin of each of these. The blood supply to the heart itself comes from the coronary arteries which spring from the aorta at its origin. Normally both atria beat together a short time before the synchronous beat of the ventricles.
Heart attack	Sections of the entire heart do not function any more due to an infarct.
Infarct	Area of dead tissue resulting from inadequate blood flow.
Intima	The innermost coat of a blood vessel.
Invasive	Medical procedure that actually invades the patient's body.
Lipoid material	Material of mixed composition, but with all of its parts some sort of lipid (i.e. fat).
Lipophages	Cells which consume fat (i.e. which "eat" lipid). They will remove certain fat deposits in the body.
Media	The middle coat of a blood vessel, generally the thickest.
Plasma	see *blood*
Reduced lumen	Flow area inside atheroma relative to the original flow area of the vessel.
Renal artery	The artery which goes from the aorta to the kidneys and supplies most of the kidneys' blood (there are left and right renal arteries supplying the left and right kidneys). If they suffer atherosclerosis there is a reduced blood supply to the kidneys and one serious consequence is dangerously high blood pressure.
Stenosis	A narrowing of a blood vessel or a valve.
Systole	The active part of the heart cycle.
Veins	The vessels carrying blood from the tissues to the atria of the heart.
Ventricles	see *heart*

Experimental Data

The numerical data of all the experiments performed is collected in this appendix. An overview in form of a table is given first. This table states hardware *settings* that differ to the reference setting of experiment 1-1 only. Any other differences ~~to~~ *in* the reference case can be found under *remarks*.

experiment	date	z-locations	number of r-locations	blockage dimensions L – D [mm]; L* - A* [/]	other settings	remarks
0-1	28.4.	z3	13	/	no settling chamber	V_{rate} ~15.3cm
0-2	29.4.	z1 – z3	15	/	no settling chamber	V_{rate} ~15.3cm
0-3	30.4.	z1	15	/	no settling chamber, no straightening section, different flexible pipes	V_{rate} ~15.3cm
0-4	8.5.	z1	15	/	no straightening section	V_{rate} ~14.8cm
0-5	15.5.	z1 – z3	15	/	no straightening section, different flexible pipes	V_{rate} ~15.6cm
0-6	20.5.	z1 – z3, z9	15	/		V_{rate} ~15.4cm
1-1	**2.7.**	**z1 – z9**	**15**	/		**REFERENCE**
1-2	2.7.	z1 – z9	15	/	no settling chamber	
1-3	3.7.	z1 – z9	15	5 – 32; 0.11 – 0.48	PVC-blockage	
1-4	3.7.	z1 – z9	15	92 – 32; 2 – 0.48	PVC-blockage	
1-5	7.7.	z1 – z9	15	92 – 32; 2 – 0.48	prestix-blockage	
1-6	8.7.	z1 – z9	15	46 – 32; 1 – 0.48	prestix-blockage	
1-7	19.8.	z1 – z4	15	/	probe horizontal, pipe turned 90° to the left	
1-8	26.8.	z1 – z4	15	/	probe horizontal, pipe turned 90° to the right	
2-1	10.7.	z1 – z9	15	46 – 40; 1 – 0.76	prestix-blockage	
2-2	8.7.	z1 – z9	15	46 – 32; 1 – 0.48	prestix-blockage	same as exp. 1-6
2-3	10.7.	z1 – z9	15	46 – 26; 1 – 0.32	prestix-blockage	
2-4	13.7.	z1 – z9	15	46 – 20; 1 – 0.19	prestix-blockage	

3-1	9.7.	z1 – z9	15	46 - *; 1 – 0.5	wooden-blockage bottom, * not circular	
3-2	9.7.	z1 – z9	15	46 - *; 1 – 0.5	wooden-blockage top, * not circular	
3-3	9.7.	z1 – z9	15	46 - *; 1 – 0.5	wooden-blockage left, * not circular	
3-4	9.7.	z1 – z9	15	46 - *; 1 – 0.5	wooden-blockage right, * not circular	
4	19.8.	p1 – p3		/, 46 - * 5 – 40, -32, -26, -20 46 – 40, -20 92 – 32		pressure loss measurement with different blockages

Table C-1: experiments performed

In the following section, the spreadsheets and the corresponding graph of velocity over radius is given for every experiment.

Experiment No 0-1

Date	28.04.												
Time	6:30am												
T ambient	20.9 C												
U (flowrate=0)	4.328V												
Flowrate	15.3cm												
Axial Location	z3												
Location x [mm]	-23	-22	-20	-17	-15	-10	0	10	15	17	20	22	23
Voltage [V]	5.55	5.66	5.86	6.03	6.1	6.22	6.28	6.05	5.66	5.42	4.97	4.8	4.97
velocity [m/s]	0.324	0.386	0.519	0.657	0.721	0.842	0.908	0.675	0.386	0.261	0.101	0.058	0.101

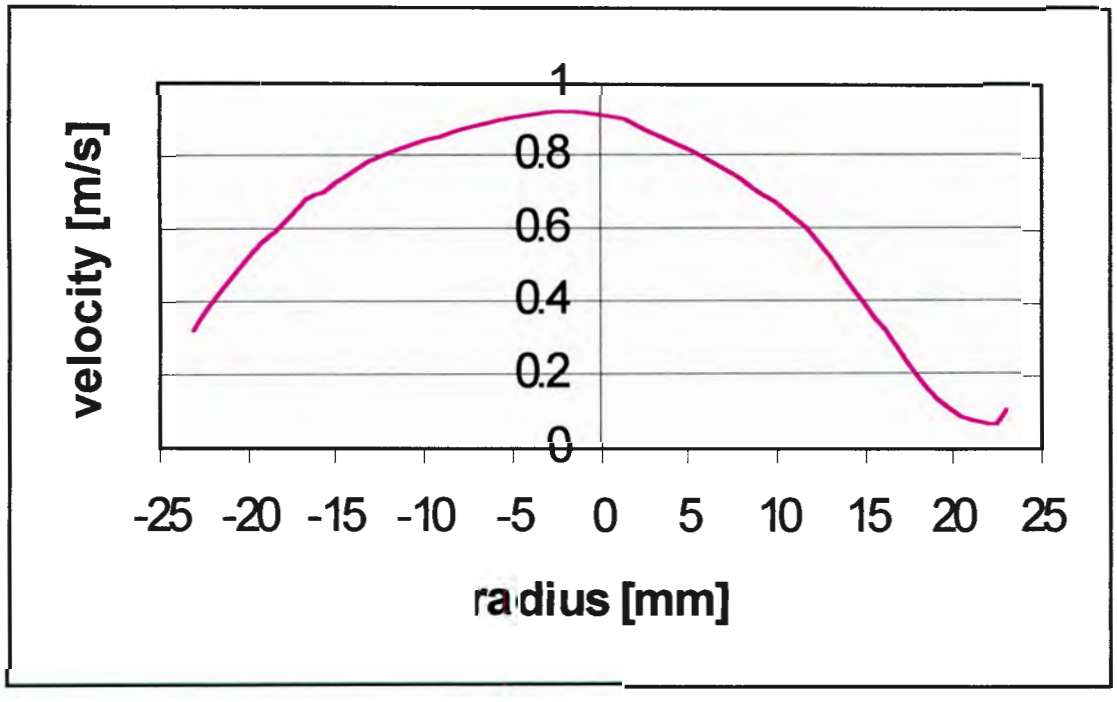

Experiment No 0-2

Date	29.04.
Time	0:00am
T ambient	21.2 C
U (flowrate=0)	4.334V
Flowrate	15.3cm

Axial Location	Z1														
Location x [mm]	-23	-22	-20	-17	-15	-10	-5	0	5	10	15	17	20	22	23
Voltage [V]	6.8	7	6.8	6	5.6	5.2	5	5	5	5	4.9	4.7	4.8	5	5
velocity [m/s]	1.67	2.07	1.67	0.63	0.35	0.17	0.11	0.11	0.11	0.11	0.08	0.04	0.06	0.11	0.11

Axial Location	Z2														
Location x [mm]	-23	-22	-20	-17	-15	-10	-5	0	5	10	15	17	20	22	23
Voltage [V]	5.35	5.42	5.58	5.73	5.8	5.9	5.99	6.06	6.08	6.03	5.78	5.49	5.26	5.23	5.17
velocity [m/s]	0.23	0.26	0.34	0.43	0.48	0.55	0.62	0.68	0.70	0.66	0.46	0.29	0.19	0.18	0.16

Axial Location	Z3														
Location x [mm]	-23	-22	-20	-17	-15	-10	-5	0	5	10	15	17	20	22	23
Voltage [V]	5.41	5.52	5.68	5.84	5.91	6.01	6.06	6.14	6.17	6.12	5.83	5.5	4.92	4.68	4.63
velocity [m/s]	0.26	0.31	0.40	0.50	0.56	0.64	0.68	0.76	0.79	0.74	0.50	0.30	0.09	0.03	0.02

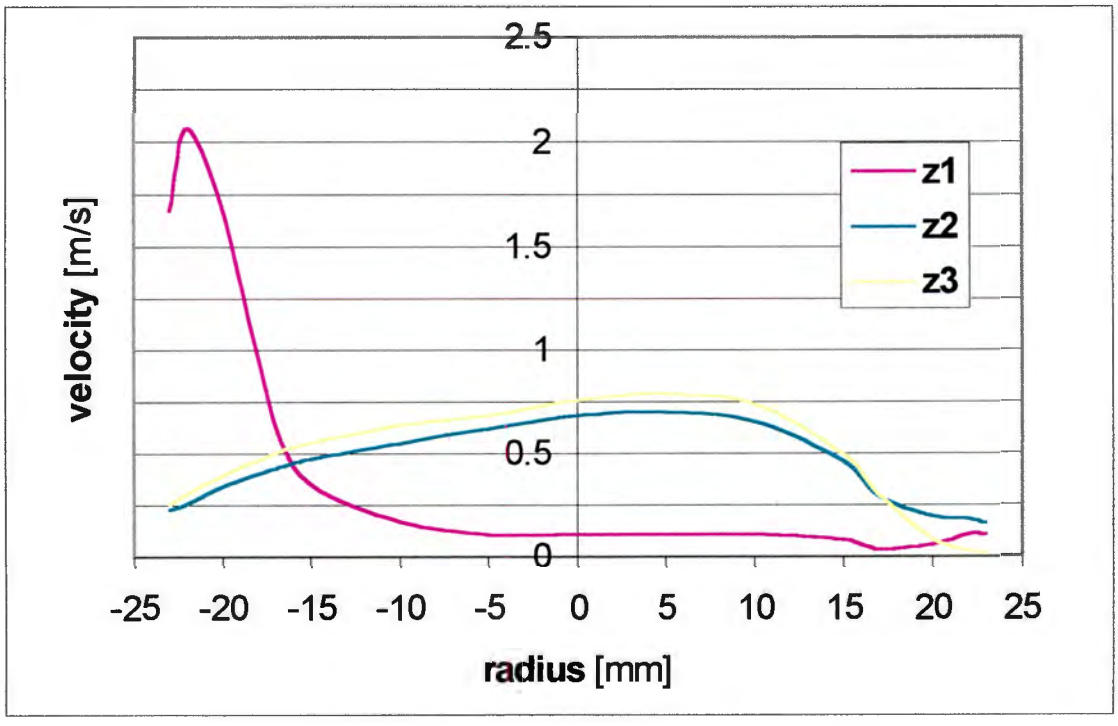

Experiment No 0-3

Date	30.04.98
Time	11:30pm
T ambient	21.1 C
Flowrate	15.3cm

without straightening section

Location Z Nr1															
Location x [mm]	-23	-22	-20	-17	-15	-10	-5	0	5	10	15	17	20	22	23
Voltage [V]	7.3	7.3	7.2	7	6.9	6.5	6.4	6.4	6.4	6.4	6.3	6.2	5.8	5.4	5.3
velocity [m/s]	2.80	2.80	2.53	2.07	1.86	1.19	1.05	1.05	1.05	1.05	0.93	0.82	0.48	0.25	0.21

without straightening section, longer elastic pipe

Location Z Nr1															
Location x [mm]	-23	-22	-20	-17	-15	-10	-5	0	5	10	15	17	20	22	23
Voltage [V]	6.6	6.5	6.5	6.5	6.5	6.6	6.5	6.6	6.7	7	7.3	7.4	6.5	5.5	5.3
velocity [m/s]	1.33	1.19	1.19	1.19	1.19	1.33	1.19	1.33	1.49	2.07	2.80	3.08	1.19	0.30	0.21

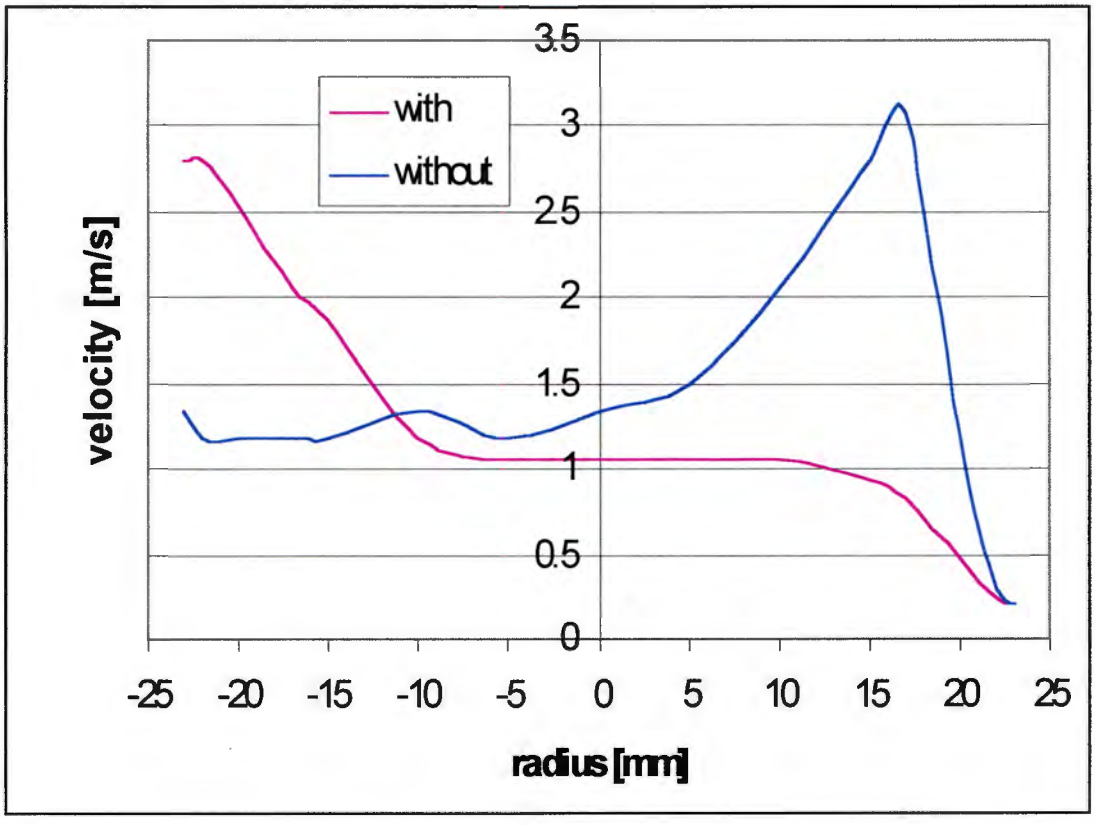

Experiment No 0-4

Date	08.05.
Time	11:45am
T ambient	19.5°C
Flowrate	14.8cm

with settling chamber, first measurement

Location Z Nr1															
Location x [mm]	-23	-22	-20	-17	-15	-10	-5	0	5	10	15	17	20	22	23
Voltage [V]	5.7	5.8	5.9	5.9	5.9	5.9	5.9	5.9	5.9	5.9	5.8	5.7	5	4.6	4.6
velocity [m/s]	0.41	0.48	0.55	0.55	0.55	0.55	0.55	0.55	0.55	0.55	0.48	0.41	0.11	0.01	0.01

with settling chamber, second measurement

Location Z Nr1															
Location x [mm]	-23	-22	-20	-17	-15	-10	-5	0	5	10	15	17	20	22	23
Voltage [V]	5.7	5.8	5.9	5.9	5.9	5.9	5.9	5.9	5.8	5.8	5.7	5.5	4.9	4.6	4.6
velocity [m/s]	0.41	0.48	0.55	0.55	0.55	0.55	0.55	0.55	0.48	0.48	0.41	0.30	0.08	0.01	0.01

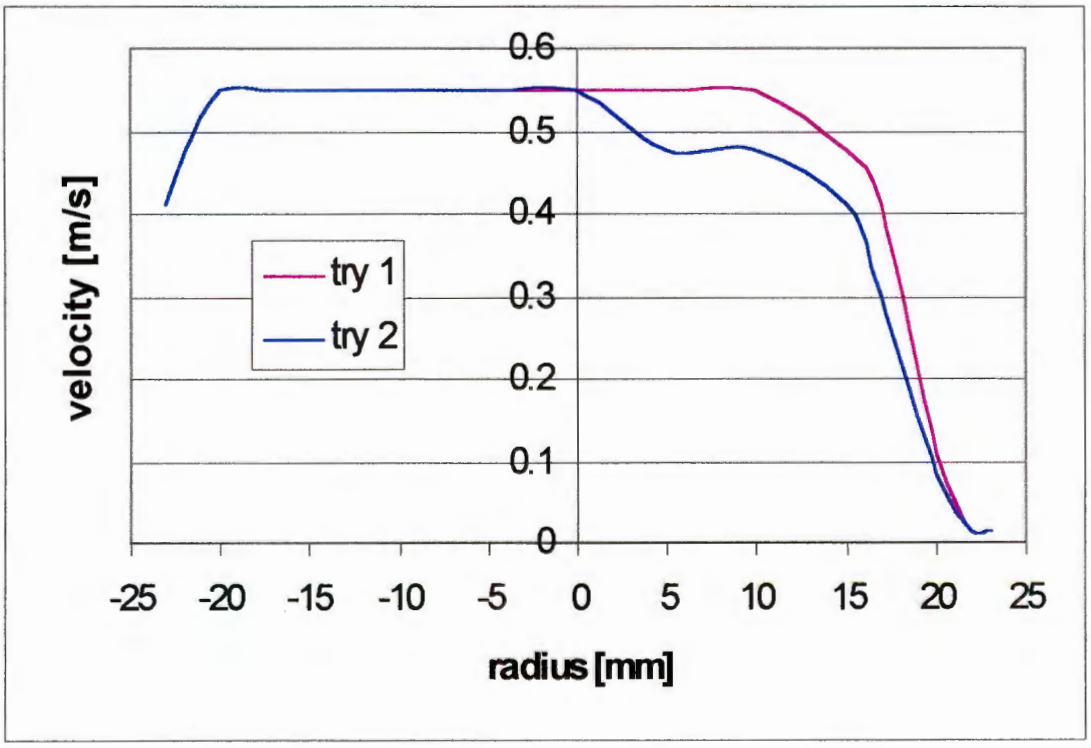

Experiment No 0-5

Date:	15.05.
Time:	13:30

Conditions	
T [°C]	20.6
$p_{ambient}$ [mmHg]	757.5
$p_{ambient}$ [Pa]	100747.5

Flowrate [cm]	15.6
Flowrate [l/min]	61.718
mean velocity [m/s]	0.619
Re [/]	1879.137

blockage type:	/						**changed bent in flex.pipe**	
z-location:	z1		z2		z3		z3	
r-koordinate [mm]	Voltage [V]	velocity 1	Voltage [V]	velocity 2	Voltage [V]	velocity 3	Voltage [V]	velocity 4
-23	5.7	0.410	5.3	0.210	5.3	0.210	5.3	0.210
-22	5.8	0.476	5.4	0.252	5.4	0.252	5.5	0.299
-20	5.8	0.476	5.6	0.351	5.6	0.351	5.6	0.351
-17	5.8	0.476	5.7	0.410	5.7	0.410	5.8	0.476
-15	5.8	0.476	5.8	0.476	5.8	0.476	5.8	0.476
-10	5.8	0.476	5.9	0.549	5.9	0.549	5.9	0.549
-5	5.8	0.476	5.9	0.549	6	0.631	6	0.631
0	5.8	0.476	6	0.631	6.1	0.721	6.1	0.721
5	5.8	0.476	6	0.631	6.1	0.721	6.1	0.721
10	5.8	0.476	6	0.631	6	0.631	6	0.631
15	5.7	0.410	5.8	0.476	5.7	0.410	5.7	0.410
17	5.6	0.351	5.5	0.299	5.4	0.252	5.4	0.252
20	5.5	0.299	5.2	0.172	5	0.109	5	0.109
22	5.3	0.210	5.2	0.172	4.8	0.058	4.8	0.058
23	5.3	0.210	5.2	0.172	4.8	0.058	4.8	0.058

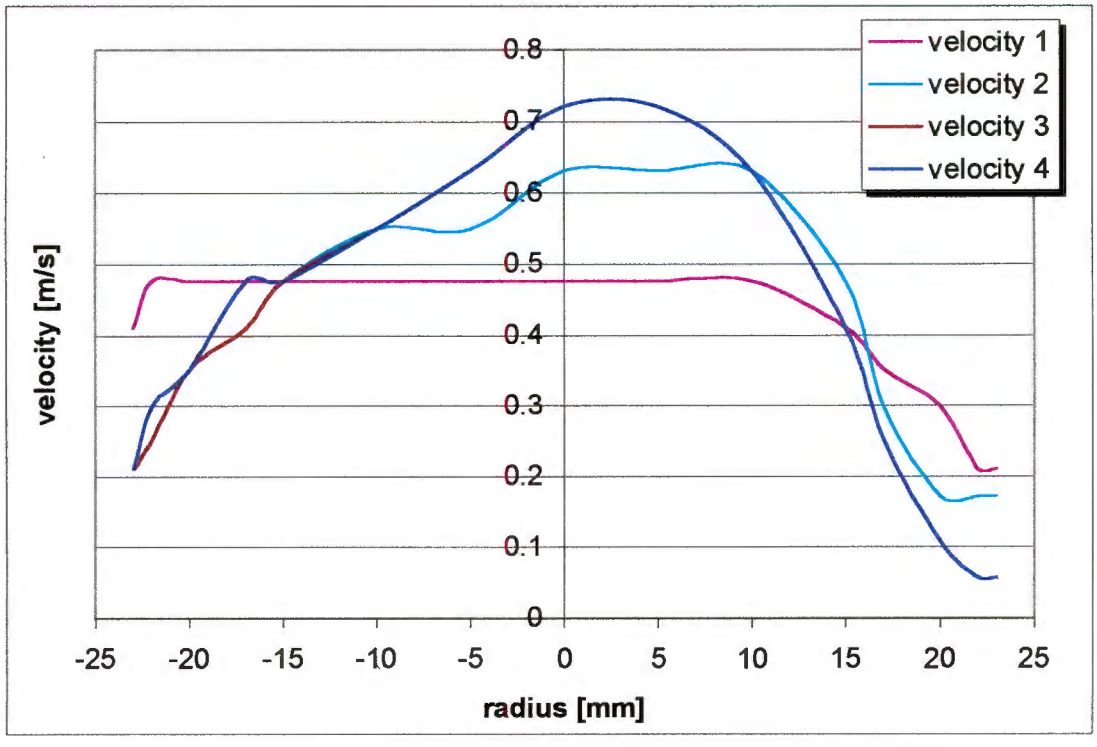

Experiment No 0-6

Date:	20.05.
Time:	1:30

Conditions				
T [C]	19.5		Flowrate [cm]	15.4
$p_{ambient}$ [mmHg]	755		Flowrate [l/min]	60.912
$p_{ambient}$ [Pa]	100415		mean velocity [m/s]	0.611
			Re [/]	1854.575

blockage type:	/							
z-location:	z1		z2		z3		Z9	
r-coordinate [mm]	Voltage [V]	velocity 1	Voltage [V]	velocity 2	Voltage [V]	velocity 3	Voltage [V]	velocity 4
-23	5.5	0.30	5.2	0.17	5.3	0.21	5.2	0.17
-22	5.6	0.35	5.3	0.21	5.3	0.21	5.3	0.21
-20	5.7	0.41	5.4	0.25	5.5	0.30	5.5	0.30
-17	5.66	0.39	5.5	0.30	5.6	0.35	5.6	0.35
-15	5.6	0.35	5.6	0.35	5.7	0.41	5.7	0.41
-10	5.7	0.41	5.7	0.41	5.8	0.48	5.8	0.48
-5	5.7	0.41	5.8	0.48	5.9	0.55	5.9	0.55
0	5.6	0.35	5.8	0.48	5.9	0.55	5.9	0.55
5	5.5	0.30	5.9	0.55	5.9	0.55	5.9	0.55
10	5.5	0.30	5.8	0.48	5.8	0.48	5.8	0.48
15	5.5	0.30	5.5	0.30	5.5	0.30	5.4	0.25
17	5.3	0.21	5.2	0.17	5.2	0.17	5.1	0.14
20	4.8	0.06	4.7	0.04	4.7	0.04	4.6	0.01
22	4.6	0.01	4.5	0.00	4.6	0.01	4.5	0.00
23	4.6	0.01	4.6	0.01	4.7	0.04	4.5	0.00

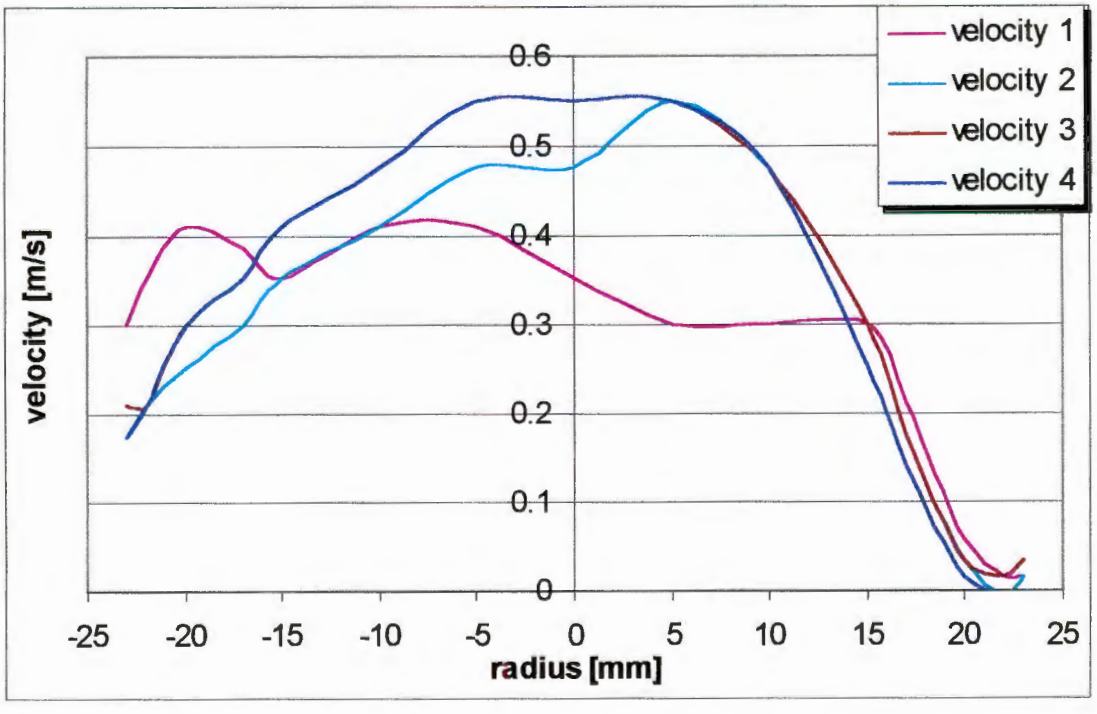

Experiment No 1-1

Date:	02.07.						
Time:	21:00						
Conditions							
T [C]	17		Flowrate [cm]	12		A* [/]	0.48
$p_{ambient}$ [mmHg]	757		Flowrate [l/min]	47.440		L* [/]	1
$p_{ambient}$ [Pa]	100681		mean velocity [m/s]	0.476		w* [m/s]	0.9912
			Re [/]	1444.3		Re* [/]	2084.8

blockage type:	no blockage																	
z-location:	1		2		3		4		5		6		7		8		9	
r-koordinate [mm]	Voltage [V]	Vel. Z 1	Voltage [V]	Ve. Z 2	Voltage [V]	Vel. Z 3	Voltage [V]	Vel. Z 4	Voltage [V]	Vel. Z 5	Voltage [V]	Vel. Z 6	Voltage [V]	Vel. Z 7	Voltage [V]	Vel. Z 8	Voltage [V]	Vel. Z 9
-23	5.63	0.37	5.33	0.22	5.33	0.22	5.33	0.22	5.38	0.24	5.33	0.22	5.36	0.23	5.36	0.23	5.39	0.25
-22	5.75	0.44	5.39	0.25	5.43	0.27	5.47	0.28	5.50	0.30	5.48	0.29	5.47	0.28	5.44	0.27	5.49	0.29
-20	5.84	0.50	5.52	0.31	5.57	0.34	5.61	0.36	5.64	0.37	5.62	0.36	5.61	0.36	5.59	0.35	5.63	0.37
-17	5.73	0.43	5.65	0.38	5.71	0.42	5.75	0.44	5.78	0.46	5.76	0.45	5.74	0.44	5.75	0.44	5.78	0.46
-15	5.76	0.45	5.71	0.42	5.80	0.48	5.83	0.50	5.84	0.50	5.83	0.50	5.82	0.49	5.82	0.49	5.84	0.50
-10	5.78	0.46	5.82	0.49	5.90	0.55	5.93	0.57	5.93	0.57	5.92	0.56	5.92	0.56	5.91	0.56	5.93	0.57
-5	5.86	0.52	5.89	0.54	6.00	0.63	6.00	0.63	6.00	0.63	5.99	0.62	6.00	0.63	5.99	0.62	6.01	0.64
0	5.75	0.44	5.97	0.61	6.06	0.68	6.05	0.67	6.05	0.67	6.04	0.67	6.06	0.68	6.05	0.67	6.05	0.67
5	5.65	0.38	6.02	0.65	6.06	0.68	6.04	0.67	6.04	0.67	6.05	0.67	6.07	0.69	6.06	0.68	6.06	0.68
10	5.67	0.39	6.02	0.65	5.96	0.60	5.90	0.55	5.92	0.56	5.95	0.59	6.00	0.63	5.98	0.61	5.95	0.59
15	5.68	0.40	5.77	0.46	5.60	0.35	5.56	0.33	5.54	0.32	5.60	0.35	5.63	0.37	5.63	0.37	5.58	0.34
17	5.68	0.40	5.48	0.29	5.32	0.22	5.27	0.20	5.26	0.19	5.32	0.22	5.33	0.22	5.37	0.24	5.26	0.19
20	5.53	0.31	5.32	0.22	5.00	0.11	4.94	0.09	4.90	0.08	4.93	0.09	4.92	0.09	4.90	0.08	4.82	0.06
22	5.37	0.24	5.20	0.17	4.83	0.06	4.71	0.04	4.63	0.02	4.72	0.04	4.76	0.05	4.74	0.04	4.67	0.03
23	5.31	0.21	5.16	0.16	4.79	0.06	4.71	0.04	4.66	0.03	4.65	0.02	4.68	0.03	4.68	0.03	4.64	0.02

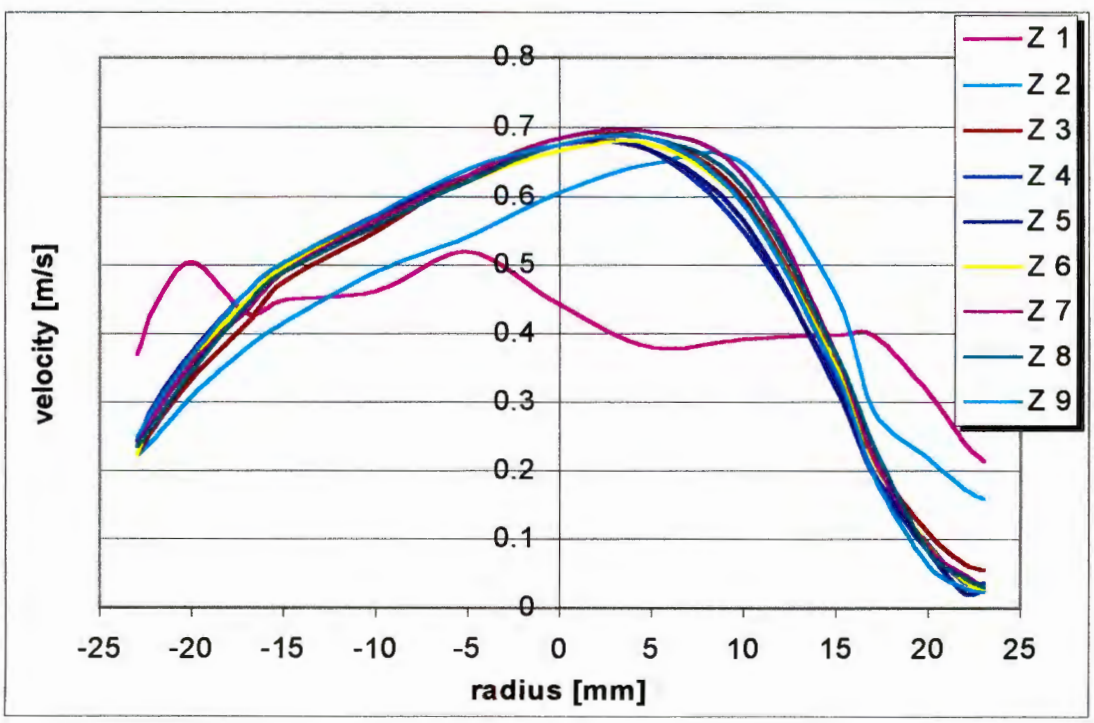

Experiment No 1-2

Date:	02.07.						
Time:	22:00						
Conditions							
T [C]	17		Flowrate [cm]	12		A* [/]	0.48
$p_{ambient}$ [mmHg]	757		Flowrate [l/min]	47.440		L* [/]	1
$p_{ambient}$ [Pa]	100681		mean velocity [m/s]	0.476		w* [m/s]	0.9912
			Re [/]	1444.3		Re* [/]	2084.8

blockage type:	no blockage, no settling chamber																	
z-location:	1		2		3		4		5		6		7		8		9	
r-koordinate [mm]	Voltage [V]	vel. 1	Voltage [V]	vel. 2	Voltage [V]	vel. 3	Voltage [V]	vel.4	Voltage [V]	vel. 5	Voltage [V]	vel. 6	Voltage [V]	vel. 7	Voltage [V]	vel. 8	Voltage [V]	vel. 9
-23	4.8	0.06	5.35	0.23	5.32	0.22	5.34	0.23	5.34	0.23	5.38	0.24	5.35	0.23	5.37	0.24	5.41	0.26
-22	4.9	0.08	5.45	0.27	5.45	0.27	5.44	0.27	5.48	0.29	5.49	0.29	5.47	0.28	5.49	0.29	5.52	0.31
-20	4.9	0.08	5.57	0.34	5.59	0.35	5.59	0.35	5.61	0.36	5.62	0.36	5.61	0.36	5.62	0.36	5.65	0.38
-17	5.1	0.14	5.70	0.41	5.74	0.44	5.74	0.44	5.75	0.44	5.76	0.45	5.75	0.44	5.75	0.44	5.79	0.47
-15	4.9	0.08	5.78	0.46	5.81	0.48	5.81	0.48	5.83	0.50	5.82	0.49	5.82	0.49	5.83	0.50	5.86	0.52
-10	5.1	0.14	5.86	0.52	5.91	0.56	5.92	0.56	5.93	0.57	5.91	0.56	5.93	0.57	5.92	0.56	5.95	0.59
-5	5.3	0.21	5.92	0.56	5.99	0.62	6.00	0.63	6.00	0.63	6.00	0.63	6.01	0.64	6.00	0.63	6.03	0.66
0	5.3	0.21	5.99	0.62	6.06	0.68	6.04	0.67	6.07	0.69	6.07	0.69	6.07	0.69	6.06	0.68	6.09	0.71
5	5.5	0.30	6.04	0.67	6.09	0.71	6.03	0.66	6.11	0.73	6.10	0.72	6.10	0.72	6.09	0.71	6.10	0.72
10	5.7	0.41	6.02	0.65	6.05	0.67	6.06	0.68	6.05	0.67	6.05	0.67	6.05	0.67	6.04	0.67	6.03	0.66
15	5.9	0.55	5.73	0.43	5.75	0.44	5.77	0.46	5.73	0.43	5.72	0.42	5.72	0.42	5.70	0.41	5.65	0.38
17	6	0.63	5.46	0.28	5.38	0.24	5.48	0.29	5.45	0.27	5.40	0.25	5.43	0.27	5.39	0.25	5.38	0.24
20	5.7	0.41	5.29	0.21	4.97	0.10	4.99	0.11	5.00	0.11	4.96	0.10	4.95	0.10	4.97	0.10	4.82	0.06
22	5.3	0.21	5.14	0.15	4.83	0.06	4.68	0.03	4.79	0.06	4.75	0.05	4.72	0.04	4.74	0.04	4.73	0.04
23	5.2	0.17	5.02	0.11	4.73	0.04	4.62	0.02	4.73	0.04	4.72	0.04	4.65	0.02	4.66	0.03	4.61	0.02

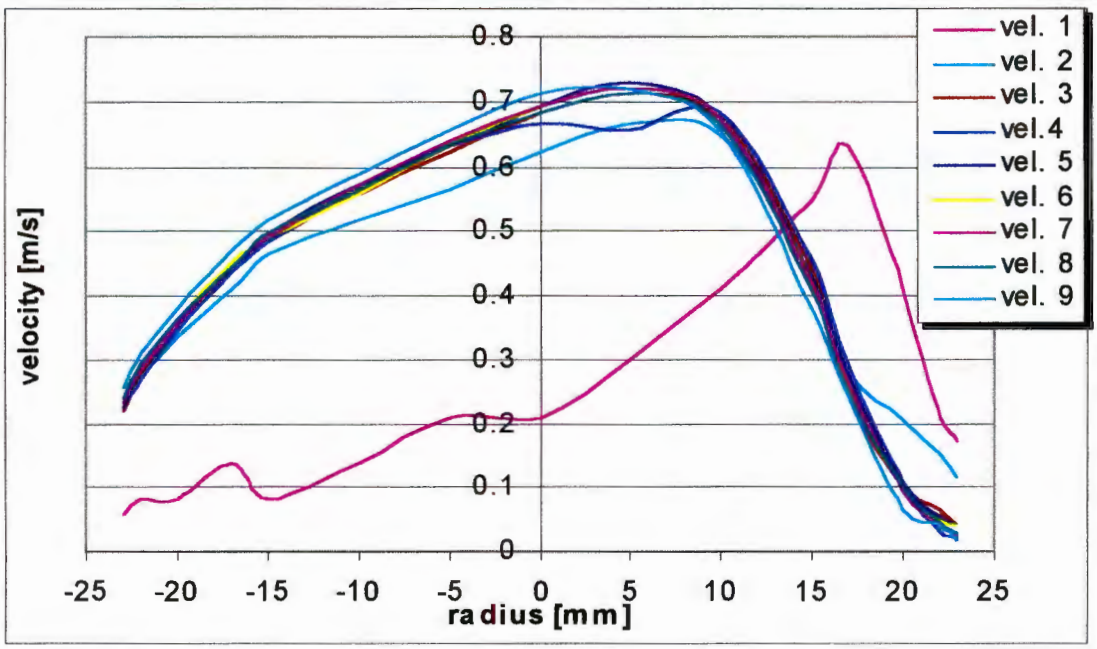

Experiment No 1-3

Date:	03.07.						
Time:	15:00						
Conditions							
T [C]	16.5		Flowrate [cm]	12		A* [/]	0.48
$p_{ambient}$ [mmHg]	757.5		Flowrate [l/min]	47.440		L* [/]	0.11
$p_{ambient}$ [Pa]	100748		mean vel. w [m/s]	0.476		w* [m/s]	0.9912
			Re [/]	1444.39		Re* [/]	2084.80

blockage type:	ring																	
z-location:	1		2		3		4		5		6		7		8		9	
r-koordinate [mm]	Voltage [V]	vel. 1	Voltage [V]	vel. 2	Voltage [V]	vel. 3	Voltage [V]	vel.4	Voltage [V]	vel. 5	Voltage [V]	vel. 6	Voltage [V]	vel. 7	Voltage [V]	vel. 8	Voltage [V]	vel. 9
-23	5.69	0.40	5.35	0.23	5.36	0.23	4.99	0.11	5.26	0.19	5.34	0.23	5.43	0.27	5.50	0.30	5.53	0.31
-22	5.82	0.49	5.45	0.27	5.45	0.27	5.07	0.13	5.44	0.27	5.49	0.29	5.56	0.33	5.64	0.37	5.63	0.37
-20	5.91	0.56	5.60	0.35	5.60	0.35	5.41	0.26	5.75	0.44	5.80	0.48	5.65	0.38	5.72	0.42	5.76	0.45
-17	5.79	0.47	5.74	0.44	5.74	0.44	6.12	0.74	6.17	0.79	6.06	0.68	5.81	0.48	5.78	0.46	5.82	0.49
-15	5.84	0.50	5.82	0.49	5.81	0.48	6.27	0.90	6.26	0.89	6.16	0.78	5.92	0.56	5.81	0.48	5.83	0.50
-10	5.84	0.50	5.92	0.56	5.92	0.56	6.33	0.97	6.32	0.95	6.24	0.86	6.07	0.69	5.88	0.53	5.84	0.50
-5	5.92	0.56	6.01	0.64	6.02	0.65	6.36	1.00	6.36	1.00	6.28	0.91	6.12	0.74	5.92	0.56	5.85	0.51
0	5.81	0.48	6.07	0.69	6.08	0.70	6.38	1.03	6.39	1.04	6.29	0.92	6.04	0.67	5.87	0.53	5.84	0.50
5	5.69	0.40	6.09	0.71	6.10	0.72	6.36	1.00	6.36	1.00	6.12	0.74	5.82	0.49	5.83	0.50	5.82	0.49
10	5.71	0.42	5.99	0.62	5.98	0.61	6.09	0.71	5.92	0.56	5.60	0.35	5.56	0.33	5.72	0.42	5.78	0.46
15	5.74	0.44	5.63	0.37	5.62	0.36	4.62	0.02	4.78	0.05	5.15	0.16	5.38	0.24	5.61	0.36	5.68	0.40
17	5.72	0.42	5.35	0.23	5.36	0.23	4.54	0.00	4.71	0.04	5.04	0.12	5.15	0.16	5.45	0.27	5.41	0.26
20	5.63	0.37	5.17	0.16	5.19	0.17	4.67	0.03	4.69	0.03	4.73	0.04	4.90	0.08	5.08	0.13	4.99	0.11
22	5.52	0.31	5.07	0.13	5.14	0.15	4.76	0.05	4.73	0.04	4.54	0.00	4.80	0.06	4.86	0.07	4.74	0.04
23	5.41	0.26	5.02	0.11	5.13	0.15	4.74	0.04	4.69	0.03	4.53	0.00	4.78	0.05	4.83	0.06	4.69	0.03

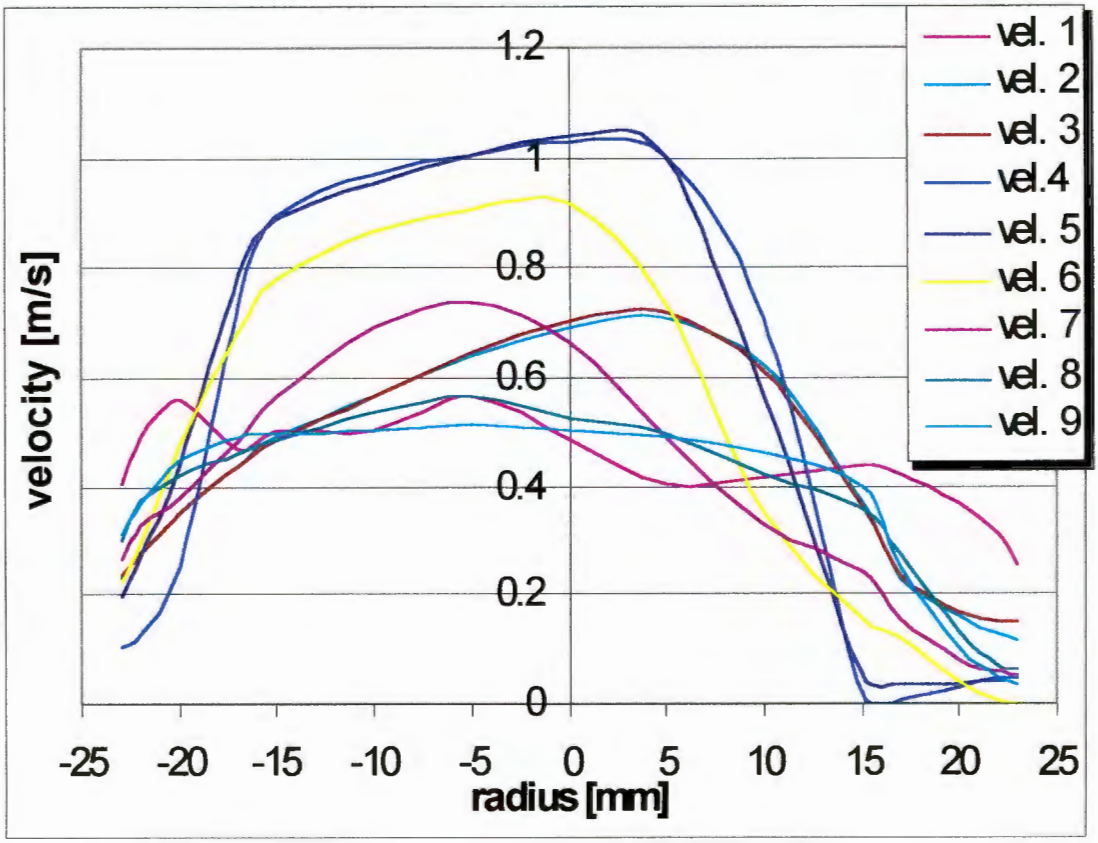

Experiment No 1-4

Date:	03.07.						
Time:	16:30						
Conditions							
T [C]	16.5		Flowrate [cm]	12		A* [/]	0.48
$p_{ambient}$ [mmHg]	757.5		Flowrate [l/min]	47.440		L* [/]	2
$p_{ambient}$ [Pa]	100748		mean vel. w [m/s]	0.476		w* [m/s]	0.9912
			Re [/]	1444.39		Re* [/]	2084.80

blockage type:	long smooth

z-location:	1		2		3		4		5		6		7		8		9	
r-koordinate [mm]	Voltage [V]	vel. 1	Voltage [V]	vel. 2	Voltage [V]	vel. 3	Voltage [V]	vel.4	Voltage [V]	vel. 5	Voltage [V]	vel. 6	Voltage [V]	vel. 7	Voltage [V]	vel. 8	Voltage [V]	vel. 9
-23	5.65	0.38	5.53	0.31	5.35	0.23	4.99	0.11	5.08	0.13	5.07	0.13	5.10	0.14	4.95	0.10	5.62	0.36
-22	5.79	0.47	5.59	0.35	5.47	0.28	5.06	0.13	5.23	0.18	5.25	0.19	5.19	0.17	5.08	0.13	5.64	0.37
-20	5.87	0.53	5.68	0.40	5.61	0.36	5.39	0.25	5.55	0.32	5.53	0.31	5.37	0.24	5.24	0.19	5.75	0.44
-17	5.76	0.45	5.81	0.48	5.75	0.44	6.00	0.63	6.05	0.67	5.97	0.61	5.82	0.49	5.47	0.28	5.79	0.47
-15	5.79	0.47	5.86	0.52	5.82	0.49	6.21	0.83	6.19	0.81	6.12	0.74	6.02	0.65	5.61	0.36	5.79	0.47
-10	5.81	0.48	5.93	0.57	5.92	0.56	6.34	0.98	6.32	0.95	6.28	0.91	6.24	0.86	5.95	0.59	5.82	0.49
-5	5.90	0.55	5.99	0.62	6.00	0.63	6.38	1.03	6.37	1.02	6.34	0.98	6.31	0.94	6.19	0.81	5.84	0.50
0	5.78	0.46	6.05	0.67	6.07	0.69	6.42	1.08	6.41	1.07	6.38	1.03	6.36	1.00	6.25	0.87	5.87	0.53
5	5.67	0.39	6.06	0.68	6.10	0.72	6.42	1.08	6.41	1.07	6.39	1.04	6.38	1.03	6.22	0.84	5.86	0.52
10	5.69	0.40	5.94	0.58	6.04	0.67	6.20	0.82	6.12	0.74	6.16	0.78	6.20	0.82	6.03	0.66	5.81	0.48
15	5.72	0.42	5.47	0.28	5.71	0.42	4.81	0.06	4.90	0.08	5.15	0.16	5.45	0.27	5.56	0.33	5.72	0.42
17	5.73	0.43	5.41	0.26	5.46	0.28	4.53	0.00	4.59	0.01	4.66	0.03	4.96	0.10	5.37	0.24	5.52	0.31
20	5.65	0.38	5.36	0.23	5.16	0.16	4.57	0.01	4.74	0.04	4.70	0.04	4.68	0.03	4.88	0.08	5.06	0.13
22	5.51	0.30	5.26	0.19	5.06	0.13	4.77	0.05	4.76	0.05	4.76	0.05	4.72	0.04	4.58	0.01	4.78	0.05
23	5.48	0.29	5.19	0.17	5.05	0.12	4.71	0.04	4.74	0.04	4.72	0.04	4.70	0.04	4.54	0.00	4.73	0.04

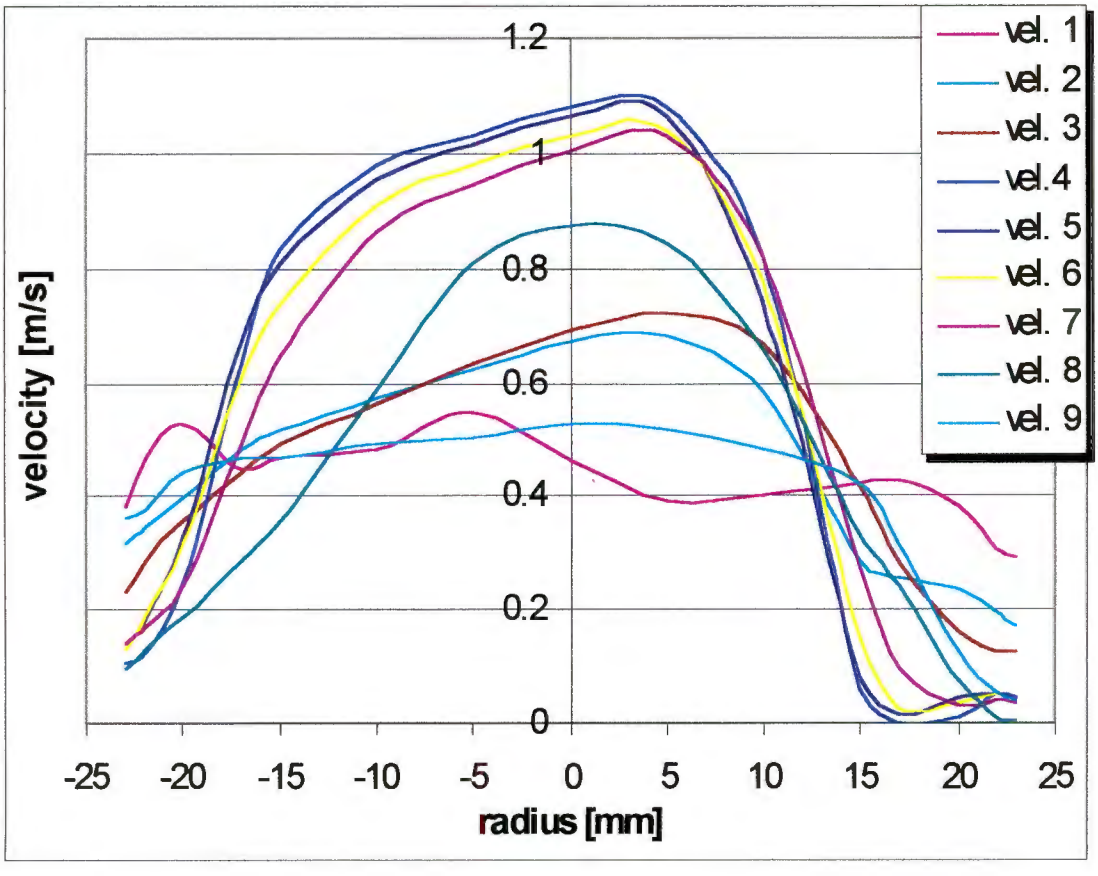

Experiment No 1-5

Date:	07.07.98							
Time:	11:30							
Conditions								
T [C]	16.3		Flowrate [cm]	12		A* [/]	0.48	
$p_{ambient}$ [mmHg]	756.5		Flowrate [l/min]	47.440		L* [/]	2	
$p_{ambient}$ [Pa]	100615		mean vel. w [m/s]	0.476		w* [m/s]	0.9912	
			Re [/]	1444.39		Re* [/]	2084.80	

blockage type:	long prestix																	
z-location:	1		2		3		4		5		6		7		8		9	
r-koordinate [mm]	Voltage [V]	vel. 1	Voltage [V]	vel. 2	Voltage [V]	vel. 3	Voltage [V]	vel.4	Voltage [V]	vel. 5	Voltage [V]	vel. 6	Voltage [V]	vel. 7	Voltage [V]	vel. 8	Voltage [V]	vel. 9
-23	5.74	0.44	5.43	0.27	5.41	0.26	5.10	0.14	5.17	0.16	5.23	0.18	5.30	0.21	5.45	0.27	5.61	0.36
-22	5.87	0.53	5.52	0.31	5.54	0.32	5.22	0.18	5.31	0.21	5.31	0.21	5.41	0.26	5.54	0.32	5.73	0.43
-20	5.96	0.60	5.67	0.39	5.68	0.40	5.61	0.36	5.68	0.40	5.58	0.34	5.56	0.33	5.61	0.36	5.80	0.48
-17	5.84	0.50	5.82	0.49	5.83	0.50	6.16	0.78	6.13	0.75	6.03	0.66	5.78	0.46	5.76	0.45	5.84	0.50
-15	5.86	0.52	5.89	0.54	5.91	0.56	6.28	0.91	6.27	0.90	6.18	0.80	5.95	0.59	5.78	0.46	5.85	0.51
-10	5.88	0.53	5.99	0.62	6.03	0.66	6.37	1.02	6.36	1.00	6.30	0.93	6.15	0.77	5.87	0.53	5.85	0.51
-5	5.97	0.61	6.08	0.70	6.11	0.73	6.42	1.08	6.41	1.07	6.36	1.00	6.23	0.85	5.96	0.60	5.89	0.54
0	5.87	0.52	6.13	0.75	6.15	0.77	6.44	1.10	6.43	1.09	6.38	1.03	6.24	0.86	6.05	0.67	5.88	0.53
5	5.74	0.44	6.14	0.76	6.13	0.75	6.40	1.05	6.37	1.02	6.30	0.93	6.09	0.71	5.99	0.62	5.87	0.53
10	5.77	0.46	6.05	0.67	6.00	0.63	5.89	0.54	5.73	0.43	5.60	0.35	5.83	0.50	5.83	0.50	5.78	0.46
15	5.79	0.47	5.70	0.41	5.64	0.37	4.59	0.01	4.84	0.07	5.01	0.11	5.38	0.24	5.71	0.42	5.65	0.38
17	5.80	0.48	5.43	0.27	5.41	0.26	4.55	0.00	4.82	0.06	4.95	0.10	5.21	0.18	5.45	0.27	5.38	0.24
20	5.70	0.41	5.35	0.23	5.17	0.16	4.82	0.06	4.75	0.05	4.79	0.06	4.88	0.08	5.01	0.11	4.93	0.09
22	5.59	0.35	5.36	0.23	5.07	0.13	4.90	0.08	4.79	0.06	4.72	0.04	4.81	0.06	4.76	0.05	4.78	0.05
23	5.54	0.32	5.31	0.21	5.01	0.11	4.89	0.08	4.80	0.06	4.66	0.03	4.78	0.05	4.75	0.05	4.73	0.04

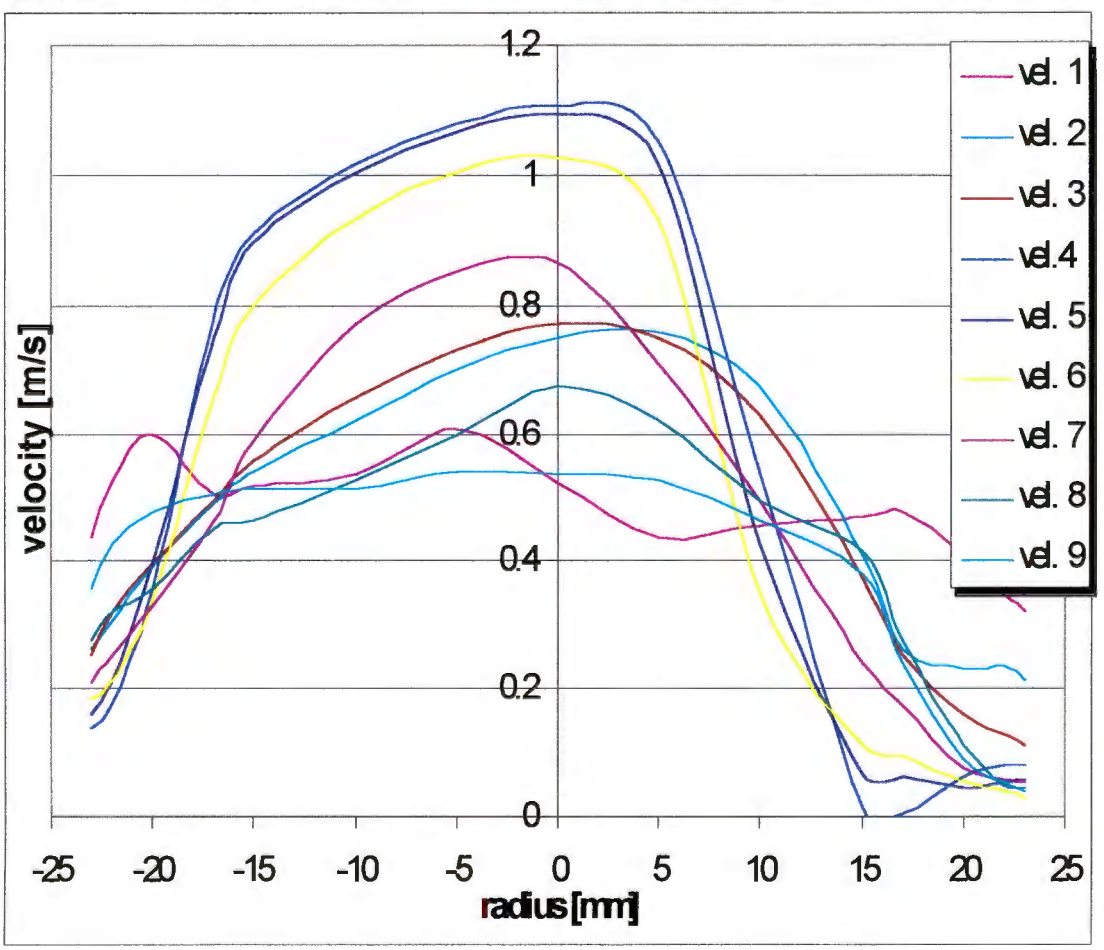

Experiment No 1-6

Date:	08.07.						
Time:	15:00						
Conditions							
T [C]	16.6		Flowrate [cm]	12		A* [/]	0.48
$p_{ambient}$ [mmHg]	755.75		Flowrate [l/min]	47.440		L* [/]	1
$p_{ambient}$ [Pa]	100515		mean vel. w [m/s]	0.476		w* [m/s]	0.9912
			Re [/]	1444.39		Re* [/]	2084.80

blockage type:	prestix short

z-location:	1		2		3		4		5		6		7		8		9	
r-koordinate [mm]	Voltage [V]	vel. 1	Voltage [V]	vel. 2	Voltage [V]	vel. 3	Voltage [V]	vel.4	Voltage [V]	vel. 5	Voltage [V]	vel. 6	Voltage [V]	vel. 7	Voltage [V]	vel. 8	Voltage [V]	vel. 9
-23	5.66	0.39	5.48	0.29	5.40	0.25	5.07	0.13	5.17	0.16	5.23	0.18	5.39	0.25	5.62	0.36	5.71	0.42
-22	5.79	0.47	5.48	0.29	5.50	0.30	5.18	0.17	5.33	0.22	5.33	0.22	5.44	0.27	5.71	0.42	5.80	0.48
-20	5.87	0.53	5.61	0.36	5.62	0.36	5.59	0.35	5.66	0.39	5.53	0.31	5.61	0.36	5.76	0.45	5.83	0.50
-17	5.77	0.46	5.74	0.44	5.76	0.45	6.13	0.75	6.11	0.73	5.94	0.58	5.75	0.44	5.81	0.48	5.86	0.52
-15	5.79	0.47	5.81	0.48	5.83	0.50	6.25	0.87	6.23	0.85	6.17	0.79	5.88	0.53	5.87	0.53	5.89	0.54
-10	5.81	0.48	5.90	0.55	5.94	0.58	6.33	0.97	6.33	0.97	6.31	0.94	6.05	0.67	5.94	0.58	5.91	0.56
-5	5.89	0.54	5.97	0.61	6.02	0.65	6.38	1.03	6.39	1.04	6.36	1.00	6.16	0.78	5.98	0.61	5.91	0.56
0	5.78	0.46	6.04	0.67	6.09	0.71	6.41	1.07	6.41	1.07	6.38	1.03	6.09	0.71	5.96	0.60	5.92	0.56
5	5.67	0.39	6.07	0.69	6.11	0.73	6.39	1.04	6.38	1.03	6.31	0.94	5.89	0.54	5.84	0.50	5.88	0.53
10	5.69	0.40	6.04	0.67	6.04	0.67	5.97	0.61	5.84	0.50	5.62	0.36	5.62	0.36	5.77	0.46	5.84	0.50
15	5.73	0.43	5.73	0.43	5.70	0.41	4.69	0.03	4.81	0.06	4.88	0.08	5.27	0.20	5.64	0.37	5.69	0.40
17	5.72	0.42	5.46	0.28	5.46	0.28	4.56	0.01	4.73	0.04	4.79	0.06	5.21	0.18	5.42	0.26	5.43	0.27
20	5.66	0.39	5.34	0.23	5.18	0.17	4.72	0.04	4.70	0.04	4.72	0.04	4.92	0.09	5.03	0.12	4.96	0.10
22	5.56	0.33	5.26	0.19	5.16	0.16	4.92	0.09	4.78	0.05	4.79	0.06	4.82	0.06	4.89	0.08	4.83	0.06
23	5.49	0.29	5.18	0.17	5.04	0.12	4.93	0.09	4.74	0.04	4.79	0.06	4.81	0.06	4.84	0.07	4.91	0.08

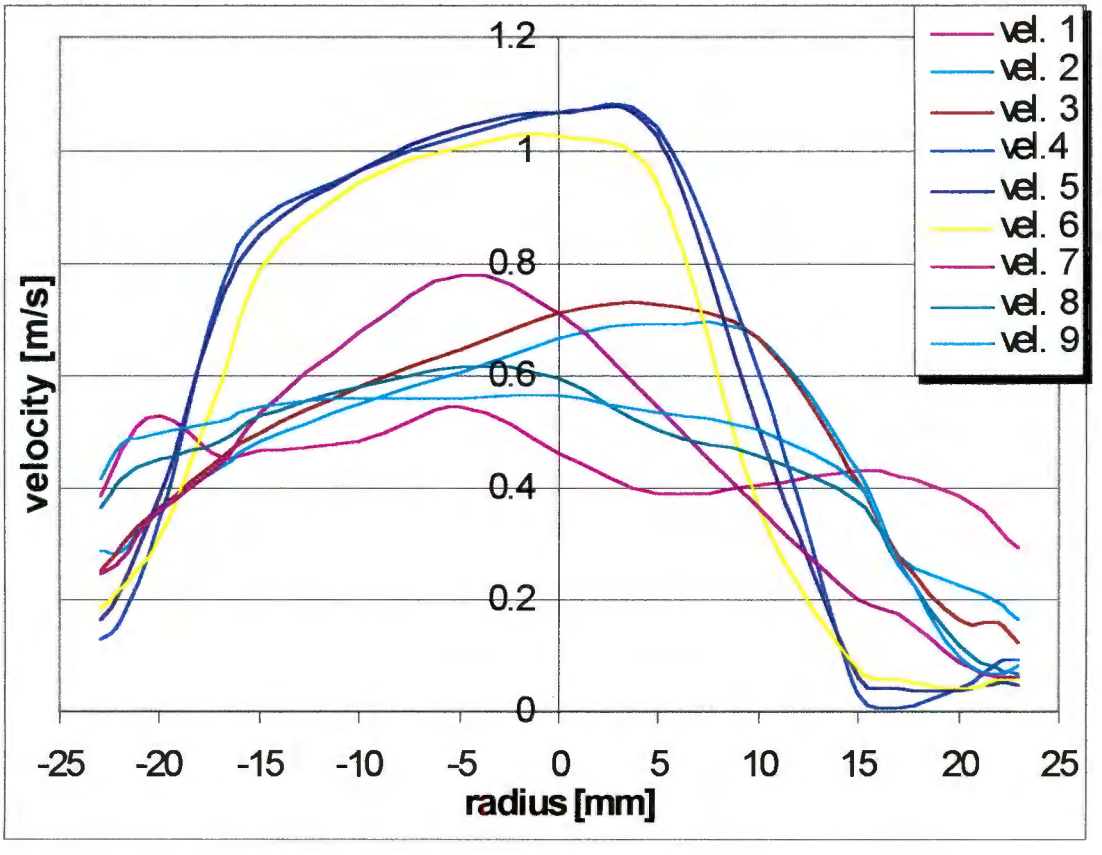

Experiment No 1-7

Date:	19.8.98			
Time:	16:00			
Conditions				
T [C]	17.6		Flowrate [cm]	12
$p_{ambient}$ [mmHg]	753		Flowrate [l/min]	47.440
$p_{ambient}$ [Pa]	100149		mean velocity [m/s]	0.476
			Re [/]	1444.392

blockage type:	no							
z-location:	1		2		3		4	
r-koordinate [mm]	Voltage [V]	velocity 1	Voltage [V]	velocity 2	Voltage [V]	velocity 3	Voltage [V]	velocity 4
-23	5.76	0.449	5.47	0.284	5.48	0.289	5.69	0.404
-22	5.84	0.504	5.56	0.330	5.59	0.346	5.75	0.442
-20	5.88	0.534	5.64	0.374	5.68	0.398	5.83	0.497
-17	5.78	0.462	5.73	0.429	5.78	0.462	5.89	0.542
-15	5.81	0.483	5.78	0.462	5.84	0.504	5.93	0.573
-10	5.83	0.497	5.84	0.504	5.9	0.549	5.97	0.605
-5	5.9	0.549	5.89	0.542	5.97	0.605	5.97	0.605
0	5.8	0.476	5.95	0.589	6.02	0.648	5.94	0.581
5	5.68	0.398	5.97	0.605	6.03	0.657	5.88	0.534
10	5.72	0.423	5.89	0.542	5.92	0.565	5.74	0.436
15	5.78	0.462	5.52	0.309	5.52	0.309	5.42	0.261
17	5.72	0.423	5.24	0.187	5.2	0.172	5.15	0.155
20	5.53	0.314	5.32	0.218	4.99	0.106	5.07	0.130
22	5.45	0.275	5.01	0.112	4.84	0.067	4.97	0.101
23	5.39	0.247	4.88	0.077	4.82	0.062	4.95	0.095

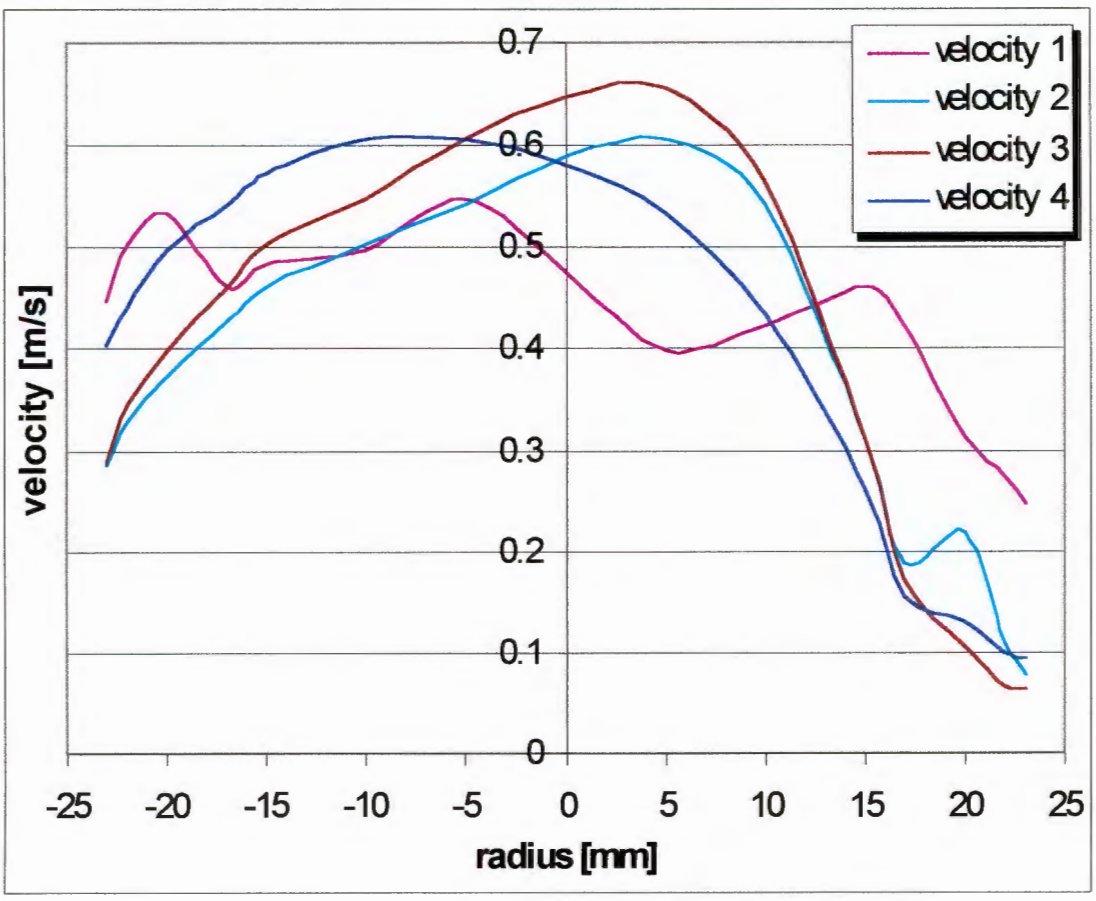

Experiment No 1-8

Date:	26.8.
Time:	17:30

Conditions				
T [C]	18.6		Flowrate [cm]	12
$p_{ambient}$ [mmHg]	756		Flowrate [l/min]	47.440
$p_{ambient}$ [Pa]	100548		mean velocity [m/s]	0.476
			Re [/]	1444.4

blockage type:	no							
z-location:	1		2		3		4	
r-koordinate [mm]	Voltage [V]	vel. 1	Voltage [V]	vel. 2	Voltage [V]	vel. 3	Voltage [V]	vel.4
-23	5.88	0.534	5.5	0.299	5.52	0.309	5.57	0.335
-22	5.85	0.512	5.56	0.330	5.61	0.357	5.67	0.392
-20	5.78	0.462	5.65	0.380	5.69	0.404	5.75	0.442
-17	5.78	0.462	5.74	0.436	5.81	0.483	5.82	0.490
-15	5.79	0.469	5.79	0.469	5.84	0.504	5.86	0.519
-10	5.82	0.490	5.84	0.504	5.89	0.542	5.91	0.557
-5	5.79	0.469	5.9	0.549	5.96	0.597	5.94	0.581
0	5.75	0.442	5.95	0.589	5.99	0.622	5.94	0.581
5	5.72	0.423	5.97	0.605	5.97	0.605	5.88	0.534
10	5.67	0.392	5.88	0.534	5.84	0.504	5.7	0.410
15	5.75	0.442	5.53	0.314	5.43	0.265	5.3	0.210
17	5.59	0.346	5.36	0.235	5.13	0.149	5.11	0.142
20	5.71	0.417	5.47	0.284	4.88	0.077	5.01	0.112
22	5.64	0.374	5.32	0.218	4.74	0.044	4.88	0.077
23	5.53	0.314	5.19	0.169	4.71	0.037	4.91	0.085

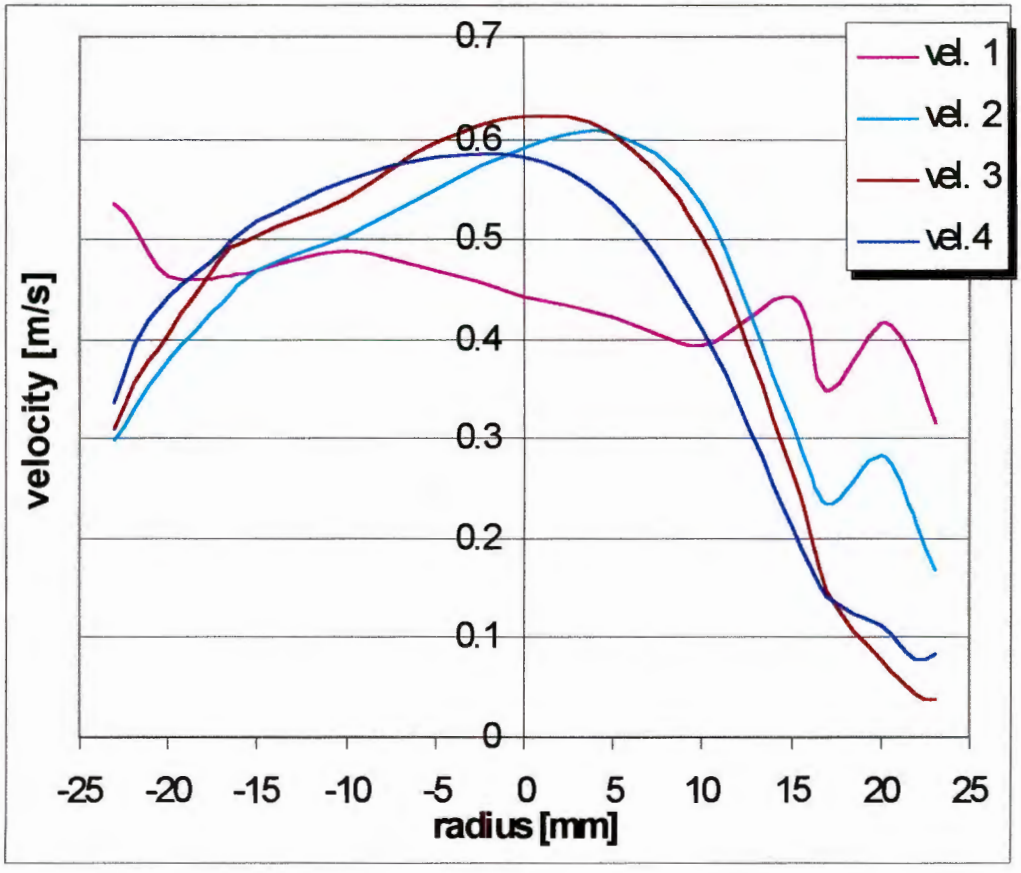

Experiment No 2-1

Date:	10.07.						
Time:	19:00						
Conditions							
T [C]	17.4		Flowrate [cm]	12		A* [/]	0.756
$p_{ambient}$ [mmHg]	761.75		Flowrate [l/min]	47.440		L* [/]	1
$p_{ambient}$ [Pa]	101313		mean velocity [m/s]	0.476		w* [m/s]	0.6293
			Re [/]	1444.39		Re* [/]	1661.21

blockage type:																		
z-location:	1		2		3		4		5		6		7		8		9	
r-koordinate [mm]	Voltage [V]	vel. 1	Voltage [V]	vel. 2	Voltage [V]	vel. 3	Voltage [V]	vel.4	Voltage [V]	vel. 5	Voltage [V]	vel. 6	Voltage [V]	vel. 7	Voltage [V]	vel. 8	Voltage [V]	vel. 9
-23	5.71	0.42	5.38	0.24	5.38	0.24	5.35	0.23	5.45	0.27	5.42	0.26	5.43	0.27	5.40	0.25	5.46	0.28
-22	5.81	0.48	5.47	0.28	5.49	0.29	5.55	0.32	5.58	0.34	5.58	0.34	5.56	0.33	5.53	0.31	5.57	0.34
-20	5.91	0.56	5.59	0.35	5.61	0.36	5.74	0.44	5.73	0.43	5.73	0.43	5.70	0.41	5.67	0.39	5.69	0.40
-17	5.79	0.47	5.72	0.42	5.75	0.44	5.90	0.55	5.87	0.53	5.87	0.53	5.85	0.51	5.83	0.50	5.84	0.50
-15	5.82	0.49	5.78	0.46	5.82	0.49	5.95	0.59	5.93	0.57	5.92	0.56	5.92	0.56	5.89	0.54	5.89	0.54
-10	5.82	0.49	5.89	0.54	5.94	0.58	6.03	0.66	6.01	0.64	6.00	0.63	6.00	0.63	5.97	0.61	5.97	0.61
-5	5.83	0.50	5.96	0.60	6.03	0.66	6.11	0.73	6.09	0.71	6.08	0.70	6.08	0.70	6.05	0.67	6.05	0.67
0	5.83	0.50	6.04	0.67	6.10	0.72	6.17	0.79	6.15	0.77	6.14	0.76	6.14	0.76	6.11	0.73	6.11	0.73
5	5.70	0.41	6.10	0.72	6.14	0.76	6.19	0.81	6.18	0.80	6.16	0.78	6.17	0.79	6.14	0.76	6.14	0.76
10	5.72	0.42	6.08	0.70	6.07	0.69	6.09	0.71	6.07	0.69	6.05	0.67	6.07	0.69	6.06	0.68	6.07	0.69
15	5.73	0.43	5.80	0.48	5.74	0.44	5.43	0.27	5.42	0.26	5.49	0.29	5.62	0.36	5.64	0.37	5.70	0.41
17	5.69	0.40	5.57	0.34	5.44	0.27	4.86	0.07	4.99	0.11	5.15	0.16	5.30	0.21	5.36	0.23	5.44	0.27
20	5.68	0.40	5.29	0.21	5.03	0.12	4.58	0.01	4.66	0.03	4.87	0.07	4.88	0.08	4.90	0.08	5.00	0.11
22	5.55	0.32	5.11	0.14	4.80	0.06	4.63	0.02	4.64	0.02	4.79	0.06	4.71	0.04	4.74	0.04	4.76	0.05
23	5.50	0.30	5.01	0.11	4.75	0.05	4.73	0.04	4.66	0.03	4.75	0.05	4.65	0.02	4.67	0.03	4.75	0.05

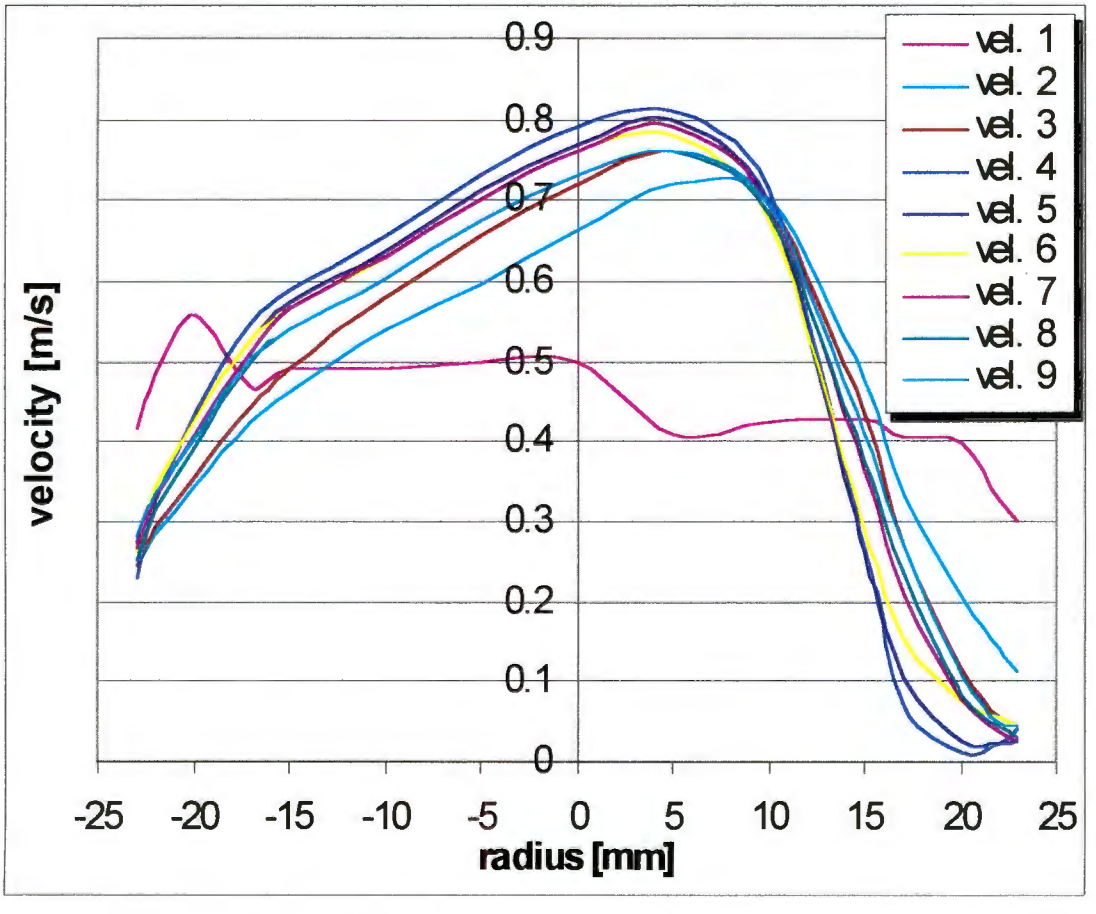

Experiment No 2-2

Date:	08.07.98						
Time:	15:00						
Conditions							
T [C]	16.6		Flowrate [cm]	12		A* [/]	0.48
$p_{ambient}$ [mmHg]	755.75		Flowrate [l/min]	47.440		L* [/]	1
$p_{ambient}$ [Pa]	100515		mean velocity [m/s]	0.476		w* [m/s]	0.9912
			Re [/]	1444.39		Re* [/]	2084.80

blockage type:	prestix short

z-location:	1		2		3		4		5		6		7		8		9	
r-koordinate [mm]	Voltage [V]	vel. 1	Voltage [V]	vel. 2	Voltage [V]	vel. 3	Voltage [V]	vel.4	Voltage [V]	vel. 5	Voltage [V]	vel. 6	Voltage [V]	vel. 7	Voltage [V]	vel. 8	Voltage [V]	vel. 9
-23	5.66	0.39	5.48	0.29	5.40	0.25	5.07	0.13	5.17	0.16	5.23	0.18	5.39	0.25	5.62	0.36	5.71	0.42
-22	5.79	0.47	5.48	0.29	5.50	0.30	5.18	0.17	5.33	0.22	5.33	0.22	5.44	0.27	5.71	0.42	5.80	0.48
-20	5.87	0.53	5.61	0.36	5.62	0.36	5.59	0.35	5.66	0.39	5.53	0.31	5.61	0.36	5.76	0.45	5.83	0.50
-17	5.77	0.46	5.74	0.44	5.76	0.45	6.13	0.75	6.11	0.73	5.94	0.58	5.75	0.44	5.81	0.48	5.86	0.52
-15	5.79	0.47	5.81	0.48	5.83	0.50	6.25	0.87	6.23	0.85	6.17	0.79	5.88	0.53	5.87	0.53	5.89	0.54
-10	5.81	0.48	5.90	0.55	5.94	0.58	6.33	0.97	6.33	0.97	6.31	0.94	6.05	0.67	5.94	0.58	5.91	0.56
-5	5.89	0.54	5.97	0.61	6.02	0.65	6.38	1.03	6.39	1.04	6.36	1.00	6.16	0.78	5.98	0.61	5.91	0.56
0	5.78	0.46	6.04	0.67	6.09	0.71	6.41	1.07	6.41	1.07	6.38	1.03	6.09	0.71	5.96	0.60	5.92	0.56
5	5.67	0.39	6.07	0.69	6.11	0.73	6.39	1.04	6.38	1.03	6.31	0.94	5.89	0.54	5.84	0.50	5.88	0.53
10	5.69	0.40	6.04	0.67	6.04	0.67	5.97	0.61	5.84	0.50	5.62	0.36	5.62	0.36	5.77	0.46	5.84	0.50
15	5.73	0.43	5.73	0.43	5.70	0.41	4.69	0.03	4.81	0.06	4.88	0.08	5.27	0.20	5.64	0.37	5.69	0.40
17	5.72	0.42	5.46	0.28	5.46	0.28	4.56	0.01	4.73	0.04	4.79	0.06	5.21	0.18	5.42	0.26	5.43	0.27
20	5.66	0.39	5.34	0.23	5.18	0.17	4.72	0.04	4.70	0.04	4.72	0.04	4.92	0.09	5.03	0.12	4.96	0.10
22	5.56	0.33	5.26	0.19	5.16	0.16	4.92	0.09	4.78	0.05	4.79	0.06	4.82	0.06	4.89	0.08	4.83	0.06
23	5.49	0.29	5.18	0.17	5.04	0.12	4.93	0.09	4.74	0.04	4.79	0.06	4.81	0.06	4.84	0.07	4.91	0.08

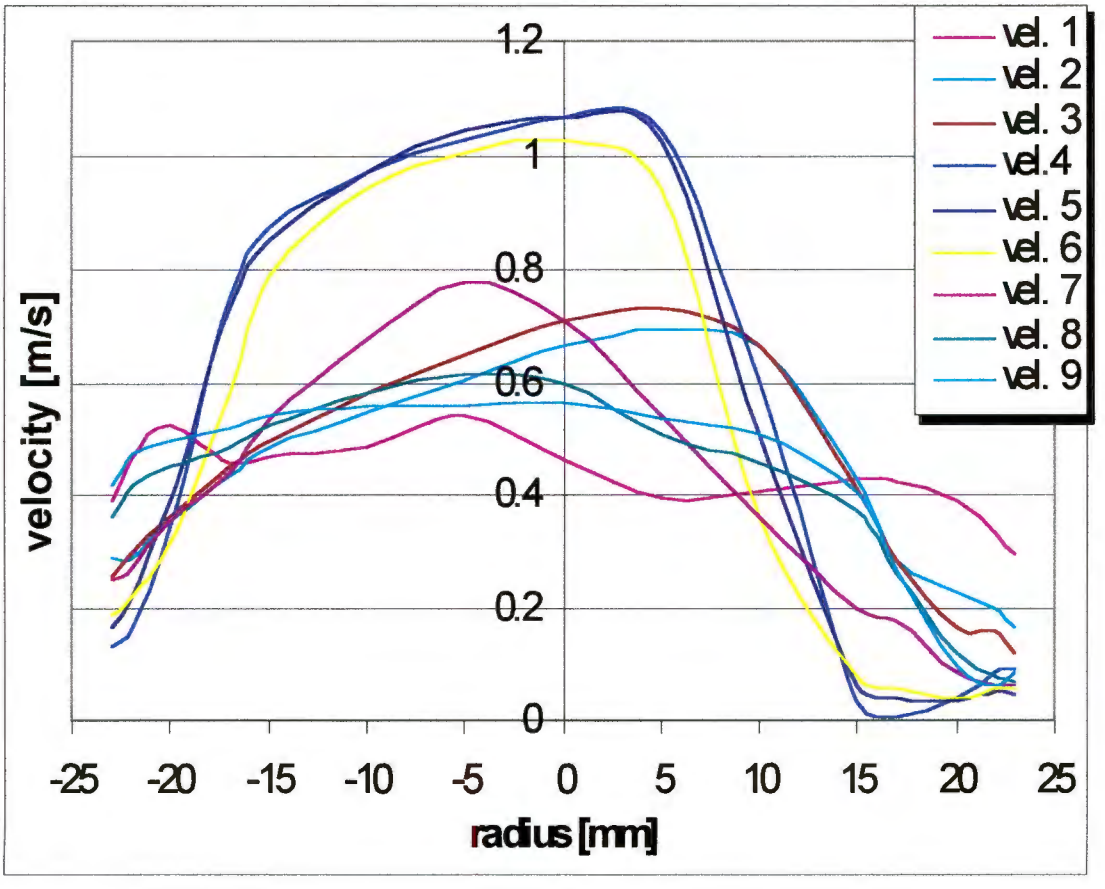

Experiment No 2-3

Date:	10.07.98						
Time:	20:30						
Conditions							
T [C]	17.4		Flowrate [cm]	12		A* [/]	0.32
$p_{ambient}$ [mmHg]	761.75		Flowrate [l/min]	47.440		L* [/]	1
$p_{ambient}$ [Pa]	101313		mean velocity [m/s]	0.476		w* [m/s]	1.4867
			Re [/]	1444.39		Re* [/]	2553.35

z-location:	1		2		3		4		5		6		7		8		9	
r-koordinate [mm]	Voltage [V]	vel. 1	Voltage [V]	vel. 2	Voltage [V]	vel. 3	Voltage [V]	vel.4	Voltage [V]	vel. 5	Voltage [V]	vel. 6	Voltage [V]	vel. 7	Voltage [V]	vel. 8	Voltage [V]	vel. 9
-23	5.71	0.42	5.39	0.25	5.39	0.25	5.05	0.12	5.24	0.19	5.55	0.32	5.36	0.23	5.54	0.32	5.64	0.37
-22	5.83	0.50	5.49	0.29	5.52	0.31	5.15	0.16	5.26	0.19	5.68	0.40	5.42	0.26	5.61	0.36	5.72	0.42
-20	5.89	0.54	5.61	0.36	5.63	0.37	5.45	0.27	5.42	0.26	5.68	0.40	5.46	0.28	5.70	0.41	5.79	0.47
-17	5.76	0.45	5.75	0.44	5.77	0.46	5.72	0.42	5.73	0.43	5.73	0.43	5.57	0.34	5.76	0.45	5.84	0.50
-15	5.78	0.46	5.82	0.49	5.84	0.50	6.13	0.75	6.16	0.78	5.93	0.57	5.71	0.42	5.78	0.46	5.86	0.52
-10	5.84	0.50	5.91	0.56	5.94	0.58	6.86	1.78	6.81	1.69	6.36	1.00	5.96	0.60	5.88	0.53	5.86	0.52
-5	5.91	0.56	5.97	0.61	6.01	0.64	6.89	1.84	6.89	1.84	6.67	1.44	6.24	0.86	5.92	0.56	5.87	0.53
0	5.82	0.49	6.04	0.67	6.08	0.70	6.89	1.84	6.88	1.82	6.74	1.56	6.21	0.83	5.93	0.57	5.86	0.52
5	5.68	0.40	6.08	0.70	6.11	0.73	6.80	1.67	6.57	1.29	6.56	1.27	6.27	0.90	5.96	0.60	5.85	0.51
10	5.70	0.41	6.06	0.68	6.05	0.67	5.13	0.15	5.06	0.13	6.11	0.73	6.02	0.65	5.83	0.50	5.80	0.48
15	5.74	0.44	5.79	0.47	5.70	0.41	4.76	0.05	4.78	0.05	5.71	0.42	5.73	0.43	5.68	0.40	5.62	0.36
17	5.74	0.44	5.61	0.36	5.53	0.31	4.78	0.05	4.75	0.05	5.35	0.23	5.57	0.34	5.67	0.39	5.37	0.24
20	5.76	0.45	5.69	0.40	5.55	0.32	5.23	0.18	5.24	0.19	5.18	0.17	5.06	0.13	5.27	0.20	5.05	0.12
22	5.74	0.44	5.70	0.41	5.70	0.41	5.18	0.17	5.15	0.16	5.03	0.12	4.73	0.04	4.90	0.08	4.78	0.05
23	5.66	0.39	5.54	0.32	5.68	0.40	5.03	0.12	5.00	0.11	4.92	0.09	4.67	0.03	4.82	0.06	4.73	0.04

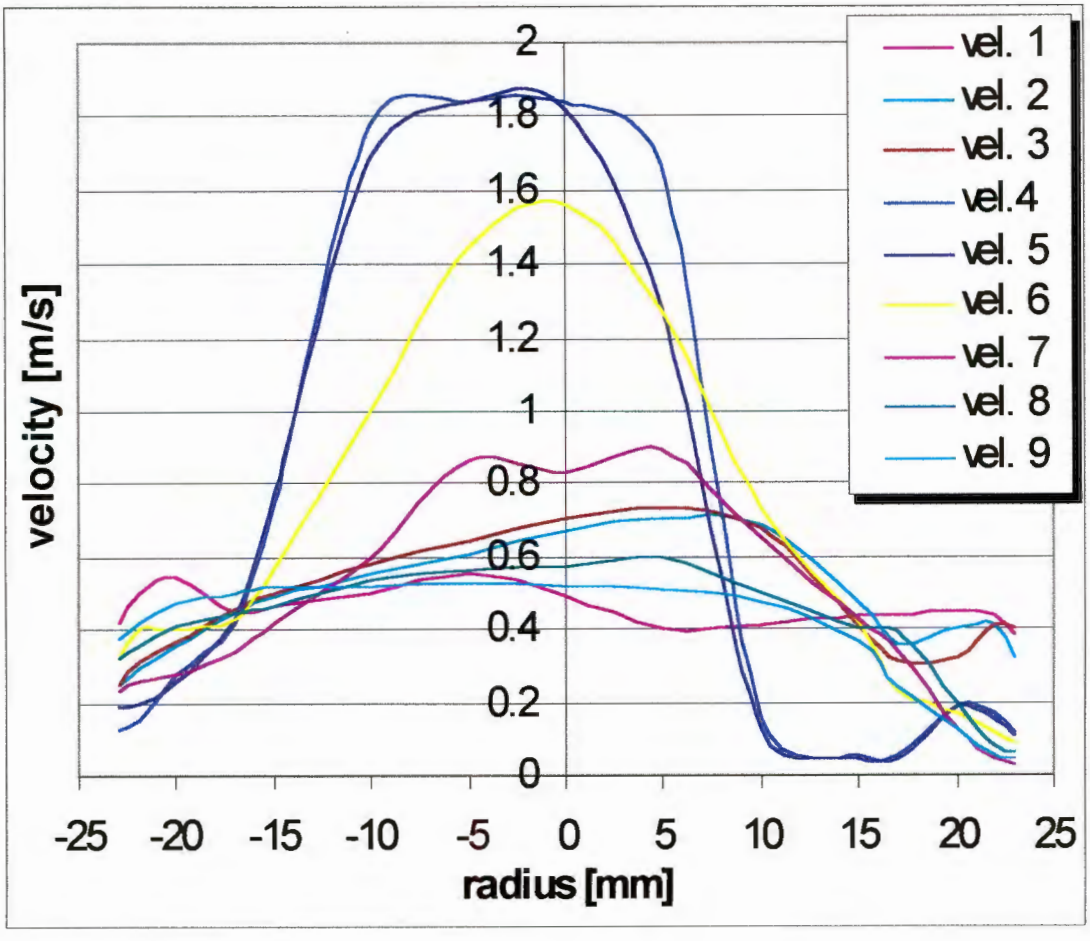

Experiment No 2-4

Date:	13.07.98						
Time:	13:45						
Conditions							
T [C]	17.7		Flowrate [cm]	12		A* [/]	0.19
$p_{ambient}$ [mmHg]	752.25		Flowrate [l/min]	47.440		L* [/]	1
$p_{ambient}$ [Pa]	100049		mean velocity [m/s]	0.476		w* [m/s]	2.504
			Re [/]	1444.39		Re* [/]	3313.66

z-location:	1		2		3		4		5		6		7		8		9	
r-koordinate [mm]	Voltage [V]	vel. 1	Voltage [V]	vel. 2	Voltage [V]	vel. 3	Voltage [V]	vel.4	Voltage [V]	vel. 5	Voltage [V]	vel. 6	Voltage [V]	vel. 7	Voltage [V]	vel. 8	Voltage [V]	vel. 9
-23	5.73	0.43	5.39	0.25	5.35	0.23	5.26	0.19	5.81	0.48	5.62	0.36	5.37	0.24	5.51	0.30	5.59	0.35
-22	5.80	0.48	5.48	0.29	5.46	0.28	5.32	0.22	5.92	0.56	5.68	0.40	5.45	0.27	5.68	0.40	5.70	0.41
-20	5.87	0.53	5.61	0.36	5.59	0.35	5.51	0.30	5.94	0.58	5.72	0.42	5.56	0.33	5.69	0.40	5.74	0.44
-17	5.75	0.44	5.74	0.44	5.73	0.43	5.77	0.46	5.96	0.60	5.76	0.45	5.63	0.37	5.72	0.42	5.82	0.49
-15	5.78	0.46	5.80	0.48	5.80	0.48	5.80	0.48	5.95	0.59	5.83	0.50	5.72	0.42	5.71	0.42	5.83	0.50
-10	5.82	0.49	5.89	0.54	5.93	0.57	7.03	2.13	6.66	1.43	6.19	0.81	5.83	0.50	5.74	0.44	5.81	0.48
-5	5.88	0.53	5.97	0.61	6.03	0.66	7.29	2.77	7.22	2.59	6.43	1.09	6.04	0.67	5.75	0.44	5.78	0.46
0	5.79	0.47	6.03	0.66	6.08	0.70	7.29	2.77	7.30	2.80	6.78	1.63	6.09	0.71	5.78	0.46	5.76	0.45
5	5.87	0.53	6.06	0.68	6.07	0.69	6.93	1.92	7.12	2.34	6.71	1.51	6.03	0.66	5.80	0.48	5.74	0.44
10	5.68	0.40	6.00	0.63	5.97	0.61	5.15	0.16	5.96	0.60	6.33	0.97	5.94	0.58	5.81	0.48	5.52	0.31
15	5.72	0.42	5.72	0.42	5.64	0.37	5.20	0.17	5.26	0.19	6.02	0.65	5.66	0.39	5.61	0.36	5.29	0.21
17	5.78	0.46	5.59	0.35	5.47	0.28	5.28	0.20	5.10	0.14	5.68	0.40	5.67	0.39	5.44	0.27	5.10	0.14
20	5.97	0.61	5.86	0.52	5.70	0.41	5.46	0.28	5.43	0.27	5.29	0.21	5.07	0.13	5.05	0.12	4.95	0.10
22	5.98	0.61	6.00	0.63	6.04	0.67	5.36	0.23	5.38	0.24	4.91	0.08	4.71	0.04	4.84	0.07	4.76	0.05
23	5.97	0.61	5.91	0.56	6.06	0.68	5.28	0.20	5.16	0.16	4.96	0.10	4.68	0.03	4.79	0.06	4.69	0.03

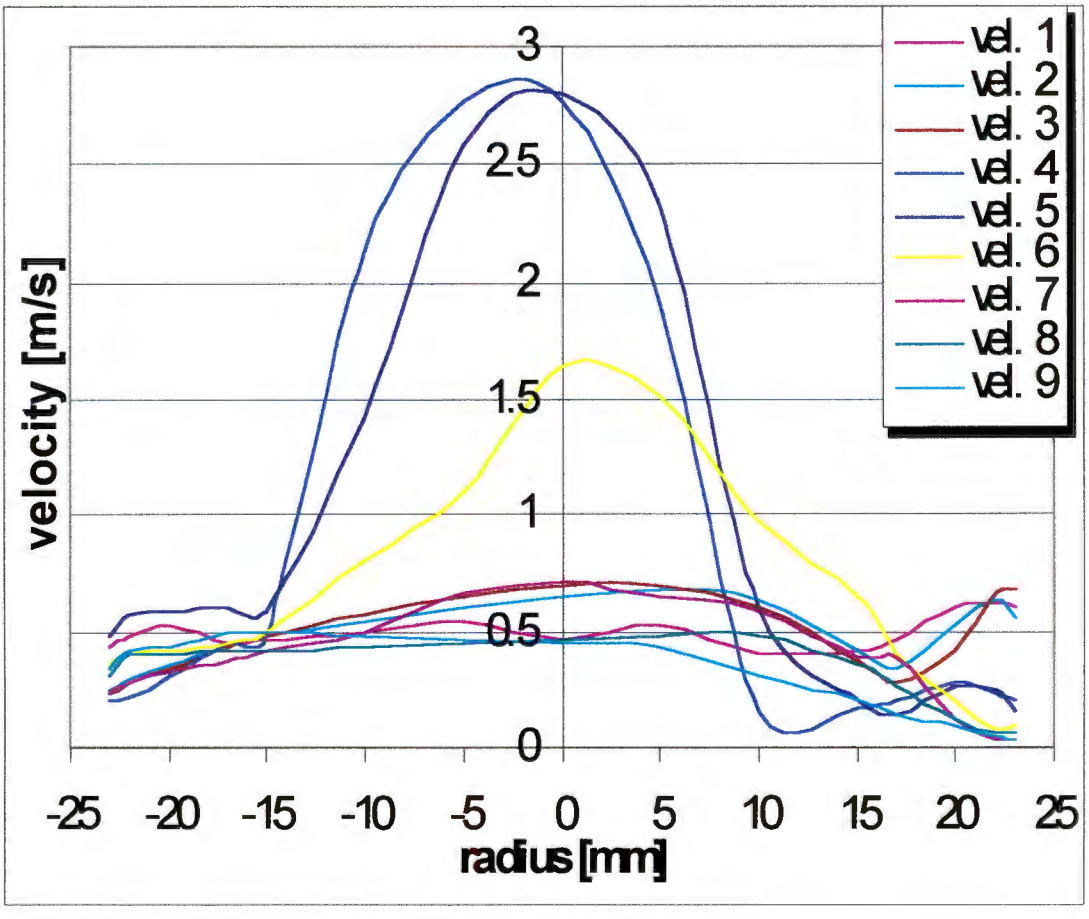

Experiment No 3-1

Date:	09.07.98							
Time:	17:45							
Conditions								
T [C]	16.3		Flowrate [cm]	12		A* [/]	0.5	
$p_{ambient}$ [mmHg]	760.25		Flowrate [l/min]	47.440		L* [/]	1	
$p_{ambient}$ [Pa]	101113		mean velocity [m/s]	0.476		w* [m/s]	0.9515	
			Re [/]	1444.39		Re* [/]	2042.68	

z-location:	1		2		3		4		5		6		7		8		9	
r-koordinate [mm]	Voltage [V]	vel. 1	Voltage [V]	vel. 2	Voltage [V]	vel. 3	Voltage [V]	vel.4	Voltage [V]	vel. 5	Voltage [V]	vel. 6	Voltage [V]	vel. 7	Voltage [V]	vel. 8	Voltage [V]	vel. 9
-23	5.75	0.44	5.41	0.26	5.39	0.25	4.60	0.01	4.60	0.01	5.10	0.14	5.75	0.44	5.71	0.42	5.63	0.37
-22	5.84	0.50	5.50	0.30	5.49	0.29	4.61	0.02	4.68	0.03	5.26	0.19	5.82	0.49	5.79	0.47	5.74	0.44
-20	5.94	0.58	5.64	0.37	5.64	0.37	4.58	0.01	4.76	0.05	5.35	0.23	5.91	0.56	5.94	0.58	5.83	0.50
-17	5.83	0.50	5.79	0.47	5.78	0.46	4.65	0.02	4.81	0.06	5.50	0.30	5.96	0.60	6.01	0.64	5.86	0.52
-15	5.85	0.51	5.87	0.53	5.87	0.53	4.73	0.04	4.83	0.06	5.68	0.40	6.02	0.65	6.02	0.65	5.91	0.56
-10	5.87	0.53	5.97	0.61	6.00	0.63	4.96	0.10	5.20	0.17	5.97	0.61	6.16	0.78	6.00	0.63	5.88	0.53
-5	5.96	0.60	6.07	0.69	6.09	0.71	5.38	0.24	5.85	0.51	6.25	0.87	6.26	0.89	5.95	0.59	5.86	0.52
0	5.85	0.51	6.13	0.75	6.14	0.76	6.33	0.97	6.36	1.00	6.31	0.94	6.19	0.81	5.75	0.44	5.81	0.48
5	5.72	0.42	6.13	0.75	6.13	0.75	6.44	1.10	6.42	1.08	6.27	0.90	5.85	0.51	5.46	0.28	5.76	0.45
10	5.75	0.44	6.05	0.67	6.01	0.64	6.42	1.08	6.37	1.02	6.14	0.76	5.53	0.31	5.23	0.18	5.74	0.44
15	5.79	0.47	5.72	0.42	5.65	0.38	6.26	0.89	6.18	0.80	5.52	0.31	5.12	0.15	5.17	0.16	5.52	0.31
17	5.78	0.46	5.49	0.29	5.41	0.26	5.99	0.62	5.83	0.50	4.96	0.10	4.88	0.08	5.01	0.11	5.34	0.23
20	5.72	0.42	5.41	0.26	5.21	0.18	5.21	0.18	5.15	0.16	4.55	0.00	4.75	0.05	4.90	0.08	4.95	0.10
22	5.61	0.36	5.35	0.23	5.15	0.16	4.76	0.05	4.76	0.05	4.56	0.01	4.68	0.03	4.81	0.06	4.87	0.07
23	5.52	0.31	5.30	0.21	5.10	0.14	4.70	0.04	4.80	0.06	4.63	0.02	4.72	0.04	4.78	0.05	4.83	0.06

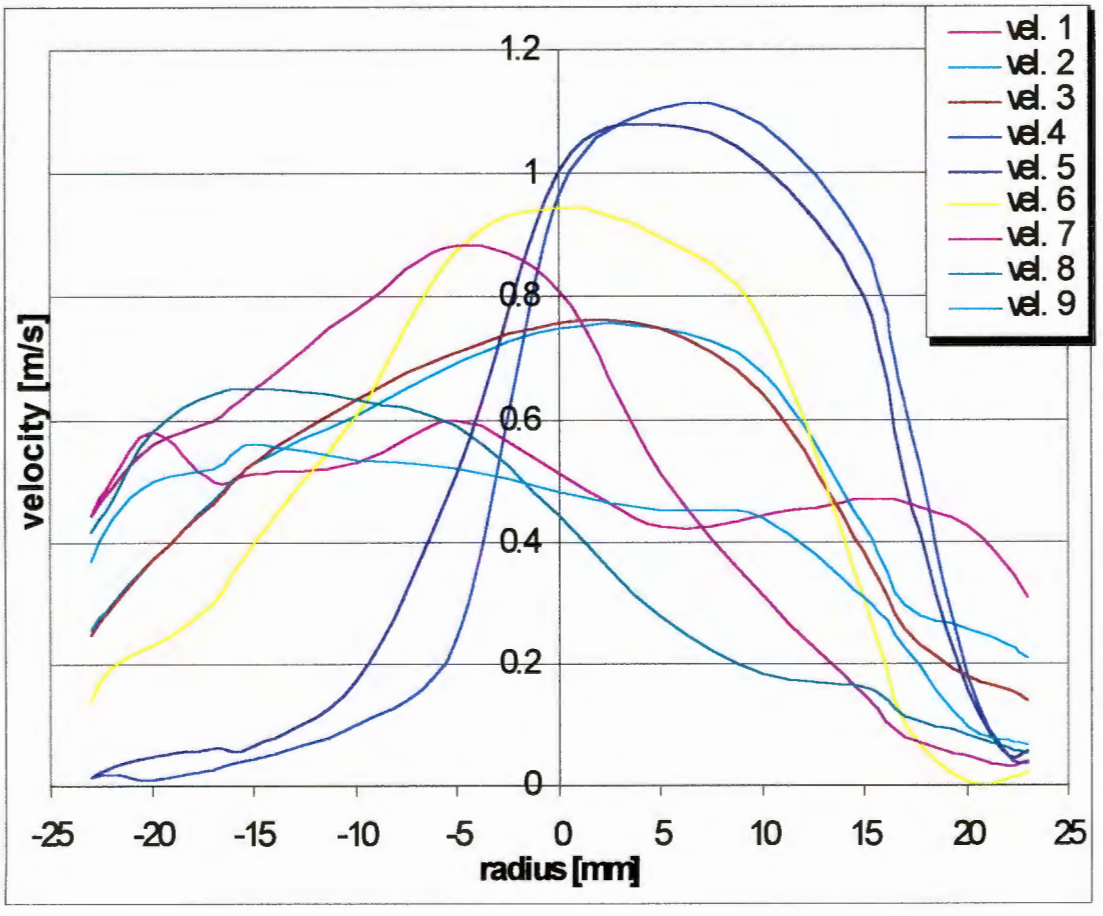

Experiment No 3-2

Date:	09.07.98						
Time:	18:45						
Conditions							
T [C]	16.3		Flowrate [cm]	12		A* [/]	0.5
$p_{ambient}$ [mmHg]	760.25		Flowrate [l/min]	47.440		L* [/]	1
$p_{ambient}$ [Pa]	101113		mean velocity [m/s]	0.476		w* [m/s]	0.9515
			Re [/]	1444.39		Re* [/]	2042.68

z-location:	1		2		3		4		5		6		7		8		9	
r-koordinate [mm]	Voltage [V]	vel. 1	Voltage [V]	vel. 2	Voltage [V]	vel. 3	Voltage [V]	vel.4	Voltage [V]	vel. 5	Voltage [V]	vel. 6	Voltage [V]	vel. 7	Voltage [V]	vel. 8	Voltage [V]	vel. 9
-23	5.68	0.40	5.43	0.27	5.42	0.26	6.17	0.79	6.05	0.67	5.38	0.24	5.43	0.27	5.52	0.31	5.59	0.35
-22	5.79	0.47	5.52	0.31	5.53	0.31	6.31	0.94	6.17	0.79	5.56	0.33	5.54	0.32	5.57	0.34	5.73	0.43
-20	5.90	0.55	5.64	0.37	5.66	0.39	6.36	1.00	6.28	0.91	5.81	0.48	5.60	0.35	5.66	0.39	5.76	0.45
-17	5.79	0.47	5.76	0.45	5.80	0.48	6.40	1.05	6.34	0.98	6.06	0.68	5.67	0.39	5.73	0.43	5.83	0.50
-15	5.80	0.48	5.83	0.50	5.87	0.53	6.42	1.08	6.38	1.03	6.13	0.75	5.71	0.42	5.71	0.42	5.85	0.51
-10	5.82	0.49	5.92	0.56	5.96	0.60	6.37	1.02	6.38	1.03	6.26	0.89	5.85	0.51	5.81	0.48	5.87	0.53
-5	5.91	0.56	5.98	0.61	6.05	0.67	6.04	0.67	6.20	0.82	6.24	0.86	6.01	0.64	5.86	0.52	5.90	0.55
0	5.81	0.48	6.05	0.67	6.12	0.74	5.01	0.11	5.87	0.53	6.13	0.75	6.06	0.68	5.93	0.57	5.92	0.56
5	5.69	0.40	6.09	0.71	6.14	0.76	4.91	0.08	5.20	0.17	5.88	0.53	6.03	0.66	5.94	0.58	5.92	0.56
10	5.71	0.42	6.08	0.70	6.07	0.69	4.83	0.06	5.23	0.18	5.50	0.30	5.83	0.50	5.86	0.52	5.90	0.55
15	5.75	0.44	5.80	0.48	5.73	0.43	4.67	0.03	5.38	0.24	5.26	0.19	5.76	0.45	5.77	0.46	5.63	0.37
17	5.68	0.40	5.57	0.34	5.49	0.29	4.70	0.04	5.35	0.23	5.11	0.14	5.54	0.32	5.64	0.37	5.44	0.27
20	5.67	0.39	5.50	0.30	5.24	0.19	4.71	0.04	4.91	0.08	4.90	0.08	5.06	0.13	5.23	0.18	4.95	0.10
22	5.54	0.32	5.48	0.29	5.15	0.16	4.78	0.05	4.83	0.06	4.78	0.05	4.89	0.08	5.01	0.11	4.73	0.04
23	5.49	0.29	5.35	0.23	5.06	0.13	4.77	0.05	4.76	0.05	4.76	0.05	4.83	0.06	4.95	0.10	4.70	0.04

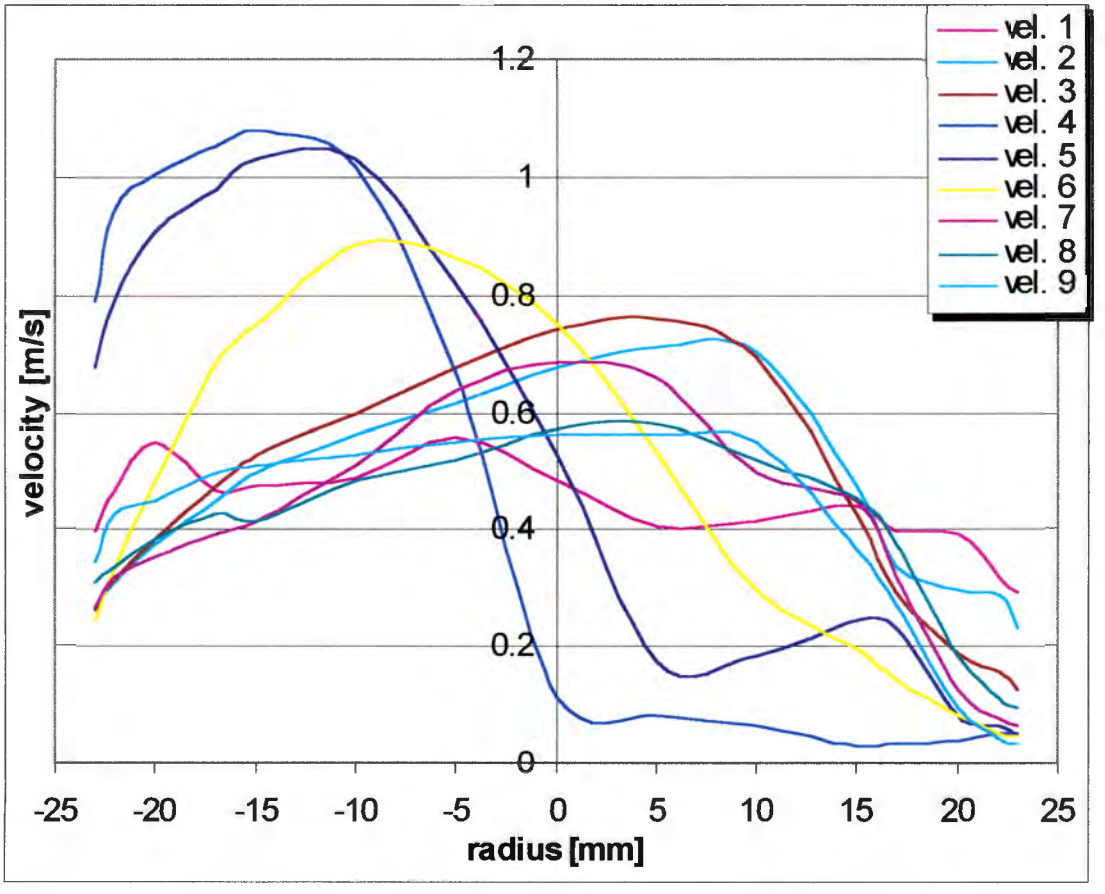

Experiment No 3-3

Date:	09.07.98																	
Time:	20:00																	
Conditions																		
T [C]	16.3			Flowrate [cm]		12			A* [/]	0.5								
$p_{ambient}$ [mmHg]	760.25			Flowrate [l/min]		47.440			L* [/]	1								
$p_{ambient}$ [Pa]	101113			mean velocity [m/s]		0.476			w* [m/s]	0.9515								
				Re [/]		1444.39			Re* [/]	2042.68								

z-location:	1		2		3		4		5		6		7		8		9	
r-koordinate [mm]	Voltage [V]	vel. 1	Voltage [V]	vel. 2	Voltage [V]	vel. 3	Voltage [V]	vel.4	Voltage [V]	vel. 5	Voltage [V]	vel. 6	Voltage [V]	vel. 7	Voltage [V]	vel. 8	Voltage [V]	vel. 9
-23	5.72	0.42	5.38	0.24	5.39	0.25	5.69	0.40	5.82	0.49	5.49	0.29	5.52	0.31	5.67	0.39	5.75	0.44
-22	5.79	0.47	5.47	0.28	5.49	0.29	5.81	0.48	5.95	0.59	5.54	0.32	5.68	0.40	5.76	0.45	5.79	0.47
-20	5.90	0.55	5.58	0.34	5.63	0.37	5.99	0.62	6.04	0.67	5.72	0.42	5.72	0.42	5.82	0.49	5.86	0.52
-17	5.80	0.48	5.71	0.42	5.77	0.46	6.05	0.67	6.07	0.69	5.96	0.60	5.82	0.49	5.88	0.53	5.91	0.56
-15	5.81	0.48	5.77	0.46	5.84	0.50	5.97	0.61	6.04	0.67	6.12	0.74	5.88	0.53	5.88	0.53	5.93	0.57
-10	5.82	0.49	5.89	0.54	5.95	0.59	5.74	0.44	5.98	0.61	6.26	0.89	6.01	0.64	5.90	0.55	5.91	0.56
-5	5.92	0.56	5.95	0.59	6.04	0.67	5.66	0.39	6.02	0.65	6.36	1.00	6.09	0.71	5.89	0.54	5.90	0.55
0	5.81	0.48	6.03	0.66	6.11	0.73	5.59	0.35	6.10	0.72	6.35	0.99	6.12	0.74	5.93	0.57	5.89	0.54
5	5.69	0.40	6.09	0.71	6.15	0.77	5.62	0.36	6.16	0.78	6.32	0.95	6.06	0.68	5.92	0.56	5.88	0.53
10	5.73	0.43	6.10	0.72	6.09	0.71	5.96	0.60	6.23	0.85	6.12	0.74	5.97	0.61	5.91	0.56	5.87	0.53
15	5.76	0.45	5.85	0.51	5.77	0.46	5.62	0.36	5.86	0.52	5.72	0.42	5.80	0.48	5.81	0.48	5.73	0.43
17	5.72	0.42	5.60	0.35	5.52	0.31	5.33	0.22	5.60	0.35	5.53	0.31	5.64	0.37	5.62	0.36	5.45	0.27
20	5.70	0.41	5.49	0.29	5.27	0.20	4.86	0.07	5.06	0.13	5.02	0.11	5.20	0.17	5.18	0.17	5.04	0.12
22	5.57	0.34	5.44	0.27	5.21	0.18	4.83	0.06	4.83	0.07	4.71	0.04	4.87	0.07	4.82	0.06	4.83	0.06
23	5.51	0.30	5.35	0.23	5.18	0.17	4.75	0.05	4.79	0.06	4.64	0.02	4.83	0.06	4.78	0.05	4.81	0.06

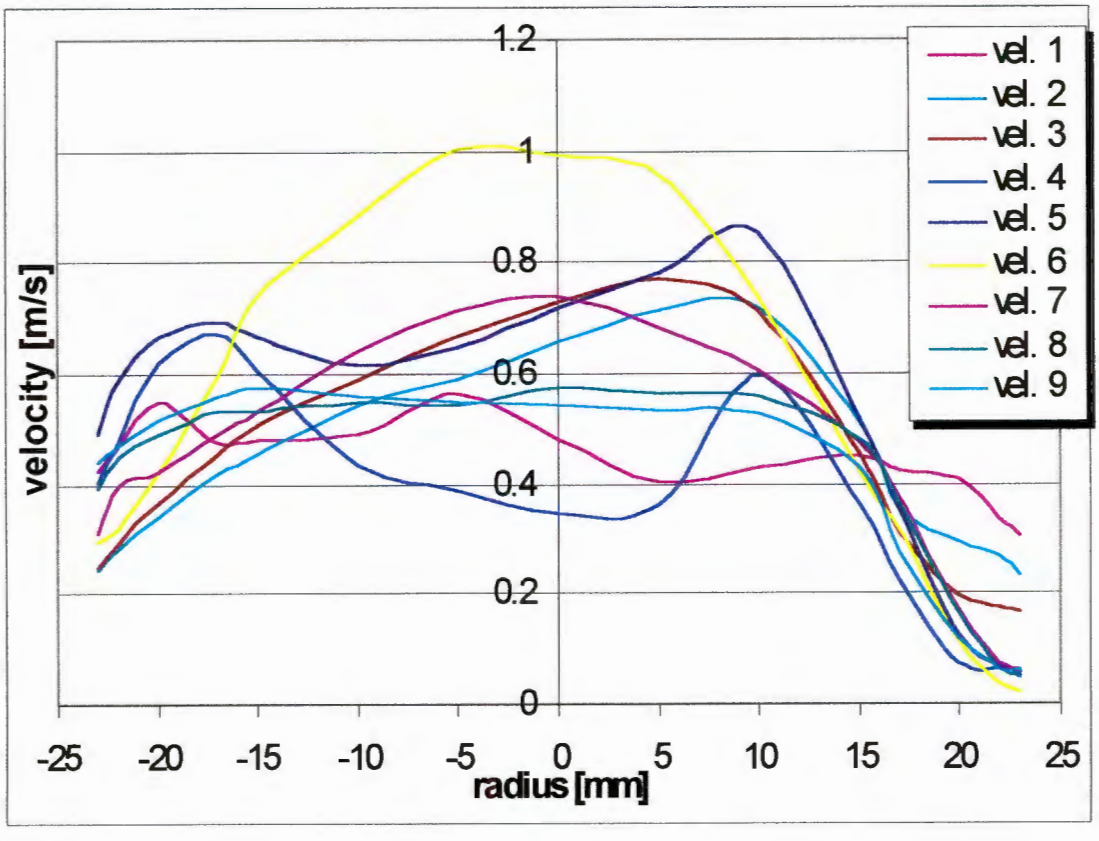

Experiment No 3-4

Date:	09.07.98						
Time:	21:30						
Conditions							
T [C]	16.3		Flowrate [cm]	12		A* [/]	0.5
$p_{ambient}$ [mmHg]	760.25		Flowrate [l/min]	47.440		L* [/]	1
$p_{ambient}$ [Pa]	101113		mean velocity [m/s]	0.476		w* [m/s]	0.9515
			Re [/]	1444.39		Re* [/]	2042.68

z-location	1		2		3		4		5		6		7		8		9	
r-koordinate [mm]	Voltage [V]	vel. 1	Voltage [V]	vel. 2	Voltage [V]	vel. 3	Voltage [V]	vel.4	Voltage [V]	vel. 5	Voltage [V]	vel. 6	Voltage [V]	vel. 7	Voltage [V]	vel. 8	Voltage [V]	vel. 9
-23	5.67	0.39	5.37	0.24	5.41	0.26	4.87	0.07	6.01	0.64	5.56	0.33	5.64	0.37	5.71	0.42	5.69	0.40
-22	5.79	0.47	5.49	0.29	5.51	0.30	4.92	0.09	6.09	0.71	5.69	0.40	5.72	0.42	5.79	0.47	5.74	0.44
-20	5.89	0.54	5.61	0.36	5.64	0.37	4.98	0.10	6.18	0.80	5.79	0.47	5.71	0.42	5.81	0.48	5.85	0.51
-17	5.77	0.46	5.73	0.43	5.77	0.46	5.03	0.12	6.21	0.83	5.87	0.53	5.73	0.43	5.85	0.51	5.88	0.53
-15	5.79	0.47	5.80	0.48	5.84	0.50	5.04	0.12	6.18	0.80	6.06	0.68	5.86	0.52	5.86	0.52	5.88	0.53
-10	5.84	0.50	5.89	0.54	5.94	0.58	5.03	0.12	6.17	0.79	6.23	0.85	6.01	0.64	5.84	0.50	5.87	0.53
-5	5.91	0.56	5.96	0.60	6.02	0.65	5.18	0.17	6.23	0.85	6.28	0.91	6.04	0.67	5.87	0.53	5.87	0.53
0	5.82	0.49	6.03	0.66	6.09	0.71	5.38	0.24	6.20	0.82	6.29	0.92	6.02	0.65	5.86	0.52	5.84	0.50
5	5.69	0.40	6.07	0.69	6.11	0.73	5.29	0.21	6.22	0.84	6.29	0.92	5.99	0.62	5.85	0.51	5.83	0.50
10	5.71	0.42	6.06	0.68	6.05	0.67	5.42	0.26	6.15	0.77	6.07	0.69	5.88	0.53	5.88	0.53	5.84	0.50
15	5.73	0.43	5.81	0.48	5.72	0.42	5.19	0.17	5.88	0.53	5.78	0.46	5.74	0.44	5.78	0.46	5.71	0.42
17	5.73	0.43	5.63	0.37	5.47	0.28	4.97	0.10	5.68	0.40	5.63	0.37	5.55	0.32	5.64	0.37	5.49	0.29
20	5.68	0.40	5.53	0.31	5.22	0.18	4.85	0.07	5.08	0.13	5.11	0.14	5.18	0.17	5.28	0.20	4.98	0.10
22	5.57	0.34	5.49	0.29	5.14	0.15	4.96	0.10	4.81	0.06	4.81	0.06	4.82	0.06	4.93	0.09	4.79	0.06
23	5.48	0.29	5.47	0.28	5.11	0.14	4.94	0.09	4.76	0.05	4.67	0.03	4.79	0.06	4.84	0.07	4.73	0.04

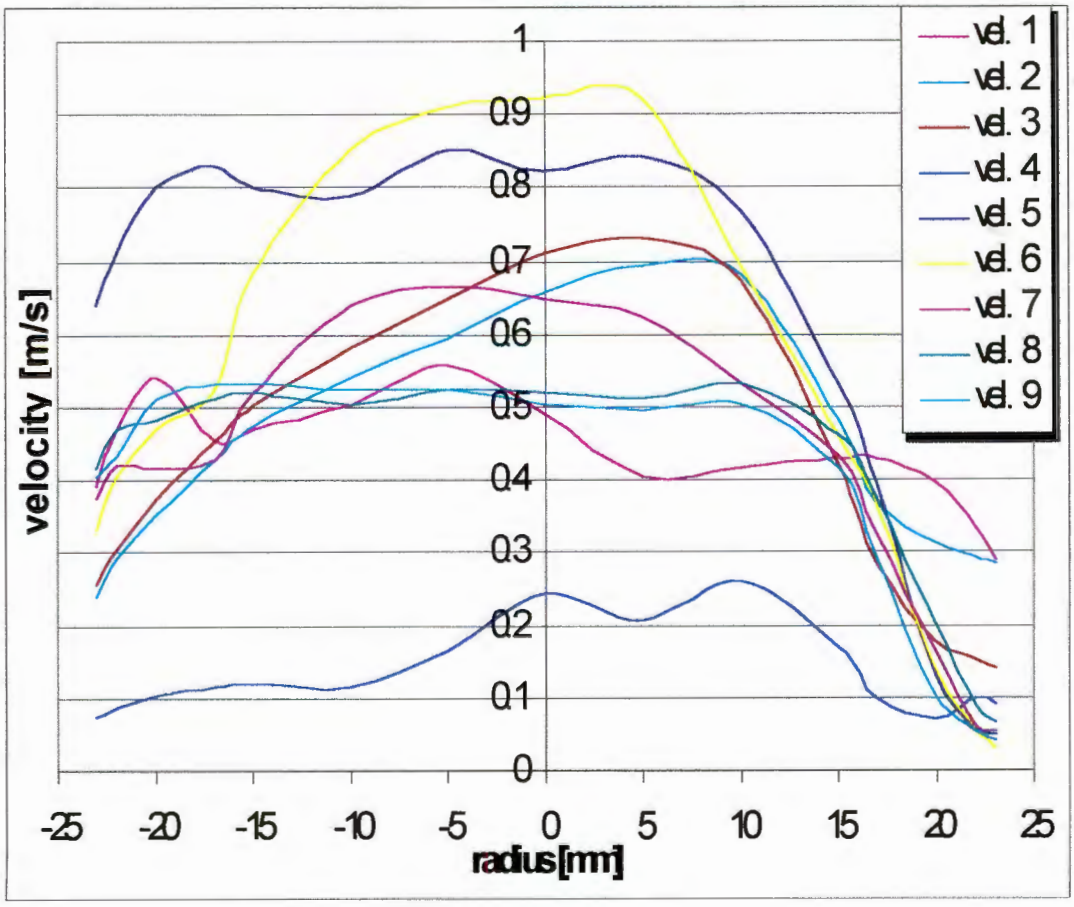

Experiment No 4

Date:	19-8-98			
Time:	18:00			
Conditions				
T [C]	17.6		Flowrate [cm]	12
$p_{ambient}$ [mmHg]	753		Flowrate [l/min]	47.440
$p_{ambient}$ [Pa]	100149		mean velocity [m/s]	0.476
			Re [/]	1444.392

blockage type	delta p1 [Pa]	delta p2 [Pa]	delta p3 [Pa]	pressure loss pipe	pressure loss blockage
no blockage	0.72	0.11	0.03	0.61	0.08
wood	0.99	0.39	0.02	0.6	0.37
smooth PVC L2	0.94	0.330	0.02	0.61	0.31
ring d40	0.73	0.120	0.02	0.61	0.1
ring d32	0.93	0.320	0.02	0.61	0.3
ring d26	1.68	1.050	0.01	0.63	1.04
ring d20	4.53	3.910	0.02	0.62	3.89
prestix d40 L1	0.74	0.110	0.01	0.63	0.1
prestix d20 L1	4.39	3.750	0.01	0.64	3.74

Numerical Results

This Appendix first shows the chosen common parameters in the numerical simulations, followed by a table of all simulations. After that, all the used pre-processing files are shown and this appendix ends with a standard post-processing file.

Common conditions for all simulations

- *Fluid conditions:*

Temperature T=20°C
Density ρ=1.18kg/m^3
Viscosity ν=1.85e-5
Pressure p=10000Pa
Constant mass flux=7.821e-4 kg/s

- *Reference Conditions*

Reference Temperature Tref=273.15K
Reference specific Heat =1006.0 J/kg K
Initial turbulent kinetic energy k=0.001
Initial turbulent dissipation ε=0.001
Reference Pressure=10000Pa
Gravitation forces all 0

- *Boundary conditions:*

Inlet: "inlet" boundary with known mass flux, constant Inlet velocity normal to inlet area w=0.476m/s
Outlet: "outlet" boundary, total flow is leaving the geometry, zero-gradients for the velocity components are imposed
Pressure Gradient at walls extrapolated

- *Numerical conditions*

Convergence condition:	1e-3
Sweeps for the individual equations of U, V, W, K and ε:	100
Sweeps for the individual equation of P:	1000
Relaxation factors for the individual equations of U, V, W, K and ε:	0.7
Relaxation factors for the individual equation of P:	0.2
Residual values for the individual equations of U, V, W, K and ε:	0.1
Residual values for the individual equation of P:	0.05

- *Geometry*

Circular main pipe with inner diameter of 46mm and length of 5.92m. Z-coordinate is in flow direction starting at the inlet with the value 0. R-coordinate is in radial direction, starting in the middle of the pipe with the value 0. Phi-coordinate is in circumferential direction.
Different blockages are inserted in the different simulations. All the blockages have their downstream ending at z=5.1m, independent of their dimensions.

simulation	blockage	flow	# cells [r,phi,z]	# iter.	CPU time	Conv.	Max. vel. num sim	Corr. Exp.	Max vel. theory	Max. vel. exp.
No 1	No	lam	72000 [10,36,200]	600	34.8h	No - pressure	(1.173)	1-1	0.95	0.7
No 2	No	lam	9000 [10,18,50]	114	24min	Yes	0.934	1-1	0.95	0.7
No 3	No	lam	36000 [10,24,150]	205	4.98h	Yes	0.792	1-1	0.95	0.7
No 4	No	Stand. K-ε	36000 [10,24,150]	295	6.48h	Yes	0.6371	1-1	0.95	0.7
No 5	No	Low Re k-ε	36000 [10,24,150]	296	6.41h	Yes	0.6307	1-1	0.95	0.7
No 6	no	Stand. K-ε, rough wall	36000 [10,24,150]	295	6.56h	Yes	0.6371	1-1	0.95	0.7
No 7	L5mm Di32mm	lam	35928 [10-7-10, 24, 134-1-15]	261	4.94h	Yes	1.098	1-3	1.98	1.05
No 7b	L5mm Di32mm	lam	35712 [10-7-10, 24,131-4-15]	261	1.55h	Yes	1.057	1-3	1.98	1.05
No 8	L46mm Di32mm	lam	35856 [10-7-10,24, 133-2-15]	261	5.22h	Yes	1.132	1-6	1.98	1.08
No 8b	L46mm Di32mm	lam	35712 [10-7-10, 24,131-4-15]	261	4.4h	Yes	1.120	1-6	1.98	1.08
No 9	L92mm Di32mm	lam	35712 [10-7-10, 24, 131-4-15]	260	4.87h	Yes	1.163	1-4, 1-5	1.98	1.1
No 10	L46mm Di40mm	lam	28752 [8-7-8,24, 133-2-15]	231	3.76h	Yes	0.8431	2-1	1.25	0.82
No 10b	L46mm Di40mm	lam	40224 [15-13-15,24, 100-2-10]	330	9.15h	Yes	0.8648	2-1	1.25	0.82
No 11	L46mm Halfcirc. A*=0.5	Lam	35760 [10,24-12-24, 133-2-15]	260	3.91h	Yes	1.090	3-1 to 3-4	1.90	0.95 to 1.1
No 12	L46mm Di26mm	Lam	32208 [9-5-9,24, 133-2-15]	235	3.76h	Yes	1.651	2-3	2.97	1.9
No 13	L46mm Di20mm	Lam	41808 [16-7-16, 24, 98-2-10]	1100	9.68h	No: p~3e-3 w~1e-2	2.946	2-4	5.00	2.8

Simulation No1

Pre-processing file

```
// *** noblolamPre : Flo++ input file
// *** for simulation of LAMINAR pipe flow
// *** without any blockage
reset
// *** Mesh generation ****************************
// *** cylindrical coordinates
// *** dimensions: length=5.92m
// *** number of cells: 72000
// *** number of vertex: 81807
// *** number of boundaries: 8640
csys 1
mcrea 0 0.023 10 0 360 36 0 5.92 200 0.9 1 1
plty hwire
view 1 0 23
cp
bview 2
bzone 1 b
bzone 2 f
view 1 0 23
// *** Fluid type definition ***********************
// energy on
turb off
// tref 273
pref 100000 1
// *** Material properties and initial conditions ***
dens const 1.18
visc const 1.85e-5
initial stand 0 0 0.476 0 20 0.001 0.001
// *** Cell and boundary group definitions ********
// *** homgene inlet velocity profile
// *** axial velocity w=0.476m/s
bgdef 1 inlet
1 0 0 0.476 1.18 20 0.001 0.001
// *** pressure boundary
bgdef 2 outlet
1
// *** Solution control ****************************
restart previous
iter 300 50
conv 0.001
monit 4
// *** Writing data for the solution stage **********
vmerge all
wmesh
wdef
// *** Save the modelling status ******************
save
view 1 0 23
plty hwire
bp
```

Simulation No2

Pre-processing file

```
// *** noblolamless1Pre : Flo++ input file
// *** for simulation of TURBULENT pipe flow
// *** without any blockage
// *** half the number of cells in
// *** all 3 directions are used
reset
// *** Mesh generation ****************************
// *** cylindrical coordinates
// *** number of cells: 9000
// *** number of vertex: 10659
// *** number of boundaries: 2160
csys 1
mcrea 0 0.023 10 0 360 18 0 5.92 50 0.9 1 1
plty hwire
view 1 0 23
cp
bview 2
bzone 1 b
bzone 2 f
view 1 0 23
// *** Fluid type definition ***********************
// energy on
turb off
// tref 273
pref 100000 1
// *** Material properties and initial conditions ***
dens const 1.18
visc const 1.85e-5
initial stand 0 0 0.476 0 20 0.001 0.001
// *** Cell and boundary group definitions ********
// *** homgene inlet velocity profile
// *** axial velocity w=0.476m/s
bgdef 1 inlet
1 0 0 0.476 1.18 20 0.001 0.001
// *** outlet
// *** pressure boundary
bgdef 2 outlet
1
// *** Solution control ********************************
iter 300 50
conv 0.001
monit 4
// *** Writing data for the solution stage **********
vmerge all
wmesh
wdef
// *** Save the modelling status ******************
save
view 1 0 23
plty hwire
bp
```

Simulation No 3

Pre-processing file

```
// *** noblolmedcel : Flo++ input file
// *** for simulation of turbulent pipe flow
// *** without any blockage
// *** medium large number of cells
// *** with rough walls
reset
// *** Mesh generation ****************************
// *** cylindrical coordinates
// *** number of cells: 36000
csys 1
mcrea 0 0.023 10 0 360 24 0 5.92 150 0.9 1 1
plty hwire
view 1 0 23
cp
bview 2
bzone 1 b
bzone 2 f
view 1 0 23
// *** Fluid type definition ***********************
// energy on
turb on
// tref 273
pref 100000 1
// *** Material properties and initial conditions ***
dens const 1.18
visc const 1.85e-5
initial stand 0 0 0.476 0 20 0.001 0.001
// *** Cell and boundary group definitions ********
// *** homgene inlet velocity profile
// *** axial velocity w=0.476m/s
bgdef 1 inlet
1 0 0 0.476 1 20 0.001 0.001
// *** pressure boundary
bgdef 2 outlet
1
// *** Solution control ******************************
iter 500 50
conv 0.001
monit 4
// *** Writing data for the solution stage **********
vmerge all
wmesh
wdef
// *** Save the modelling status ******************
save
view 1 0 23
plty hwire
bp
```

Simulation No 4

Pre-processing file

```
// *** noblohire : Flo++ input file
// *** for simulation of turbulent pipe flow
// *** without any blockage
// *** medium large number of cells
// *** standard k-epsilon
reset
// *** Mesh generation ****************************
// *** cylindrical coordinates
// *** number of cells: 36000
// *** number of vertex: 41525
csys 1mcrea 0 0.023 10 0 360 24 0 5.92 150 0.9 1 1
plty hwire
view 1 0 23
cp
bview 2
bzone 1 b
bzone 2 f
view 1 0 23
// *** Fluid type definition ***********************
// energy on
turb on
// tref 273
pref 100000 1
// *** Material properties and initial conditions ***
dens const 1.18
visc const 1.85e-5
initial stand 0 0 0.476 0 20 0.001 0.001
// *** Cell and boundary group definitions ********
// *** homgene inlet velocity profile
// *** axial velocity w=0.476m/s
bgdef 1 inlet
1 0 0 0.476 1 20 0.001 0.001
// *** pressure boundary
bgdef 2 outlet
1
// *** Solution control ***************************
iter 300 50
conv 0.001
monit 4
// *** Writing data for the solution stage **********
vmerge all
wmesh
wdef
// *** Save the modelling status ******************
save
view 1 0 23
plty hwire
bp
************************************************************
```

Simulation No 5

Pre-processing file

```
// *** noblolore : Flo++ input file
// ***Low Reynolds number k-ε model
// *** without any blockage
// *** medium large number of cells
reset
// *** Mesh generation ****************************
// *** cylindrical coordinates
// *** number of cells: 36000
// *** number of vertex: 41525
csys 1
mcrea 0 0.023 10 0 360 24 0 5.92 150 0.9 1 1
plty hwire
view 1 0 23
cp
bview 2
bzone 1 b
bzone 2 f
view 1 0 23
// *** Fluid type definition ***********************
// energy on
turb lowrey
// tref 273
pref 100000 1
// *** Material properties and initial conditions ***
dens const 1.18
visc const 1.85e-5
initial stand 0 0 0.476 0 20 0.001 0.001
// *** Cell and boundary group definitions ********
// *** homgene inlet velocity profile
// *** axial velocity w=0.476m/s
bgdef 1 inlet
1 0 0 0.476 1 20 0.001 0.001
// *** pressure boundary
bgdef 2 outlet
1
// *** Solution control ******************************
iter 300 50
conv 0.001
monit 4
// *** Writing data for the solution stage **********
vmerge all
wmesh
wdef
// *** Save the modelling status ******************
save
view 1 0 23
plty hwire
bp
```

Simulation No 6

Pre-processing file

```
// *** noblorough : Flo++ input file
// *** for simulation of turbulent pipe flow
// *** without any blockage
// *** with rough walls
reset
// *** Mesh generation ****************************
// *** cylindrical coordinates
// *** number of cells: 36000
csys 1
mcrea 0 0.023 10 0 360 24 0 5.92 150 0.9 1 1
plty hwire
view 1 0 23
cp
bview 2
bzone 1 b
bzone 2 f
bzone 3 n
bzone 4 e
bzone 5 w
bzone 6 s
view 1 0 23
// *** Fluid type definition ***********************
turb on
pref 100000 1
// *** Material properties and initial conditions ***
dens const 1.18
visc const 1.85e-5
initial stand 0 0 0.476 0 20 0.001 0.001
// *** Cell and boundary group definitions ********
// *** homgene inlet velocity profile
// *** axial velocity w=0.476m/s
bgdef 1 inlet
1 0 0 0.476 1 20 0.001 0.001
// *** pressure boundary
bgdef 2 outlet
1
// *** rough wall
// *** elog [1.14 9], 9~smooth
// *** chosen value elog=1.14 (=minimum)
bgdef 3 wall
1 0 0 0 1.14
bgdef 4 wall
1 0 0 0 1.14
bgdef 5 wall
1 0 0 0 1.14
bgdef 6 wall
1 0 0 0 1.14
 // *** Solution control ********************************
iter 300 50
conv 0.001
monit 4
// *** Writing data for the solution stage **********
vmerge all
wmesh
wdef
// *** Save the modelling status ******************
save
```

```
view 1 0 23
plty hwire
bp
```

Simulation No 7

Pre-processing file

```
// *** ring2 : Flo++ input file
// *** simulation of flow with ring2
// *** di=32mm
// *** l=5mm
reset
// *** Mesh generation ****************************
// *** cylindrical coordinates
// *** number of cells: 35928
csys 1
cgro 1
mcrea 0 0.023 10 0 360 24 0 5.095 134
view 1 0 1
plty hwire
cp
cset none
cgro 2
mcrea 0 0.016 7 0 360 24 5.095 5.1 1
view 1 0 1
plty hwire
cp
cset none
cgro 3
mcrea 0 0.023 10 0 360 24 5.1 5.92 15
view 1 0 1
plty hwire
cp
cset all
vmerge all
// ***** Create boundary cells
// *** Inlet
cset none
cnum off
cset xyzr 0 0.023 0 360 0 0.04
plty hsurf
bview 1
bface 1 b
view 1 0 1
// *** Outlet
cset none
cset xyzr 0 0.023 0 360 5.88 5.92
bview 2
bface 2 f
view 1 0 1
plty hwire
cp
cset all
// *** Fluid type definition ***********************
turb off
pref 100000 1
// *** Material properties and initial conditions ***
dens const 1.18
visc const 1.85e-5
```

```
initial stand 0 0 0.476 0 20 0.001 0.001
// *** Cell and boundary group definitions ********
bgdef 1 inlet
1 0 0 0.476 1 20 0.001 0.001
bgdef 2 outlet
1
// *** Solution control ******************************
iter 500 50
conv 0.001
monit 4
// *** Writing data for the solution stage **********
vmerge all
wmesh
wdef
// *** Save the modelling status ********************
save
view 1 0 23
plty hwire
bp
```

Simulation No 7b

Pre-processing file

```
// *** ring2b : Flo++ input file
// *** simulation of flow with ring2
// *** di=32mm
// *** l=5mm
reset
// *** Mesh generation ****************************
// *** cylindrical coordinates
// *** number of cells: 35928
csys 1
cgro 1
mcrea 0 0.023 10 0 360 24 0 5.095 131
view 1 0 1
plty hwire
cp
cset none
cgro 2
mcrea 0 0.016 7 0 360 24 5.095 5.1 4
view 1 0 1
plty hwire
cp
cset none
cgro 3
mcrea 0 0.023 10 0 360 24 5.1 5.92 15
view 1 0 1
plty hwire
cp
cset all
vmerge all
// ***** Create boundary cells
// *** Inlet
cset none
cnum off
cset xyzr 0 0.023 0 360 0 0.04
plty hsurf
bview 1
bface 1 b
view 1 0 1
```

```
// *** Outlet
cset none
cset xyzr 0 0.023 0 360 5.88 5.92
bview 2
bface 2 f
view 1 0 1
plty hwire
cp
cset all
// *** Fluid type definition ************************
turb off
pref 100000 1
// *** Material properties and initial conditions ***
dens const 1.18
visc const 1.85e-5
initial stand 0 0 0.476 0 20 0.001 0.001
// *** Cell and boundary group definitions ********
bgdef 1 inlet
1 0 0 0.476 1 20 0.001 0.001
bgdef 2 outlet
1
// *** Solution control *******************************
iter 500 50
conv 0.001
monit 4
// *** Writing data for the solution stage **********
vmerge all
wmesh
wdef
// *** Save the modelling status ********************
save
view 1 0 23
plty hwire
bp
```

Simulation No 8

Pre-processing file

```
// *** block-d2-l1 : Flo++ input file
// *** simulation of flow with ring2
// *** di=32mm (d2)
// *** l=46mm
reset
// *** Mesh generation ******************************
// *** cylindrical coordinates
// *** number of cells: 35856
csys 1
cgro 1
mcrea 0 0.023 10 0 360 24 0 5.054 133
view 1 0 1
plty hwire
cp
cset none
cgro 2
mcrea 0 0.016 7 0 360 24 5.054 5.1 2
view 1 0 1
plty hwire
cp
cset none
cgro 3
```

```
mcrea 0 0.023 10 0 360 24 5.1 5.92 15
view 1 0 1
plty hwire
cp
cset all
vmerge all
// ***** Create boundary cells
// *** Inlet
cset none
cnum off
cset xyzr 0 0.023 0 360 0 0.04
plty hsurf
bview 1
bface 1 b
view 1 0 1
// *** Outlet
cset none
cset xyzr 0 0.023 0 360 5.88 5.92
bview 2
bface 2 f
view 1 0 1
plty hwire
cp
cset all
// *** Fluid type definition ************************
turb off
pref 100000 1
// *** Material properties and initial conditions ***
dens const 1.18
visc const 1.85e-5
initial stand 0 0 0.476 0 20 0.001 0.001
// *** Cell and boundary group definitions ********
bgdef 1 inlet
1 0 0 0.476 1 20 0.001 0.001
bgdef 2 outlet
1
// *** Solution control *******************************
iter 500 50
conv 0.001
monit 4
// *** Writing data for the solution stage **********
vmerge all
wmesh
wdef
// *** Save the modelling status ********************
save
view 1 0 23
plty hwire
bp
```

Simulation No 8b

Pre-processing file

```
// *** block-d2-l1b : Flo++ input file
// *** simulation of flow with ring2
// *** di=32mm (d2)
// *** l=46mm
```

```
reset
// *** Mesh generation ****************************
// *** cylindrical coordinates
// *** number of cells: 35712
csys 1
cgro 1
mcrea 0 0.023 10 0 360 24 0 5.054 131
view 1 0 1
plty hwire
cp
cset none
cgro 2
mcrea 0 0.016 7 0 360 24 5.054 5.1 4
view 1 0 1
plty hwire
cp
cset none
cgro 3
mcrea 0 0.023 10 0 360 24 5.1 5.92 15
view 1 0 1
plty hwire
cp
cset all
vmerge all
// ***** Create boundary cells
// *** Inlet
cset none
cnum off
cset xyzr 0 0.023 0 360 0 0.04
plty hsurf
bview 1
bface 1 b
view 1 0 1
// *** Outlet
cset none
cset xyzr 0 0.023 0 360 5.88 5.92
bview 2
bface 2 f
view 1 0 1
plty hwire
cp
cset all
// *** Fluid type definition **************************
turb off
pref 100000 1
// *** Material properties and initial conditions ***
dens const 1.18
visc const 1.85e-5
initial stand 0 0 0.476 0 20 0.001 0.001
// *** Cell and boundary group definitions ********
bgdef 1 inlet
1 0 0 0.476 1 20 0.001 0.001
bgdef 2 outlet
1
// *** Solution control *******************************
iter 500 50
conv 0.001
monit 4
// *** Writing data for the solution stage **********
vmerge all
```

```
wmesh
wdef
// *** Save the modelling status ********************
save
view 1 0 23
plty hwire
bp
```

Simulation No 9

Pre-processing file

```
// *** block-d2-l2 : Flo++ input file
// *** simulation of flow with ring2
// *** di=32mm (d2)
// *** l=92mm
reset
// *** Mesh generation ******************************
// *** cylindrical coordinates
// *** number of cells: 35712
csys 1
cgro 1
mcrea 0 0.023 10 0 360 24 0 5.008 131
view 1 0 1
plty hwire
cp
cset none
cgro 2
mcrea 0 0.016 7 0 360 24 5.008 5.1 4
view 1 0 1
plty hwire
cp
cset none
cgro 3
mcrea 0 0.023 10 0 360 24 5.1 5.92 15
view 1 0 1
plty hwire
cp
cset all
vmerge all
// ***** Create boundary cells
// *** Inlet
cset none
cnum off
cset xyzr 0 0.023 0 360 0 0.04
plty hsurf
bview 1
bface 1 b
view 1 0 1
// *** Outlet
cset none
cset xyzr 0 0.023 0 360 5.88 5.92
bview 2
bface 2 f
view 1 0 1
plty hwire
cp
cset all
```

```
// *** Fluid type definition ************************
turb off
pref 100000 1
// *** Material properties and initial conditions ***
dens const 1.18
visc const 1.85e-5
initial stand 0 0 0.476 0 20 0.001 0.001
// *** Cell and boundary group definitions ********
bgdef 1 inlet
1 0 0 0.476 1 20 0.001 0.001
bgdef 2 outlet
1
// *** Solution control *******************************
iter 500 50
conv 0.001
monit 4
// *** Writing data for the solution stage **********
vmerge all
wmesh
wdef
// *** Save the modelling status ********************
save
view 1 0 23
plty hwire
bp
```

Simulation No 10

Pre-processing file

```
// *** block-d1-l1 : Flo++ input file
// *** simulation of flow with ring1
// *** di=40mm (d1)
// *** l=46mm
reset
// *** Mesh generation ****************************
// *** cylindrical coordinates
// *** number of cells: 28752
// *** ratio 0.02/0.023=0.8696
// *** possible combinations to match:
// *** 7/8=0.875 ****************
// *** 13-15=0.8667
csys 1
cgro 1
mcrea 0 0.023 8 0 360 24 0 5.054 133 1.005 1 1
view 1 0 23
plty hwire
cp
cset none
cgro 2
mcrea 0 0.02 7 0 360 24 5.054 5.1 2
view 1 0 23
plty hwire
cp
cset all
view 0 0 1
plty hwire
cp
cset none
cgro 3
mcrea 0 0.023 8 0 360 24 5.1 5.92 15 1.005 1 1
```

```
view 1 0 23
plty hwire
cp
cset all
view 1 0 23
plty hwire
cp
vmerge all
// ***** Create boundary cells
// *** Inlet
cset none
cnum off
cset xyzr 0 0.023 0 360 0 0.04
plty hsurf
bview 1
bface 1 b
view 1 0 1
// *** Outlet
cset none
cset xyzr 0 0.023 0 360 5.88 5.92
bview 2
bface 2 f
view 1 0 1
plty hwire
cp
cset all
// *** Fluid type definition ************************
turb off
pref 100000 1
// *** Material properties and initial conditions ***
dens const 1.18
visc const 1.85e-5
initial stand 0 0 0.476 0 20 0.001 0.001
// *** Cell and boundary group definitions *********
bgdef 1 inlet
1 0 0 0.476 1 20 0.001 0.001
bgdef 2 outlet
1
// *** Solution control ***************************
iter 500 50
conv 0.001
monit 4
// *** Writing data for the solution stage **********
vmerge all
wmesh
wdef
// *** Save the modelling status ******************
save
view 1 0 23
plty hwire
bp
```

Simulation No 10b

Pre-processing file

```
// *** block-l1-d1 : Flo++ input file
// *** simulation of flow with ring1
// *** di=40mm (d1)
// *** l=46mm
reset
// *** Mesh generation ****************************
// *** cylindrical coordinates
// *** number of cells: 40224
// *** ratio 0.02/0.023=0.8696
// *** possible combinations to match:
// *** 7/8=0.875
// *** 13-15=0.8667 ****************
csys 1
cgro 1
mcrea 0 0.023 15 0 360 24 0 5.054 100 0.998 1 1
view 1 0 23
plty hwire
cp
cset none
cgro 2
mcrea 0 0.02 13 0 360 24 5.054 5.1 2
view 1 0 23
plty hwire
cp
cset all
view 0 0 1
plty hwire
cp
cset none
cgro 3
mcrea 0 0.023 15 0 360 24 5.1 5.92 10 0.998 1 1
view 1 0 23
plty hwire
cp
cset all
view 1 0 23
plty hwire
cp
vmerge all
// ***** Create boundary cells
// *** Inlet
cset none
cnum off
cset xyzr 0 0.023 0 360 0 0.04
plty hsurf
bview 1
bface 1 b
view 1 0 23
cp
// *** Outlet
cset none
cset xyzr 0 0.023 0 360 5.82 5.92
bview 2
bface 2 f
view 1 0 23
plty hwire
```

```
cp
cset all
// *** Fluid type definition ***************************
turb off
pref 100000 1
// *** Material properties and initial conditions ***
dens const 1.18
visc const 1.85e-5
initial stand 0 0 0.476 0 20 0.001 0.001
// *** Cell and boundary group definitions ********
bgdef 1 inlet
1 0 0 0.476 1 20 0.001 0.001
bgdef 2 outlet
1
// *** Solution control ********************************
iter 500 50
conv 0.001
monit 4
// *** Writing data for the solution stage **********
vmerge all
wmesh
wdef
// *** Save the modelling status *******************
save
view 1 0 23
plty hwire
bp
```

Simulation No 11

Pre-processing file

```
// *** half-wood : Flo++ input file
// *** simulation of flow with
// *** halfcylindrical blockage
// *** di=23mm
// *** l=46mm
reset
// *** Mesh generation ***************************
// *** cylindrical coordinates
// *** number of cells: 35760
csys 1
cgro 1
mcrea 0 0.023 10 0 360 24 0 5.054 133
view 1 0 23
plty hwire
cp
cset none
cgro 2
mcrea 0 0.023 10 0 180 12 5.054 5.1 2
view 1 0 23
plty hwire
cp
cset none
cgro 3
mcrea 0 0.023 10 0 360 24 5.1 5.92 15
view 1 0 23
plty hwire
cp
```

```
cset all
vmerge all
// ***** Create boundary cells
// *** Inlet
cset none
cnum off
cset xyzr 0 0.023 0 360 0 0.04
plty hsurf
bview 1
bface 1 b
view 1 0 1
// *** Outlet
cset none
cset xyzr 0 0.023 0 360 5.88 5.92
bview 2
bface 2 f
view 1 0 1
plty hwire
cp
cset all
// *** Fluid type definition ************************
turb off
pref 100000 1
// *** Material properties and initial conditions ***
dens const 1.18
visc const 1.85e-5
initial stand 0 0 0.476 0 20 0.001 0.001
// *** Cell and boundary group definitions ********
bgdef 1 inlet
1 0 0 0.476 1 20 0.001 0.001
bgdef 2 outlet
1
// *** Solution control *******************************
restart  PREVIOUS
iter 500 50
conv 0.001
monit 4
// *** Writing data for the solution stage **********
vmerge all
wmesh
wdef
// *** Save the modelling status ******************
save
view 1 0 23
plty hwire
bp
```

Simulation No 12

Pre-processing file

```
// *** block-d3-l3-tryPre
// *** di=26mm (d3)
// *** l=46mm
reset
// *** Mesh generation ****************************
// *** cylindrical coordinates
// *** number of cells: 32208
csys 1
```

```
cgro 1
mcrea 0 0.023 9 0 360 24 0 5.054 133 0.99 1 1
view 1 0 23
plty hwire
cp
cset none
cgro 2
mcrea 0 0.013 5 0 360 24 5.054 5.1 2
view 1 0 23
plty hwire
cp
cset all
view 0 0 1
plty hwire
cp
cset none
cgro 3
mcrea 0 0.023 9 0 360 24 5.1 5.92 15 0.99 1 1
view 1 0 23
plty hwire
cp
cset all
vmerge all
// ***** Create boundary cells
// *** Inlet
cset none
cnum off
cset xyzr 0 0.023 0 360 0 0.04
plty hsurf
bview 1
bface 1 b
view 1 0 1
// *** Outlet
cset none
cset xyzr 0 0.023 0 360 5.88 5.92
bview 2
bface 2 f
view 1 0 1
plty hwire
cp
cset all
// *** Fluid type definition ************************
turb off
pref 100000 1
// *** Material properties and initial conditions ***
dens const 1.18
visc const 1.85e-5
initial stand 0 0 0.476 0 20 0.001 0.001
// *** Cell and boundary group definitions ********
bgdef 1 inlet
1 0 0 0.476 1 20 0.001 0.001
bgdef 2 outlet
1
// *** Solution control *******************************
iter 500 50
conv 0.001
monit 4
// *** Writing data for the solution stage **********
vmerge all
wmesh
```

```
wdef
// *** Save the modelling status ******************
save
view 1 0 23
plty hwire
bp
```

Simulation No 13

Pre-processing file

```
// *** block-l1d4 : Flo++ input file
// *** di=20mm (d4)
// *** l=46mm
reset
// *** Mesh generation ****************************
// *** cylindrical coordinates
// *** number of cells: 41808
csys 1
cgro 1
mcrea 0 0.023 16 0 360 24 0 5.054 98 1.001 1 1
view 1 0 23
plty hwire
cp
cset none
cgro 2
mcrea 0 0.01 7 0 360 24 5.054 5.1 2
view 1 0 23
plty hwire
cp
cset all
view 0 0 1
plty hwire
cp
cset none
cgro 3
mcrea 0 0.023 16 0 360 24 5.1 5.92 10 1.001 1 1
view 1 0 23
plty hwire
cp
cset all
vmerge all
// ***** Create boundary cells
// *** Inlet
cset none
cnum off
cset xyzr 0 0.023 0 360 0 0.04
plty hsurf
bview 1
bface 1 b
view 1 0 1
// *** Outlet
cset none
cset xyzr 0 0.023 0 360 5.82 5.92
bview 2
bface 2 f
view 1 0 1
plty hwire
cp
cset all
// *** Fluid type definition ***********************
```

```
turb off
pref 100000 1
// *** Material properties and initial conditions ***
dens const 1.18
visc const 1.85e-5
initial stand 0 0 0.476 0 20 0.001 0.001
// *** Cell and boundary group definitions ********
bgdef 1 inlet
1 0 0 0.476 1 20 0.001 0.001
bgdef 2 outlet
1
// *** Solution control ********************************
relaxation 0.5 0.5 0.5 0.2 0.7 0.7 0.7
//sweeps 100 100 100 1000 100 100 100
residuals 0.01 0.01 0.01 0.005 0.01 0.01 0.01
restart previous
iter 500 50
conv 0.001
monit 4
// *** Writing data for the solution stage **********
vmerge all
wmesh
wdef
// *** Save the modelling status *******************
save
view 1 0 23
plty hwire
bp
```

General Postprocessing file

```
// *** block : Flo++ post-processing file ************************
// ************************************************************
// *** Resume from the previous settings
resume
// *** Read the results
rresults
// *** Prepare a contour plot of magnitude velocity and pressure
view -1 0 23
plty hwire
bp
pltype plane
ploption contour
COLSCALE 10  USER 0 1.7
pnorm 1 0 0
ppoi 0 0 2.5
vload m
cp
COLSCALE 10  GLOBAL
vload p
cp
// *** next plane
pltype plane
ploption contour
COLSCALE 10  USER 0 3
pnorm 0 0 1
ppoi 0 0 5.1
vload m
cp
```